

HUMAN Nav1.5 F1486 DELETION ASSOCIATED WITH LONG-QT SYNDROME  
LEADS TO DEFICIENCY IN INACTIVATION AND  
REDUCES LIDOCAINE SENSITIVITY

Weihua Song

Submitted to the faculty of the University Graduate School  
in partial fulfillment of the requirements  
for the degree of  
Doctor of Philosophy  
in the Department of Pharmacology and Toxicology  
Indiana University

May 2011

Accepted by the Faculty of Indiana University, in partial fulfillment of the requirements for the degree of Doctor of Philosophy.

Doctoral Committee

---

Weinian Shou, Ph.D., Chair

---

Theodore R. Cummins, Ph.D., Chair

---

Peng-Sheng Chen, MD.

March 3, 2011

---

Andy Hudmon, Ph.D.

---

Richard Nass, Ph.D.

---

Rajesh Khanna, PhD.

## **DEDICATION**

To my parents Yufang Wang, and Yuhui Song, my sisters, my brother, and my husband for their unconditional love and support.

## ACKNOWLEDGEMENTS

There are special moments in my life that I want to express my great appreciation and gratitude to those who have supported me and given me the strength to become a better person. Upon finishing my thesis, I would like to thank all of the individuals that have impacted me directly or indirectly throughout my journey toward the Ph.D. degree.

My dissertation work would not have been completed without the inspiration, guidance, generous support, encouragement, and strong motivation from several persons with whom I have had the great opportunity to work directly or indirectly and those that have influenced me on my journey.

I would like to extend my deepest appreciation to Dr. Weinian Shou for believing in me, taking me into his lab as his graduate student and generously giving me the great opportunity to explore the current thesis project that I have had such a passion to pursue. I also appreciate him for providing me with scientific guidance, detailed advice, and enormous support in many ways. Without his support and advice, I would have never accomplished my goal of getting the Ph.D. degree. His “three-p” advice (passion, patience, and persistence) has shaped me to become a better scientist. My deepest gratitude also goes to Dr. Theodore R. Cummins, for his generosity in providing me with scientific guidance, endless encouragement, detailed advice, manuscript revisions, and other tremendous amounts of help he has provided throughout my study. Without his scientific guidance and support, I would have never been able

to advance this far. Throughout my Ph.D. study, Dr. Andy Hudmon also gave me scientific support and encouragement. He has taught me numerous skills to become a successful scientist. Without his help, I would not have been able to finish the study based on cardiomyocytes. Much appreciation should also be given to Dr. Peng-sheng Chen, Dr. Rajesh Khanna, and Dr. Richard Nass for taking time to be a part of my thesis committee. They all continuously gave me great guidance and suggestions during our discussions. The ideas generated by them helped me move forward and motivated me to always ask questions. Their encouragement made me confident when I was struggling. These advisors are my role models in science. Furthermore, they have shown me that enthusiasm is an essential component of a rewarding scientific career. All I can hope for is to accomplish as much as they have in science.

I would also like to thank my parents for giving me life. Due to a disease condition, my father could not live long enough to watch me grow up and pursue an academic career that he, himself used to do. Nonetheless, the integrity and sincerity that he and my mother have shown me shaped and guided me toward the right track to be a good scientist, and more importantly, a good mother to educate and guide my own son. It is because of the self-motivation, diligence, sacrifice and dedication learned from both of them that has motivated me to achieve the current goal and will drive me to further pursue an academic career. My brother and sisters have also helped me throughout each step of my life. The way that each of them act both in the community and in academic institutions will encourage me throughout my life. I appreciate my mom, sisters,

and brother for always having faith in me. I would also like to extend my appreciation to my sister-in-law and my two brother-in-laws, who have been constantly encouraging and supporting me. Lastly, I would like to thank my husband, Peilin Ma, for his endless support and unconditional love, which have made me strong and ambitious whenever I was facing difficulty. I also appreciate him for our scientific discussions. I look forward to our beautiful life years ahead.

## ABSTRACT

Weihua Song

Human Nav1.5 F1486 deletion associated with long-QT syndrome leads to deficiency in inactivation and reduces lidocaine sensitivity

The cardiac voltage-gated sodium channel  $\alpha$  subunit Nav1.5 generates the cardiac sodium current, which is essential for the initiation and propagation of the cardiac action potentials. Mutations of *SCN5A*, the gene that encodes Nav1.5, have been well documented to cause long-QT syndrome (LQTS) by disrupting channel inactivation and increasing late sodium current. Previous studies have revealed the importance of the intracellular loop region between transmembrane domain III and IV of sodium channel  $\alpha$  subunit in regulating the fast inactivation. A recent clinical case study reported an infant patient with LQTS carrying a phenylalanine (F) deletion at amino acid 1486 of the Nav1.5 channel. This study reported that the patient showed severe cardiac arrhythmia reflected as LQTS and subsequent ventricular tachycardia, which was refractory to antiarrhythmic drug lidocaine treatment. Therefore, it was hypothesized that the deletion of F1486 on Nav1.5 would substantially alter electrophysiological properties of the channel and reduce the potency of lidocaine on sodium channel. Using HEK293 cells and neonatal rat cardiomyocytes, the F1486del channel was functionally characterized by whole-cell patch-clamp techniques. Studies revealed that the deletion of F1486 causes a combination of changes including a loss-of-function alteration reflected as a substantial reduction of peak current density and a

number of gain-of-function alterations including reduced channel inactivation, substantial augmentation of late sodium current, and an increase in ramp current. In addition, lidocaine sensitivity was dramatically reduced. By contrast, the voltage for half maximal activation ( $V_{1/2}$ ) and the time constant for channel deactivation for the F1486del channel were identical to the wild type channels. Using neonatal rat cardiomyocytes, we were able to study the functional consequence of F1484del on action potential duration (APD). Cardiomyocytes expressing F1486del channel have substantial APD prolongation and prominent spontaneous early afterdepolarizations, which likely underlie the subsequent LQTS in the patient. Taken together, despite the reduction in peak current density, the substantial gain-of-function changes are sufficient to cause the APD prolongation, which is a prominent characteristic of LQTS. These findings provide knowledge for understanding the relationships between sodium channel structure, pharmacology and the physiological consequence of sodium channel mutations that underlie LQTS.

Weinian Shou, Ph.D., Chair

## TABLE OF CONTENTS

<b>LIST OF TABLES</b> .....	xv
<b>LIST OF FIGURES</b> .....	xvi
<b>LIST OF ABBREVIATIONS</b> .....	xx
<b>I. INTRODUCTION</b> .....	1
A. Overview of the thesis project .....	1
B. Basic methodology used in studying the function of VGSCs: patch-clamp techniques .....	3
C. Background information of VGSCs: research history, structure, function, and modulation .....	7
D. Introduction and the characteristics of cardiac sodium channel Nav1.5 $\alpha$ subunit: tissue distribution, TTX sensitivity and other properties .....	15
E. Introduction of sodium channel $\beta$ subunits .....	17
F. Action potential and its correlation with ECG study .....	18
G. Overview of the LQTS .....	24
1. History of the identification of the LQTS .....	24
2. Diagnosis of the LQTS .....	24
3. Classification of the LQTS .....	25
a. Genesis of the acquired LQTS .....	25
b. The molecular basis of the congenital inherited LQTS .....	26

H. Sodium channel $\alpha$ subunit mutations and cardiac arrhythmias .....	31
1. Role of the cardiac sodium channels in the genesis of the inherited cardiac arrhythmias .....	31
2. Inherited LQTs and its relationship with sodium channel gain-of-function mutations .....	31
3. Sodium channel loss-of-function mutations .....	32
a. Brugada syndrome .....	32
b. Progressive conduction system defects.....	33
I. Antiarrhythmic drug binding sites on sodium channel .....	34
J. Hypothesis and specific aims .....	34
<b>II. MATERIALS AND METHODS .....</b>	<b>39</b>
A. Ethical information and animal protocols .....	39
B. Animals .....	39
C. Patch-clamp recording related instrument set up and general experimental procedures .....	39
D. Preparation of the patch-clamp recording chamber .....	40
E. Mutagenesis of VGSCs .....	41
F. Large-scale bacteria culture and DNA purification .....	45
G. Cell culture .....	46
1. Culture of HEK293 cells .....	46
2. Harvest, isolation and culture of neonatal rat cardiomyocytes .....	46
H. Gene transfection .....	48
1. Plasmid map of cDNA construct for human Nav1.5 .....	48

2. Plasmid map of cDNA construct for N <sub>2</sub> -EGFP .....	48
3. Transient transfection of HEK293 cells .....	51
4. Transfection of neonatal rat cardiomyocytes .....	53
I. Chemicals .....	54
J. Solutions .....	55
1. Preparation of lidocaine hydrochloride stock solution .....	55
2. Preparation of tetrodotoxin stock solution .....	55
3. Standard extracellular bathing solution for voltage clamp recordings from HEK293 cells .....	55
4. Standard intracellular pipette solution for voltage clamp recordings from HEK293 cells .....	56
5. Standard extracellular bathing solution for I <sub>Na</sub> recordings from neonatal rat cardiomyocytes .....	56
6. Standard intracellular pipette solution for I <sub>Na</sub> recordings from neonatal rat cardiomyocytes .....	56
7. Standard extracellular solution for action potential recordings from neonatal rat cardiomyocytes .....	57
8. Standard intracellular pipette solution for action potential recordings from neonatal rat cardiomyocytes .....	57
K. Whole cell patch-clamp recordings on HEK293 cells .....	58
L. Whole cell patch-clamp recordings from neonatal rat cardiomyocytes .....	58

M. Cysteine, lysine and arginine specific cell surface biotinylation assay .....	61
N. Preparation of cell lysate .....	62
O. Protein concentration measurement .....	63
P. SDS-polyacrylamide gel electrophoresis of protein and transfer .....	63
Q. Western immunoblotting analysis .....	64
R. Data analysis .....	65
<b>III. RESULTS</b> .....	<b>67</b>
A. Deletion of F1486 within the intracellular loop between DIII-DIV of hNav1.5 reduces peak current density in HEK293 cells and neonatal rat cardiomyocytes .....	67
B. Deletion of F1486 decreases sodium channel surface expression in HEK293 cells .....	74
C. Deletion of F1486 augments late sodium current (late $I_{Na}$ ) in HEK293 cells and neonatal rat cardiomyocytes .....	76
D. F1486del does not alter voltage dependence of activation in both HEK293 cells and neonatal rat cardiomyocytes .....	81
E. F1486del does not alter the time constants for channel deactivation in HEK293 cells .....	88
F. Multiple biophysical consequences of the F1486del may lead to delayed repolarization and APD prolongation .....	90

G. F1486del leads to the increased time constants for recovery from inactivation .....	97
H. F1486del produces augmented ramp current in both HEK293 cells and neonatal rat cardiomyocytes .....	98
I. F1486del on hNav.15 prolongs APD and generates EADs in neonatal rat cardiomyocytes .....	104
J. F1486del attenuates the response to antiarrhythmic drug lidocaine in HEK293 cells .....	109

## **SUPPLEMENTAL RESULTS**

K. Sodium channel mutation G1481E within the intracellular loop between DIII-DIV of hNav1.5 increases peak current density in HEK293 cells .....	116
L. G1481E mutation causes a leftward shift of the steady-state activation curve in HEK293 cells .....	119
M. The G1481E mutation does not affect sodium channel steady-state fast inactivation .....	121
N. Sodium channel G1481E mutation does not affect late $I_{Na}$ .....	123
O. The G1481E mutation enhances window current .....	125
P. The G1481E mutation does not affect the slow inactivation .....	127
<b>IV. DISCUSSION</b> .....	130
A. Overview of the dissertation research .....	130
B. Voltage-clamp studies on the F1486del channel .....	131

C. Therapeutic outcomes of lidocaine on F1486del channels .....	133
D. Current-clamp studies on neonatal cardiomyocytes ectopically expressing recombinant F1486del channels .....	134
E. Trafficking and cellular localization of voltage-gated F1486del sodium channels .....	135
F. Summary and conclusions .....	138
G. Discussion on supplemental results: G1481E mutation increases window current and may lead to LQT3 in patients .....	141
<b>V. REFERENCE LIST .....</b>	<b>142</b>

**CURRICULUM VITAE**

## LIST OF TABLES

Table 1. Summary of LQTs .....	30
Table 2. Primers used for generating hNav1.5 mutant cDNA constructs .....	43
Table 3. Primers used in full-length sequence analysis of sodium channel .....	44
Table 4. Chemical reagents and drugs used in the study .....	54
Table 5. Voltage-dependent gating parameters for WT and F1486del mutant Na <sup>+</sup> channels in HEK293 cells .....	86
Table 6. Voltage-dependent gating parameters for WT and F1486del channels expressed in cardiomyocytes .....	87
Table 7. Summary of IC <sub>50</sub> values estimated for lidocaine inhibition of hNav1.5 channels in different states .....	115

## LIST OF FIGURES

Figure 1. Illustration of four gigaseal recording methods .....	6
Figure 2. Schematic representation of the linear structure of voltage-gated sodium channels (VGSCs) .....	13
Figure 3. Schematic representation of three-dimensional arrangement of sodium channel $\alpha$ subunit .....	14
Figure 4. Electrical and chemical gradients for sodium and potassium channel in the resting state .....	22
Figure 5. Action potential and its relationship with the ECG study .....	23
Figure 6. Schematic representation and sequence alignment of <i>Homo Sapiens</i> VGSCs .....	38
Figure 7. Plasmid map of pcDNA3.1 (+) carrying the gene of <i>Homo Sapiens</i> full-length <i>SCN5A</i> encoding hNav1.5 .....	49
Figure 8. Plasmid map of cDNA construct for N <sub>2</sub> -EGFP .....	50
Figure 9. Illustration of the cDNA sequences coding for recombinant sodium channels that are highly resistant to tetrodotoxin (TTX) .....	60
Figure 10. F1486del within the intracellular loop between DIII-DIV of hNav1.5 reduced peak current density in HEK293 cells .....	69
Figure 11. Endogenous sodium currents in neonatal cardiomyocytes were blocked by TTX at a final concentration of 20 $\mu$ M .....	71

Figure 12. F1486del results in decrease in membrane current density in neonatal rat cardiomyocytes .....	72
Figure 13. Deletion of F1486 decreases sodium channel surface expression in HEK293 cells .....	75
Figure 14. F1486del augments late $I_{Na}$ in HEK293 cells .....	78
Figure 15. F1486del augments late $I_{Na}$ in neonatal rat cardiomyocytes .....	80
Figure 16. F1486del does not affect the voltage dependence of $Na^+$ channel activation in HEK293 cells .....	83
Figure 17. F1486del does not affect the voltage dependence of $Na^+$ channel activation in neonatal rat cardiomyocytes .....	85
Figure 18. F1486del does not alter the time constants of channel deactivation in HEK293 cells .....	89
Figure 19. F1486del causes a depolarizing shift in the voltage dependence of inactivation in HEK293 cells .....	92
Figure 20. F1486del increases window sodium current in HEK293 cells .....	93
Figure 21. F1486del causes a depolarizing shift in the voltage dependence of inactivation in neonatal rat cardiomyocytes .....	94
Figure 22. F1486del causes an augmentation of window sodium current in neonatal rat cardiomyocytes .....	95
Figure 23. F1486del increases ramp current in HEK293 cells .....	100

Figure 24. F1486del causes an augmentation of ramp current in neonatal rat cardiomyocytes .....	102
Figure 25. hNav1.5 F1486del prolongs APD in neonatal rat cardiomyocytes .....	106
Figure 26. Cardiomyocytes expressing F1486del mutant channels presented with spontaneous EADs .....	108
Figure 27. Dose-response curve for the inhibitory effect of lidocaine on hNav1.5 WT and F1486del channels in the resting state .....	111
Figure 28. Deletion of F1486 attenuates the effect of 100 $\mu$ M lidocaine on sodium channels in the resting state .....	112
Figure 29. Dose-response curve for the inhibitory effect of lidocaine on inactivated hNav1.5 channels .....	113
Figure 30. F1486del reduces the effect of lidocaine on sodium channels in the inactivated state .....	114
Figure 31. Sodium channel mutation G1481E within the intracellular loop between DIII-DIV of hNav1.5 increases peak current density in HEK293 cells .....	118
Figure 32. G1481E mutation causes a leftward shift of the steady-state activation in HEK293 cells .....	120
Figure 33. G1481E mutation does not affect sodium channel steady-state fast inactivation in HEK293 cells .....	122
Figure 34. G1481E mutation does not affect late $I_{Na}$ .....	124

Figure 35. The G1481E mutation increases sodium  
channel window current in HEK293 cells ..... 126

Figure 36. G1481E mutation does not affect the slow inactivation ..... 129

## LIST OF ABBREVIATIONS

ANOVA	Analysis of Variance
AP	Action Potential
APD	Action Potential Duration
Ca <sup>2+</sup>	Calcium Ion
cDNA	Complementary DNA
CsOH	Cesium Hydroxide
DMEM	Dulbecco's Modified Eagle Medium
EADs	Early Afterdepolarizations
ECG	Electrocardiogram
EGFP	Enhanced Green Fluorescence Protein
EGTA	Ethylene Glycol Tetraacetic Acid
E <sub>Na</sub>	Reversal Potential of Sodium Channel
E <sub>K</sub>	Reversal Potential of Potassium Channel
ER	Endoplasmic Reticulum
FBS	Fetal Bovine Serum
HBSS	Hanks' Balanced Salt Solution
HEK293	Human Embryonic Kidney 293 Cell
HERG	The Human Ether-a-go-go Related Gene
hH1	Human heart sodium channel
IFM	Isoleucine, Phenylalanine, and Methionine
I <sub>Na</sub>	Sodium Current

K <sup>+</sup>	Potassium Ion
LQTS	Long-QT Syndrome
LQT3	Long-QT Syndrome Type 3
Met (M)	Methionine
Na <sup>+</sup>	Sodium Ion
Nav	Voltage-Gated Sodium Channel
Nav1.5	Voltage-Gated Sodium Channel 1.5
NaCl	Sodium Chloride
NaOH	Sodium Hydroxide
Phe (F)	Phenylalanine
PVDF	Polyvinylidene Fluoride
QTc	Corrected QT Interval
S1-S6	Interdomain Segments of the Voltage-Gated Sodium Channel
S.E.M	Standard Error of the Mean
SIDS	Sudden Infant Death Syndrome
STX	Saxitotxin
TdP	Torsade de Pointes
TTX	Tetrodotoxin
TTX-r	Tetrodotoxin Resistant
TTX-s	Tetrodotoxin Sensitive
V <sub>1/2</sub>	Voltage at Which Channel Is Half Activated or Inactivated

VGSCs	Voltage-Gated Sodium Channels
V <sub>m</sub>	Membrane Potential or Membrane Voltage
VT	Ventricular Tachycardia
WT	Wild Type

## I. INTRODUCTION

### A. Overview of the thesis Project

Inherited long-QT syndrome (LQTS) is an infrequent but serious medical problem of the heart's rhythm. It usually affects children and young adults. Patients with LQTS who have symptoms often exhibit syncope and cardiac arrhythmia, which potentially could cause sudden death. Genetic mutation of the gene *SCN5A* encoding human voltage-gated cardiac sodium channel hNav1.5 can put patients at risk of type 3 LQT syndrome (LQT3), a type of cardiac arrhythmia that is typically associated with a gain-of-function mutation in the cardiac sodium channel.

Nav1.5 is the predominant form of sodium channel that expresses in the heart. Over the last twenty years, numerous studies have investigated the role of Nav1.5 channels in cardiac arrhythmia, especially LQT3. The vast majority of studies have focused on the biophysical properties of Nav1.5 sodium channel carrying specific polymorphisms associated with LQT3. There is overwhelming evidence suggesting that LQT3 might be predominantly caused by sodium channel gain-of-function mutations. Although the potential outcome of this disease can be lethal, it is a treatable disease. In general, there are treatments for LQTS, including medications such as  $\beta$  blockers that block sodium current in a manner similar to the blocking by local anesthetics (Bankston & Kass, 2010). Sometimes, a surgical procedure can be performed, and some patients may benefit from an implantable defibrillator. Treatment for LQT3 includes therapeutic

drugs such as Mexiletine, a sodium channel blocker, which is predicted to be especially effective when other drugs fail. As a long-term goal, it is of importance to reveal effective drugs for specific sodium channel mutations, which is now called “mutation/gene-specific approach” (An *et al.*, 1998; Benhorin *et al.*, 2000) .

Previous studies on the neuronal sodium channel Nav1.2 indicated that the intracellular loop III between transmembrane domain III and IV is critical for sodium channel fast inactivation (West *et al.*, 1992). Using a mutagenesis approach, West *et al.* have demonstrated the essential role of a three amino acid residue cluster IFM in channel fast inactivation. Nonetheless, these works on the electrophysiology properties of the sodium channels were carried out mostly using the heterologous expression systems such as Chinese Hamster Ovary cells and *Xenopus* oocytes. In addition, it is not clear whether these amino acids work in the cardiac sodium channel Nav1.5 through the same mechanism.

This thesis is mainly focused on the biophysical and pharmacological properties of the human cardiac sodium channel Nav1.5 carrying the phenylalanine (Phe, F) deletion at amino acid F1486, an intriguing site that is believed to be critical for channel inactivation (West *et al.*, 1992). Based on the data collected from both HEK293 cells and primary cultured neonatal rat cardiomyocytes, this thesis provides strong evidence indicating that the F1486del disrupts sodium channel inactivation and increases late sodium current. Like other LQT3-associated mutations, the F1486del leads to a series of sodium channel gain-of-function alterations. Surprisingly, F486del causes decreased current density in both cell types, indicating a loss-of-function alteration. Action

potential duration prolongation and the prominent early afterdepolarizations were observed in cultured ventricular cardiomyocytes, which underline the mechanism of long-QT syndrome and the subsequent ventricular tachycardia in the newborn patient. More importantly, this thesis revealed the mechanism for the refractory response of the patient to antiarrhythmic drug lidocaine. This particular finding provides strong evidence supporting the idea that certain mutations can alter the channel's response to antiarrhythmic drugs. Thus, it is of great importance to identify the effective drugs that can be used for mutation specific individualized therapy in the future.

## **B. Basic methodology used in studying the function of VGSCs:**

### **patch-clamp techniques**

So far, the most direct way of investigating ion channel function is to record the current that flows through the channel across the cell membrane, or, to measure the membrane potential changes that the current produces. The profound advance in electrophysiology came with the development of patch-clamp methods. This technique was invented by Erwin Neher and Bert Sakmann, who were awarded with the Nobel Prize in "Physiology or Medicine" in 1991 for their discoveries concerning the function of single ion channels in cells. In 1976, Neher and Sakmann first tried to record current from a tiny area of cell surface membrane (so called "patch") by pressing a heat-polished pipette against a living cell. The first evidence of the success of this technique was published in the paper by Neher and Sakmann in 1976 (Neher & Sakmann, 1976). In 1981, another breakthrough was made by them when the clean glass pipette can fuse

to the cell membrane to form a seal resistance called gigaseal ( $10^9$ ) in comparison with the conventional seal level of mega ohm. The high resistance of this seal ensures that most of the currents originating in a small patch of membrane flow into the pipette, and from there into the current-measurement circuitry. The level of seal resistance is critical also because it determines the level of background noise in recordings.

Four recording configurations can be formed based on the high seal resistance (Figure 1): 1) On-cell or cell-attached mode: this configuration can be achieved as soon as the pipette is sealed to the cell membrane with a high level of resistance of gigaseal. Under this recording mode, single channel recordings can be obtained. 2) Inside-out or excised-patch mode: this configuration is achieved by getting a stable high seal resistance first, and then pulling off the cell that is still tightly sealed to the pipette. By bathing the pulled-off part in the bathing solution, the functional changes can be studied specifically in the inside part (intracellular cytosolic side) of the cell membrane (ion channels) by replacing the component in the bathing solution. 3) Whole-cell configuration: this mode is achieved by deliberately rupturing the on-cell patch by gentle suction without disrupting the seal. After the whole-cell configuration is made, the pipette solution will diffuse into the cell cytoplasm and the composition of these two solutions will exchange and finally reach equilibrium within a few minutes. Typically, the functions of ion channels have been studied using this configuration. Since the pipette solution exchanges molecules with the cytoplasmic component under the whole-cell configuration, this configuration has become a useful tool to deliver

metabolites, inhibitors of signal transduction pathways, or fluorescent dyes during the recordings. 4) Out-side out patch mode: this configuration is formed by pulling the pipette away from the cell in whole-cell mode making the cytoplasmic face of the outer membrane of the cell being exposed to the pipette solution, and its extracellular face to the bath solution. By varying the composition of the bath solution, the effect of drug or ion concentration changes on currents can be investigated at either the cytoplasmic or the extracellular face of the membrane.

In my thesis work, all of the sodium channel recordings were made using whole-cell configuration.

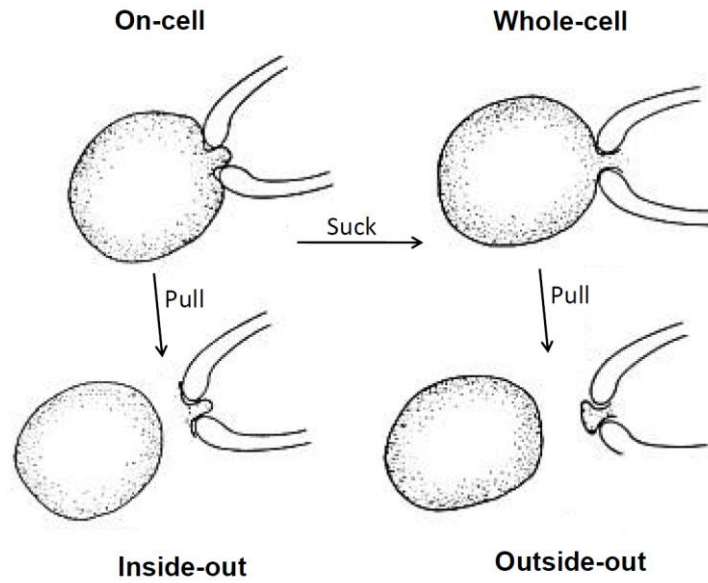


**Figure 1. Illustration of four gigaseal recording methods.** This figure was modified from Hamill *et al*, 1981; Pflügers Arch 391, 85-100 and Hille B, 1992 Sinauer Associates Inc.. The cell configuration used in this thesis work is solely whole-cell configuration.

### **C. Background information of VGSCs: research history, structure, function, and modulation**

Sodium channels are integral membrane proteins. In general, sodium channel can be classified into two categories: one category is the sodium channels that are not voltage-gated; the epithelial sodium channel (EnaC)/degenerin (DEG) gene family that mediate sodium transport in epithelial and other cell types (Palmer & Frindt, 1986; Roudier-Pujol *et al.*, 1996; Kellenberger & Schild, 2002). The other is voltage-gated sodium channels (VGSCs), with the characteristic of altering the gating kinetics in response to the membrane voltage changes. The epithelial sodium channel is structurally unrelated to the voltage-gated sodium channel. In the following context, the term “sodium channel” will be solely used to refer to the “voltage-gated sodium channel”.

As the first member of the ion channel super family that has been discovered, the function of sodium channel was discovered by Hodgkin and Huxley in 1952. The other member that was very first uncovered in the early years was the potassium channel. Voltage-gated  $\text{Ca}^{2+}$  channel was recognized almost a decade later. Using squid axons, Hodgkin and Huxley observed transient inward and sustained outward currents that they believe to carry enough charges to contribute to the rapid rise and fall of the action potential. With the help of the early stage voltage-clamp technique, Hodgkin and Huxley advanced the conceptual knowledge of ionic currents. They identified two major components of the membrane current:  $I_{\text{Na}}$  and  $I_{\text{K}}$  (Hodgkin & Huxley, 1952a;

Hodgkin, 1958; Hille, 2001). By replacing the external solution with choline chloride, Hodgkin and Huxley confirmed the early transient component in the ionic current as the  $I_{Na}$ , since removal of the external  $Na^+$  could completely abolish this current (Hille, 2001). Several years after Hodgkin and Huxley's work, the formal terminology emerges for the axon ion channel description: "sodium channels" which have a positive reversal potential,  $E_{Na}$ , and "potassium channels" with a negative reversal potential  $E_K$  (Hille, 2001).

The identification of sodium channel proteins began as radioactive tetrodotoxin (TTX) and saxitoxin (STX) became available (Henderson & Wang, 1972). Using electric eel organs, the size of the protein that can bind to the radioactive TTX and STX was revealed to be around 230 kDa (Levinson & Ellory, 1973). It was predicted that this protein should also contain an additional 30% by weight of covalently attached sugar chains and 6% fatty acids (Agnew *et al.*, 1978; Miller & Robyt, 1983; Levinson *et al.*, 1990). With the evolution of the protein chemistry and molecular biology techniques, we now know the complete amino acid sequence of the voltage-gated sodium channels. In addition, we now know that sodium channels display developmental and tissue specific expression (Mandel, 1992; Black & Waxman, 1996; Goldin, 2001; Dominguez *et al.*, 2008; Chopra *et al.*, 2010). We also know that the sodium channel  $\alpha$  subunit has a molecular weight of about 260 kD. The high molecular weight is caused by glycosylation (Schmidt & Catterall, 1986, 1987). So far, we know not only the amino acid sequences that form the aqueous conduction pore, but also the

details about the gating charges that contribute to the voltage sensitivity of the sodium channel.

Sodium channel consists of a pore-forming  $\alpha$  subunit and one or more modulatory auxiliary  $\beta$  subunits (Figure 2). The  $\alpha$  subunit is composed of four structurally homologous domains (Sato *et al.*, 1998), namely DI (domain I) to DIV (domain IV). Each domain contains six transmembrane segments (S1-S6). The extracellular linker region between each segment 5 and 6 joins together forming the channel pore referred to as “P loop” or “P segment”, which controls ion selectivity and permeation (Figure 2, 3). This loop exhibits a high degree of conservation among the various tissue and organ-specific isoforms across species, and determines ion selectivity and conductance properties of the channel. In each domain, the P loop exerts a unique contribution towards the ion selectivity, ion and toxin binding properties and permeation properties of the sodium channel. The pore contains the selectivity filter which is referred to as the DEKA ring. The DEKA ring is composed by amino acids of aspartic acid (D), glutamate (E), lysine (K), alanine (A). It was found that the DEKA ring contains one of these amino acids in each P-loop. It was found that the DEKA ring attracts positive  $\text{Na}^+$  ions and repels negatively charged ions (Backx *et al.*, 1992). Importantly, the P loops in DIII and DIV play an important role in sodium ion selectivity. Using mutagenesis techniques, a lysine residue in the P loop of DIII (K1418 in Nav1.5) was demonstrated to be critical for discrimination for  $\text{Na}^+$  over the divalent charged ion  $\text{Ca}^{2+}$  (Heinemann *et al.*, 1992; Perez-Garcia *et al.*, 1997). In other studies using the same technique, the tetrad WDGL in DIV of the human

cardiac sodium channel Nav1.5 (residues 1713 to 1716) were demonstrated to affect the selectivity among monovalent cations (Chiamvimonvat *et al.*, 1996). Positively charged residues at every third position (with mostly nonpolar residues intervening between the basics residues) on S4 segments act as voltage sensors, which can lead to the fast activation (opening) of the sodium channel when the membrane potential is depolarized. Stuhmer *et al.* performed site-directed mutagenesis to identify the functional regions on S4 of the sodium channel (Stuhmer *et al.*, 1989). To test the proposed role of S4 as a voltage sensor, they introduced point mutations into the S4 region so that positively charged amino acid residues are replaced by either negatively or neutral charged residues. They saw a decrease in the steepness of the voltage dependence of activation due to the reduction of the net positive charge. Their studies provide experimental evidence for the direct involvement of the positive charged residues in this segment in the voltage sensing process for activation.

After the channel is activated, for a period of time varying from milliseconds to a few seconds, the channel is unable to open again due to the channel gating process called “inactivation”. Inactivation is the process that terminates the current (Hodgkin & Huxley, 1952a). There are two types of inactivation: one is fast steady-state inactivation, which happens for a period of milliseconds. The other type of inactivation is the so-called “slow inactivation”, which was comes into play when the channel is depolarized for hundreds of milliseconds. The slow inactivation can be sustained for a few seconds.

With the development of the molecular biology and advanced biochemistry techniques, we now know that certain regions of the sodium channel are responsible for channel fast inactivation. These regions are: the IFM motif with three hydrophobic amino acids Ile-Phe-Met (West *et al.*, 1992) in the segment between transmembrane domain III and IV (DIII, DIV), the intracellular linker between S4 and S5 of DIII and DIV, the P loop, and the C-terminal domain of the sodium channel (Glaaser *et al.*, 2006).

Studies for identifying the intracellular cytosolic loop as the structure that is responsible for inactivation include: 1) Realization of the inactivation as a process that can terminate the transient inward Na<sup>+</sup> current (Hodgkin & Huxley, 1952a). 2) Perfusion of the intracellular surface of the sodium channel with proteolytic enzyme prevents inactivation, which implicates the requirement of an intracellular structure in the inactivation process (Armstrong, 1981). 3) Antibodies targeted at the intracellular linker between homologous domain III and domain IV completely blocked the fast inactivation of affected single sodium channel (Vassilev *et al.*, 1988; Vassilev *et al.*, 1989). 4) Expression of the sodium channel as two single individual polypeptides with a cut between domain III and domain IV causes an ~20 fold delay of channel inactivation (Stuhmer *et al.*, 1989). 5) Small insertion of the amino acids within the intracellular loop III between domain III and IV also slows inactivation (Patton & Goldin, 1991). 6) Post translation modification of the serine residue through phosphorylation by protein kinase C slows inactivation (West *et al.*, 1991). 7) Deletion of a segment containing 10 amino acids within the intracellular loop III completely blocks fast inactivation

(Patton *et al.*, 1992). The above mentioned studies support the hypothesis that loop III between DIII and DIV plays an integral role in the inactivation of the Na<sup>+</sup> channel.

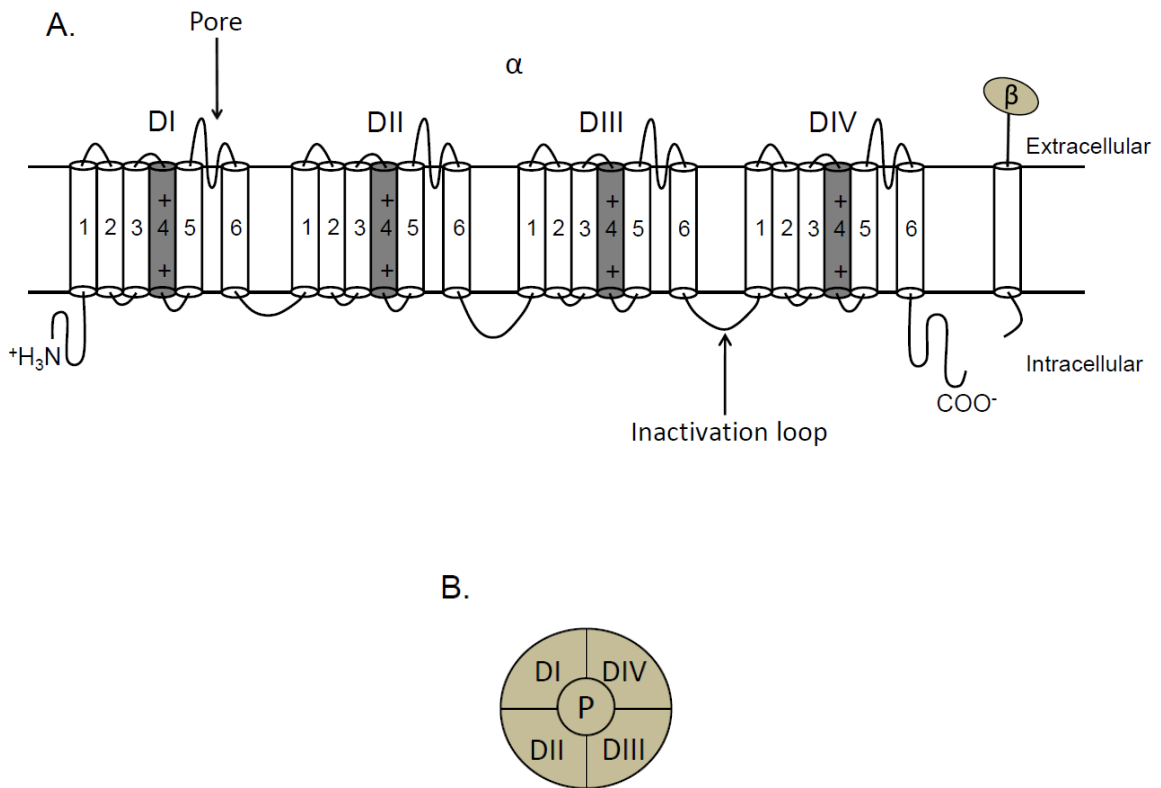


**Figure 2. Schematic representation of the linear structure of voltage-gated sodium channels (VGSCs).** A. The linear schematic structure of voltage-gated sodium channel  $\alpha$  subunit. The  $\alpha$  subunit of the voltage-gated sodium channel is a membrane integrated protein, which consists of four transmembrane domains. Each domain contains six transmembrane segments (S1-S6), a pore-forming region between S5-S6, and a voltage sensor (S4). The  $\alpha$  subunit can assemble with one or more auxiliary  $\beta$  subunits namely  $\beta_1$ - $\beta_4$ . The inactivation gate is located on the intracellular loop between transmembrane domain III and IV. B. Indicates four of the subunit fold together to form a functional voltage-gated sodium channel. "P" represents channel pore region. Panel A and B are modified from the review paper written by Yu and Catterall (Yu & Catterall, 2003).

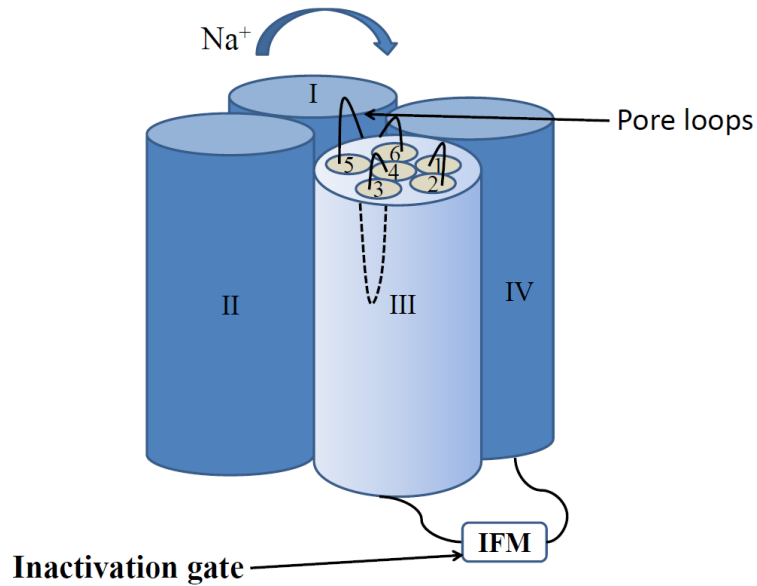


**Figure 3. Schematic representation of three-dimensional arrangement of sodium channel  $\alpha$  subunit.** Four homologous domains (I - IV) are fold together and each domain contains six hydrophobic transmembrane  $\alpha$  helices segments (S1-S6). This model was first hypothesized and confirmed by Sato and his colleagues (Sato *et al.*, 2001). Within each domain, the S5 and S6 are positioned adjacent to the central pore region of the channel. Extracellular linker between S5 and S6 in each domain forms the P-loop. S1-S3 forms the outer edge of the complex and S4 is positioned in the center of the six segments. Putative IFM motif with intracellular linker connecting transmembrane domain III (DIII) and domain IV (DIV) forms the inactivation gate.

#### **D. Introduction and the characteristics of cardiac sodium channel Nav1.5 $\alpha$ subunit: tissue distribution, TTX sensitivity and other properties**

Voltage-gated sodium channel family contains at least nine members, and each of them is responsible for action potential initiation and propagation. The human cardiac voltage-gated sodium channel is a member of the voltage-dependent sodium channels. The major cardiac sodium channel in the heart is Nav1.5 (Yu & Catterall, 2003). Cardiomyocytes also express the neuronal Nav channel isoforms, such as Nav1.1, Nav1.3, and 1.6, but the location of these channels are solely on the T-tubules (Maier *et al.*, 2004). The Nav1.5 isoform was found at high levels in adult rat heart (Rogart *et al.*, 1989). Although Nav1.5 was found in the heart tissue, it is not detectable in adult skeletal muscle. However, Nav1.5 isoform is detectable in embryonic, neonatal skeletal muscle and denervated skeletal muscle (Kallen *et al.*, 1990). Like other types of voltage-gated sodium channels, these channels contain a principle  $\alpha$  subunit and one or more auxiliary  $\beta$  subunits. The  $\alpha$  subunit is the pore forming subunit, and it can form a functional channel when it is expressed alone in the expression system. When expressed, this large  $\alpha$  subunit accounts for the defining properties of the voltage-gated sodium channels. It contains characteristic toxin-binding sites, pore, gates, and a voltage sensor. The  $\alpha$  subunit is encoded by the *SCN5A* gene. Most mutations that affect the cardiac sodium channel are located on this gene. The functions of the auxiliary  $\beta$  subunits are discussed later.

The tissue distribution of the cardiac sodium channel was demonstrated by both immunohistochemistry and RT-PCR experiments. It was found that these

channels are localized not only on the cardiomyocyte surface, but also on the surface of T-tubules. Later on, it was also demonstrated that the cardiac sodium channel also exists at the terminal of the intercalated disc (Cohen, 1996; Maier *et al.*, 2004). As specialized membrane domains, intercalated discs separate adjacent cells and contain gap junctions that are responsible for propagating the cardiac action potential. The specialized distribution of Nav1.5 as compared to the neuronal forms of sodium channel in the heart suggest that it may be crucial for action potential initiation while the action potential jumps from one cell to the other within the fibers. However, the distribution of the neuronal forms of sodium channels within the heart suggests that they are responsible for conducting the action potential into the inside of the cell to activate the contractile machinery (Cusdin *et al.*, 2008).

One of the characteristics of the cardiac sodium channel Nav1.5 is lacking the sensitivity to a toxin called tetrodotoxin (named by K.S. Cole as “TTX”), a paralytic poison from puffer fish such as fugu. The low sensitivity to TTX makes the cardiac sodium channel Nav1.5 different from the neuronal and skeletal muscle isoforms (Leffler *et al.*, 2005). For those sodium channels that are TTX sensitive, their currents can be blocked by nanomolar concentrations of TTX (Leffler *et al.*, 2005). The identity of a single amino acid residue in the P loop within domain I (DI) determines the differential sensitivities to TTX. It is tyrosine 401 in Nav1.4, serine 356 in Nav1.8 and serine 355 in Nav1.9 that determines the channel’s sensitivity to TTX. TTX sensitive sodium channels carry aromatic residues (Phe, or Tyr) at extracellular pore openings. The presence of a

hydrophilic cysteine residue at amino acid 374 instead of an aromatic residue within the cardiac Nav1.5 channel renders the channel relatively resistant to TTX (Satin *et al.*, 1992a; Leffler *et al.*, 2005), such that the current can be blocked only by applying micromolar concentrations of TTX.

The electrophysiological properties of Nav1.5 are generally similar to those of the CNS channels, but there are some important differences. The membrane potential at which Nav1.5 inactivates is more negative than that of other isoforms of sodium channels such as the CNS isoforms (16 mV more negative compared to Nav1.2) when the  $\alpha$  subunit is expressed alone in *Xenopus* oocytes (Mantegazza *et al.*, 2001). Nav1.5 inactivates more slowly than other isoforms such as Nav1.2 (White *et al.*, 1991; Satin *et al.*, 1992b; Mantegazza *et al.*, 2001).

#### **E. Introduction of sodium channel $\beta$ subunits**

There are four sodium channel  $\beta$  subunits ( $\beta_1$  to  $\beta_4$ ) that have been identified so far. These four subunits can be divided into two groups. One group contains  $\beta_1$  (encoded by *SCN1B*, localized in brain neuronal tissues, skeletal muscle and cardiac tissue (Makita *et al.*, 1994)), and  $\beta_3$  (encoded by *SCN3B*, localized primarily in neuronal tissue (Morgan *et al.*, 2000).  $\beta_3$  has been detected in the heart (Morgan *et al.*, 2000; Dhar Malhotra *et al.*, 2001; Fahmi *et al.*, 2001).  $\beta_1$  and  $\beta_3$  are very similar in amino acid sequence and they are classified as noncovalently linked with  $\alpha$  subunits (Isom *et al.*, 1992; Morgan *et al.*, 2000). Studies indicates that the  $\beta_1$  subunit interacts with DI and DIV of the  $\alpha$  subunit (Makita *et al.*, 1996). Co-expression of  $\beta_1$  subunit with  $\alpha$  subunit modulates

channel gating kinetics. It has been shown that co-expression of the  $\beta_1$  subunit with the neuronal or skeletal muscle  $\alpha$  subunit in *Xenopus* oocytes increases the cell surface channel expression. Further, channel inactivation and activation rates were both altered. Channel inactivation curve was shifted to more negative potentials when  $\beta_1$  subunit was co-expressed with the cardiac sodium channel  $\alpha$  subunit (Makita *et al.*, 1994; Nuss *et al.*, 1995). Lori Isom's group studied the expression of  $\alpha$  and  $\beta$  subunits in heart tissue, and identified Nav1.1  $\alpha$  subunit, Nav1.5  $\alpha$  subunit,  $\beta_1$ , and  $\beta_2$ . The developmental time course of  $\beta_2$  subunit expression suggests that it is at detectable levels from postnatal day 15. Both Nav1.5 and Nav1.1 were shown to be co-expressed with  $\beta_1$  and  $\beta_2$  subunits (Dhar Malhotra *et al.*, 2001). In cardiomyocytes, it was shown that although the  $\alpha$  subunit associates with both  $\beta_1$  and  $\beta_2$  subunits, only the  $\beta_1$  subunit has a modulatory effect on the electrophysiological properties of Nav1.5. The  $\beta_2$  subunit seemingly has no detectable effects on electrophysiological properties of cardiac sodium channels, suggesting that the effects of  $\beta_2$  in heart *in vivo* may involve cell adhesion and cytoskeletal communication instead of directly modulating channel gating (Dhar Malhotra *et al.*, 2001). Based on the above mentioned expression and functional patterns, the  $\alpha$  subunit was solely coexpressed with  $\beta_1$  subunit in my thesis work.

## **F. Action potential and its correlation with ECG study**

Ions and currents move across cell membranes in response to electrical and concentration gradients through several specific ion channels or transporters. In a normal situation, the cardiomyocyte maintains a resting membrane potential

of -80 mV to -90 mV, which is relatively negative in comparison to the exterior membrane. This gradient is maintained by the pumps such as Na<sup>+</sup>-K<sup>+</sup>-ATPase as well as fixed anionic charges in the cells (Goodman *et al.*, 2001). Although there are both electrical and chemical gradient for sodium ions, the sodium channels are voltage-gated and are closed at the negative resting membrane potentials. Therefore, Na<sup>+</sup> does not enter cardiomyocytes under resting potentials (Figure 4). However, specific types of potassium channels such as the inward rectifier potassium channels are open under negative resting membrane potentials and can allow K<sup>+</sup> to move across the cell membrane in response to electrical and chemical gradients.

When the cardiomyocyte is depolarized above a voltage threshold, the sodium channel will change its conformation from a closed resting state to an open activated conducting state. Thus, about 10<sup>7</sup> Na<sup>+</sup> ions can enter the cell per second (Goodman *et al.*, 2001). The activation of a sodium channel can only last for a few milliseconds (Ulbricht, 2005). The opening and activation of the sodium channel will lead to the depolarization phase of an action potential (called “0” phase of the action potential). The inward current generated by the inward sodium current can, in turn, cause a series of openings and inactivations of some other types of channels, such as transient outward potassium channels (4-AP sensitive transient outward K<sup>+</sup> current I<sub>to1</sub>, and Ca<sup>2+</sup>-activated Cl<sup>-</sup> current I<sub>to2</sub>) (Kenyon & Gibbons, 1979; Kenyon & Sutko, 1987), L-type and T-type calcium channels, delayed rectifier potassium channel (I<sub>Ks</sub>, I<sub>Kr</sub>, and I<sub>Kur</sub>), inward rectifier potassium channel I<sub>K1</sub> (Deal *et al.*, 1996). The above mentioned channels

constitute the repolarization phase of the action potential (phase 1 to 3 of cardiac cells). Figure 5 summarizes the relationship of ECG and the human cardiac action potential. The P wave of the electrocardiograph represents the depolarization that spreads from the sinus atrial node throughout the atria. It has a duration of 0.08-0.10 seconds (80-100 ms). The QRS complex represents ventricular depolarization. The duration of the QRS complex is usually 60 ms to 100 ms, a short period indicating that the ventricular depolarization occurs rapidly. Following the QRS complex, there is an isoelectric period, which is called “the ST segment”. The ST segment indicates the time at which the entire ventricle is depolarized and is roughly correlated to the action potential plateau phase. The T wave represents the repolarization phase of the ventricular action potential, and its duration is usually longer than the depolarization phase. In summary, the QT interval represents the time for both ventricular depolarization and repolarization. Altogether, the QT interval can be used as a parameter to estimate the duration of an average ventricular action potential, and there is a negative correlation between these two parameters. Depending on the heart rate, the QT interval can vary from 200 ms to 400 ms. In reality, physicians use the “corrected QT interval” (QTc) to assess the QT interval (Jackman *et al.*, 1988). The QTc interval is calculated by measuring QT interval and dividing it by the square root of the R-R interval (an interval between ventricular depolarization) using the “Bazett’s formula”, which was named after physiologist Henry Cuthbert Bazett. QTc is used to calculate the heart rate-correlated QT interval more accurately (Funck-Brentano & Jaillon, 1993). QTc is usually less than 440 ms, and the long-QTs

patient have a QTc interval of  $> 440$  ms (a standard originated by Peter Schwartz)  
(Schwartz, 1985).

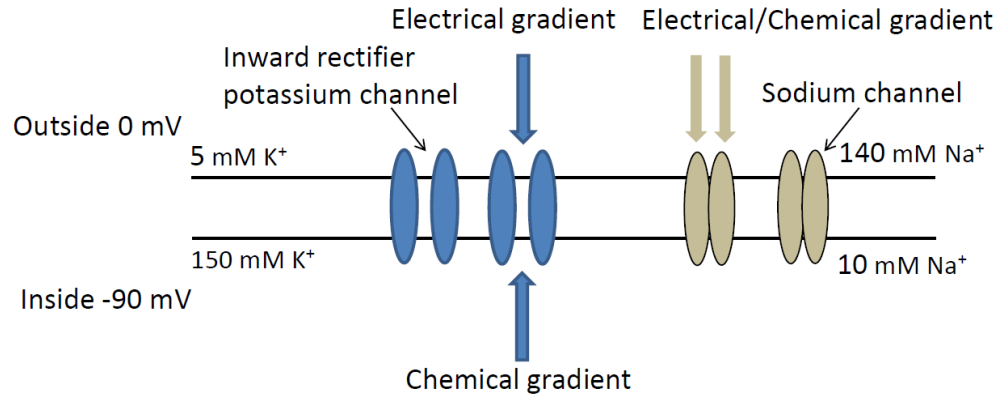


**Figure 4. Electrical and chemical gradients for sodium and potassium channel in the resting state.** In the resting state, sodium channels do not open, and  $\text{Na}^+$  does not enter the cell. In contrast, inward rectifier potassium channels are open, allowing the  $\text{K}^+$  ion moves across the membrane until the membrane potential reaches the potential that is close to the equilibrium potential for  $\text{K}^+$  ( $E_K$ ). Note: This figure is adapted from “Goodman and Gilman’s the Pharmacological basis of therapeutics” (Goodman *et al.*, 2001).

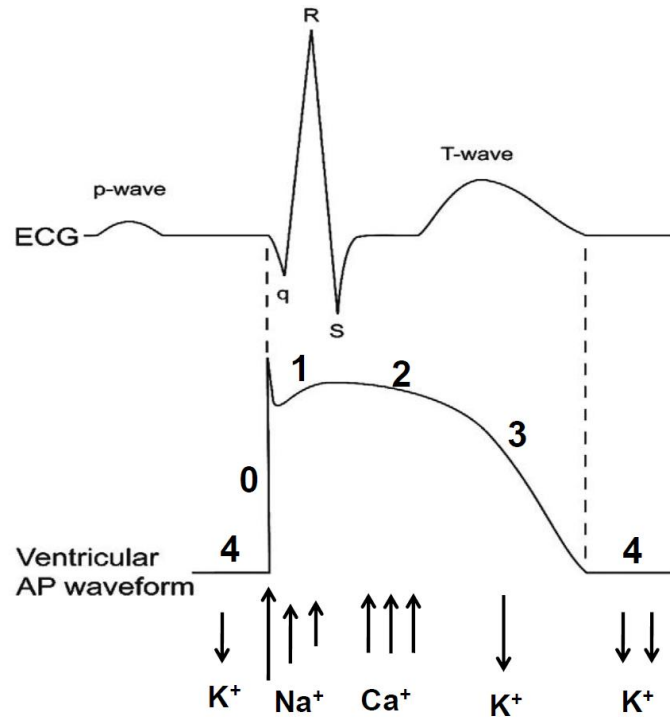


**Figure 5. Action potential and its relationship with the ECG study.** This figure is modified from Michowitz and Saenen's work. (Michowitz *et al.*, 2000; Saenen & Vrints, 2008). The top panel depicts a standard ECG trace. The lower panel represents a typical ventricular action potential. The QRS wave represents the depolarization phase of the ventricle, and the T-wave represents the repolarization phase of the ventricle. The QT-interval is the measurement of the starting point of the Q wave and the end point of the T-wave. The QT-interval is the indicator of the length of the action potential duration (APD). Indicated below are the currents participating in each phase of the action potential. Sodium current is involved in phase 0, phase 1, and phase 2 of the action potential in the ventricular cardiomyocyte.

## **G. Overview of the LQTS**

### **1. History of the identification of LQTS**

LQTS was first described by Jervell and Lange in 1957. The first case of LQTS was identified in a family in which several children had congenital bilateral neural deafness and QT prolongation manifested by electrocardiogram (ECG) study. The children carrying this disease experienced recurrent syncope and sudden death. The disease was referred to as “Jervell and Lange-Nielsen syndrome” at the time of discovery (Jervell & Lange-Nielsen, 1957). It was found that the particular inherited disease case in this family happened to be in an autosomal recessive pattern. Almost a decade later, the LQTS was found in other families with similar QT prolongation, and the family history suggested autosomal dominant inheritance. The symptom was named as “Romano-Ward syndrome”, and the affected members suffered from recurrent syncope and sudden death (Ward, 1964; Towbin & Vatta, 2001; Bloise *et al.*, 2002).

### **2. Diagnosis of the LQTS**

The diagnosis of LQTS is based on the corrected QT interval (QTc) measurement defined on page 20. The QT interval is measured from the start point of Q wave to the end point of the T wave. Usually, the ECG result from lead II allows a better measurement, since the amplitude of the T wave is large enough to allow for an accurate identification of the repolarization T wave for the ventricle. Over the years, it was found that LQTS is an inherited cardiac arrhythmia that causes abrupt loss of consciousness, seizures and sudden death (Jervell & Lange-Nielsen, 1957; Romano *et al.*, 1963; Maron *et al.*, 1976;

Towbin & Friedman, 1998; Arnestad *et al.*, 2007). The sudden death is due to the ventricular tachycardia, such as ventricular fibrillation and torsade de pointes (TdP) (Schwartz *et al.*, 1975; Moss *et al.*, 1991). Although TdP (French for “twisting of the points”) is a very rare ventricular arrhythmia, it can degenerate into ventricular fibrillation and lead to death without immediate medical intervention.

### **3. Classification of the LQTs**

There are two types of long-QT syndromes. Besides the inherited LQTs that is caused by genetic defects, there is also a type of LQTs so called “drug-induced LQT syndrome” or “acquired LQT syndrome”.

#### **a. Genesis of the acquired LQTs**

Compared to inherited LQTs, drug-induced LQTs is far more common, and can be acquired as a side-effect of treatment with clinical medications such as antiarrhythmic, antihistamine, and psychoactive medications. The “acquired” LQTs and TdP were reported in the 1970’s. The administration of certain drugs caused reversible LQTs with a high risk of sudden death. The acquired LQTs is mostly caused by drugs and/or electrolyte disturbances that alter the electrochemical conditions required for normal cardiac excitability. Theoretically, drug-induced LQTs can be caused by the reduction of any known voltage-gated potassium channel that participates in the cardiac action potential. The molecular mechanism for acquired LQTs is almost exclusively found to be the reduction of I<sub>Kr</sub> current through direct or indirect down regulation or blockade of the channel, which is encoded by the human ether-a-go-go related gene “*HERG*” (Yang *et al.*,

2002). HERG channels carry the current of  $I_{Kr}$ . There are several risk factors that can contribute to the acquired LQTS as a complication of drug therapy. These factors include gender difference (higher incidence in female), hypokalemia, hypomagnesaemia, hypocalcemia, congestive heart failure, congenital structural heart defect, left ventricular hypertrophy, bradycardia, atrial fibrillation, high plasma drug concentration (Roden, 2006).

#### **b. The molecular basis of the congenital inherited LQTS**

Since the first identification of genetic mutations that cause LQTS in 1991, mutations have been discovered in 12 different genes. The classification of the inherited LQTS was based on the chronological order in which the location of the mutation was identified. In the population that has been identified to carry LQTS, about 50% was associated with mutations. So far, more than 150 mutations have been found in the 12 different LQTS associated genes (see Table 1). Mark Keating's group was the very first group to map three LQTS loci: LQTS1 on chromosome 11p15.5 (Keating *et al.*, 1991a; Keating *et al.*, 1991b), LQTS2 on 7q35-36 and LQTS3 on 3p21-24 (Jiang *et al.*, 1994). The major strategy they used to identify LQTS genes is called "candidate gene approach", which relies on hypotheses based on the fundamental physiology knowledge. Since then, more LQTS subtypes were found and characterized. Inherited LQTS is thought to be caused by mutations on certain genes. The majority of the mutations happen to be on the genes coding for potassium channels such as *KCNQ<sub>1</sub>*, and *HERG*, and they account for about 88% of the mutations that were identified. In fact, the LQTS are predominantly ion channel disorders, although genes coding for

channel modulatory proteins were also identified a few years later to be the cause of other types of LQTS. It was found that sodium channel mutation is associated with LQT3, and sodium channel mutations account for about 7% of the total identified LQTS-causing mutations. The typical ECG study for LQT3 will indicate the long ST-segment interval before the onset of a late prominent T wave, and this is the characteristic of LQT3 phenotype. The first *SCN5A* mutation was identified by Mark T. Keating's group (Wang *et al.*, 1995). They found a three amino acid KPQ deletion at position 1505-1507 of the  $\alpha$  subunit in affected members of two distinct families with LQTS history. This deletion was not identified in the control individuals with the sample size of more than 500 healthy individuals. This three amino acid in-frame deletion Lys-1505, Pro-1506, Gln-1507 was predicted to be in the cytoplasmic linker between DIII and DIV. The presence of exactly identical deletions in two unrelated families with LQTS history strongly suggests that *SCN5A* mutation is the likely cause of LQT3. KPQ deletion is the most extensively characterized *SCN5A* mutations. In 1995, Bennett *et al.* reported the biophysical properties of this mutant channel. They showed that fast inactivation of the mutant channel is delayed since time constants for current decay were decreased in the  $\Delta$ KPQ mutant (WT-hH1:  $\tau_{fast} = 1.47 \pm 0.11$  ms,  $\tau_{slow} = 8.59 \pm 0.71$  ms;  $\Delta$ KPQ:  $\tau_{fast} = 0.98 \pm 0.07$  ms,  $\tau_{slow} = 5.40 \pm 0.55$  ms,  $p < 0.01$ ; data are means  $\pm$  s.e.m.) not increased as was predicted. However, unlike WT-hH1, there are abnormal sustained sodium current ( $I_{sus}$ ) in  $\Delta$ KPQ expressing cells. The  $I_{sus}$  ( $\sim 5\%$  of the peak inward current at -20 mV) was shown not to decay within a 200 ms depolarization pulse (Bennett *et al.*, 1995; Wang *et al.*, 1996).

Single channel recordings demonstrated that the  $\Delta$ KPQ channels present multiple intermittent reopening after the first 20 ms. This reopening induces an  $I_{\text{sus}}$  or delayed inactivation. In theory, mutations in cardiac sodium channel gene could cause LQT. Voltage-gated sodium channels underline the rapid depolarization phase in ventricular cardiomyocytes and also conduct a small portion of current during the plateau phase of the action potential (Attwell *et al.*, 1979). Therefore, a subtle abnormality of sodium channel function such as delayed sodium channel inactivation, or altered voltage dependence of channel inactivation, this could delay the cardiac repolarization phase. As a result, sodium channel functional defects can lead to QT interval prolongation and arrhythmia.

So far, there are transgenic mouse models of  $\Delta$ KPQ and N1325 mutants. *In vivo* studies from these mice indicate the presence of prolonged QT interval, spontaneous ventricular tachycardia and ventricular fibrillation. *In vitro* electrophysiology studies indicated that cardiomyocytes from these mice have prolonged APD, increased  $I_{\text{sus}}$ , and early afterdepolarizations (Fabritz *et al.*, 2003; Tian *et al.*, 2004). Typically, the *SCN5A* mutations that are correlated with LQT3 are gain-of-function mutations. Studies have demonstrated that gain-of-function mutations disturb the delicate balance between outward and inward currents which are involved in the plateau phase of the action potential repolarization process. In the presence of APD prolongation, there is a propensity for cardiomyocytes to develop early afterdepolarizations, which can trigger TdP. Under normal conditions, during the plateau phase nearly 99% of the channels become inactivated and transitioned into a non-conducting state while the

remaining channels stay in the open activated state, sustaining a small window-current that contributes to the plateau phase. Therefore, mutations that disrupt the inactivation process will dramatically enhance the window-current and give rise to the prolonged action potential duration (Bennett *et al.*, 1995).

Table 1. Summary of LQTS

Type of LQT (time of discovery)	Genes affected	Chromosomal locus	Affected protein	Disease mechanism	Function affected	Frequency in patients
LQT1 (1991)	KCNQ1 (KVLQT1)	11p15.5	Kv7.1 ( $\alpha$ subunit $I_{Ks}$ )	Loss-of-function	$\downarrow$ of slowly activating delayed rectifier $I_{Ks}$ current ( $I_{Ks}$ )	30-35%
LQT2 (1994)	HERG	7q35-36	Kv11.1 ( $\alpha$ subunit $I_{Kr}$ )	Loss-of-function	$\downarrow$ of rapidly activating delayed rectifier $I_{Kr}$ current ( $I_{Kr}$ )	25%-30%
LQT3 (1994)	SCN5A	3p21-24	Nav1.5 ( $\alpha$ subunit $I_{Na}$ )	Gain-of-function	$\uparrow$ Sodium channel function caused by delaying inactivation and cause $\uparrow$ of late $I_{Na}$	5%-10%
LQT4 (1995)	Ankyrin	4q25-27	Ankyrin B (adaptor for $I_{Na}$ , $I_{Na-Cx}$ , $I_{Na-K}$ )	Loss-of-function	$\downarrow$ coordination of proteins such as Na/Ca exchange, lead to LQTS	rare
LQT5 (1997)	KCNE1 (Mink)	21q22.1-22.2	Mink ( $\beta$ subunit of $I_{Ks}$ )	Loss-of-function	$\downarrow$ surface $I_{Ks}$ , $\downarrow I_{Ks}$ current	rare
LQT6 (1999)	KCNE2 (MiRP1)	21q22.1-22.2	MiRP1 ( $\beta$ subunit of $I_{Ks}$ )	Loss-of-function	$\downarrow I_{Kr}$ current, prolong QT interval	rare
LQT7 (2001)	KCNJ2	17q23.1-17q24.2	Kir2.1 ( $\alpha$ subunit of $I_{K1}$ )	Loss-of-function	$\downarrow$ flux of $I_{Kir2.1}$ current, prolong QT interval	rare
LQT8 (2005)	CACNA1C	12p13.3	Cav1.2 ( $\alpha$ subunit of $I_{Ca}$ )	Gain-of-function	Mutations result in complete loss of $I_{Ca}$ inactivation, delay action potential repolarization	rare
LQT9 (2006)	CAV3	3p25	M-caveolin (adaptor for $I_{Na}$ )	Loss-of-function	$\downarrow$ of interaction of CAV3 and Nav1.5, cause 2-5 fold $\uparrow$ of late $I_{Na}$	rare
LQT10 (2007)	SCN4B	11q23	Nav $\beta_4$ ( $\beta$ subunit of $I_{Na}$ )	Loss-of-function	Nav $\beta_4$ slightly inhibit $I_{Na}$ in the normal situation. Mutation of SCN4B cause 8-fold $\uparrow$ of late $I_{Na}$	rare
LQT11 (2007)	AKAP9	7q21-7q22	Youtiao (adaptor protein)	Loss-of-function	$\downarrow$ interaction with $I_{Ks}$ , $\downarrow$ Kv7.1 phosphorylation. $\uparrow$ QT-time	rare
LQT12 (2008)	SNTA1	20q11.2	$\alpha 1$ -synnrophin (Scaffolding protein)	Loss-of-function	$\uparrow$ nitrosylation of Nav1.5, $\uparrow$ late $I_{Na}$	rare

Note: This table summarizes the classification and molecular mechanisms of LQTS. It was modified from a review by Hedley *et al.* (Hedley *et al.*, 2009).

## **H. Sodium channel $\alpha$ subunit mutations and cardiac arrhythmias**

### **1. Role of the cardiac sodium channels in the genesis of the inherited cardiac arrhythmias**

In general, as has been discussed before, sodium channels contribute predominantly to two phases of the action potential: phase 0, the period of fast depolarization of the action potential; and phase 2, the plateau phase of the action potential. Mutations in the cardiac sodium channel are associated with cardiac arrhythmia. Mutations in the sodium channel contributes to the genesis of cardiac arrhythmia through two basic mechanisms: one is loss-of-function mutations that lead to the non-functional sodium channels, or channels that can inactivate faster; the other mechanism is gain-of-function mutations which consequently cause slowing of inactivation and an increase in the late sodium current. Increase in the late sodium current leads to the prolongation in cardiac action potential duration and the corrected QT interval on ECG.

### **2. Inherited LQTS and its relationship with sodium channel gain-of-function mutations**

LQTS is an abnormality of cardiac muscle repolarization that predisposes affected individuals to a ventricular arrhythmia that can degenerate into ventricular fibrillation and cause sudden death. LQTS patients often present with a series of symptoms such as QT interval prolongation, polymorphic ventricular tachycardia, and sudden death (Jervell & Lange-Nielsen, 1957; Romano *et al.*, 1963; Ward, 1964). While QT prolongation by itself is not harmful, it can provide

the basis for the life-threatening ventricular tachycardia (VT) such as Torsade de Points due to its morphological characteristic of changing QRS amplitude.

### **3. Sodium channel loss-of-function mutations**

#### **a. Brugada syndrome**

It was first described by Brugada in 1992 (Brugada & Brugada, 1992). This is described as a syndrome with recurrent episodes of aborted sudden death, right bundle branch block, persistent ST segment elevation, and normal QT interval. These patients have structurally normal hearts.

The first gene that is linked to the Brugada syndrome was reported in 1998 by Chen and colleagues in Dr. Wang's and Towbin's laboratory (Chen *et al.*, 1998). Using a candidate gene approach, Chen *et al.* examined six families with Brugada syndrome and identified C to T base substitutions in exon 21 and exon 28 of the cardiac sodium channel gene *SCN5A*. These mutations lead to the substitution of an arginine (R) by a tryptophan (W) at codon 1232, and the substitution of a highly conserved amino acid threonine (T) by a methionine (M) at 1620. The R1232W missense mutation was found to be located in the S1-S2 extracellular loop of DIII. The T1620M missense mutation was identified to be located in the extracellular loop S3-S4 of DIV. Using *Xenopus* oocytes, Wang demonstrated that sodium channels with the missense mutation recover from inactivation more rapidly than normal. In addition, the voltage dependence of steady-inactivation was shifted almost 10 mV towards more positive potentials in oocytes expressing both R1232W and T1620 mutant channels. Unlike LQTS-related mutants, these two missense mutants do not cause persistent,

inactivation-resistant currents. Electrophysiological studies carried out by Baroudi *et al.* suggested that in mammalian cells such as tsA 201 cells, the T1620 mutation led to a slower recovery from inactivation with no effect on steady-state inactivation (Baroudi *et al.*, 2000). Baroudi's finding supports the idea that the slower recovery from inactivation could decrease sodium current density during the cardiac cycle. Therefore, his finding could explain part of the arrhythmia phenotypes seen in patients with Brugada syndrome. Other mutations indentified by Chen (Chen *et al.*, 1998) were found to produce a stop codon, resulting in the elimination of DIII/S6 and DIV/S1-S6. Therefore, the number of functional sodium channels will be reduced as a consequence of the stop codon. So far, Brugada syndrome related sodium channel mutations are considered to reduce the number of functional sodium channels or accelerate their inactivation.

#### **b. Progressive conduction system defects**

Progressive conduction system defects were first described by Lenegre and Lev *et al.* (Lenegre, 1964; Lev *et al.*, 1970). This disease has a characteristic of right or left bundle branch block, which may lead to complete heart block. Patients with conduction system defects usually presented with syncope and heart block. Later, the gene that causes this defect was mapped to the cardiac sodium channel gene *SCN5A*, which produced a channel lacking S4 of DIII. It was shown by histology studies that the heart with conduction system defects develops significant fibrosis in the conduction system.

## **I. Antiarrhythmic drug binding sites on sodium channel**

Sodium channel blockers such as lidocaine and quinidine are still widely used drugs in terminating cardiac arrhythmia by slowing cardiac conduction and prolonging refractoriness period. Hille and Hondeghem proposed models of drug actions by binding to a specific site on the channel protein (Hille, 1977; Hondeghem & Katzung, 1977). Using alanine scanning mutagenesis method, DIV/S6 was examined as a site of action of sodium channel blockers such as local anesthetics (Ragsdale *et al.*, 1994). The corresponding regions of the cardiac sodium channel were confirmed to have similar function as the drug access and binding sites (Ragsdale *et al.*, 1996). Work by Sunami *et al.* also explored the cysteine residue in the linker region between S5 and S6 in domain I, and showed that this site may contribute to the cardiac selective binding site for sodium channel blocker (Sunami *et al.*, 1997). Further studies need to be performed to identify other residues that bind to local anesthetics and antiarrhythmic drugs.

## **J. Hypothesis and specific aims**

As a rare but lethal inherited cardiovascular disorder, congenital LQTS carries a hallmark of prolonged QT interval measured by a surface electrocardiograph (ECG). The incidence of congenital LQTS has been estimated to be 1 in 5000 to 10000 live births (Nemec *et al.*, 2003; Crotti *et al.*, 2008; Schwartz *et al.*, 2009). The episodic ventricular tachycardia such as ventricular fibrillation and torsade de points can consequently be triggered by LQTS. So far, congenital LQTS has been linked to mutations in 12 different genes including

*SCN5A*, the gene that encodes the cardiac sodium channel Nav1.5 (Hedley *et al.*, 2009).

Nav1.5 is the major form of voltage-gated sodium channels (VGSCs) in the heart (Rogart *et al.*, 1989), and these channels are essential for the initiation and propagation of action potentials throughout different cardiac tissues. These channel proteins are composed of a complex of a ~260 kD pore forming  $\alpha$  subunit and one or more auxiliary  $\beta$  subunits (32-36 kD). Like other types of VGSCs, Nav1.5 can undergo conformational changes between closed non-conducting, open ion-conducting and inactivated non-conducting states in response to the changes in the local electric potential across the cell membrane. Mutation of *SCN5A* is considered as the cause of LQT3 (Wang *et al.*, 1995). Typically, gain-of-function *SCN5A* mutations increase late sodium current by disruption of sodium channel inactivation, which was predicted to lead to the prolongation of action potential duration (Bankston *et al.*, 2007b).

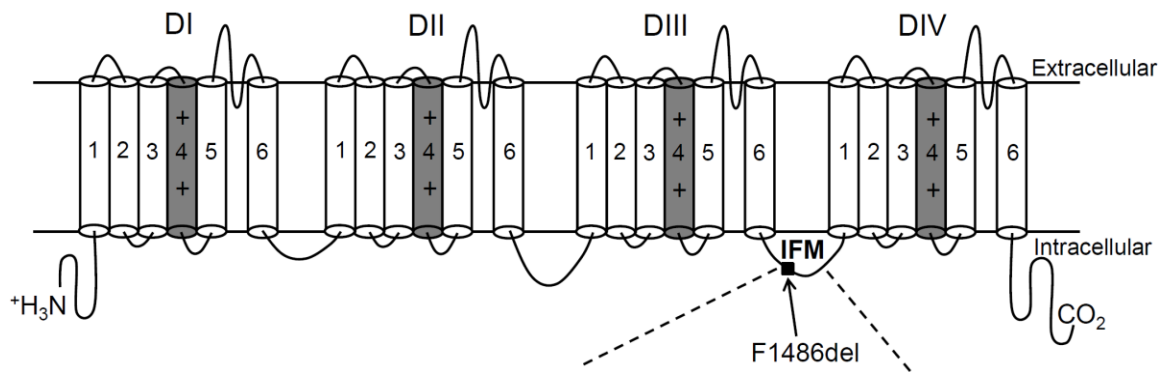
The  $\alpha$  subunit of sodium channel consists of four structurally homologous domains (DI-DIV), each containing six transmembrane segments. The intracellular loop between domain III and IV is thought to play an important role in channel fast inactivation (Figure 6). Within this region, the motif with three hydrophobic amino acid IFM (Isoleucine, Phenylalanine, Methionine) was demonstrated to be critical for channel inactivation (West *et al.*, 1992). Triple mutation of IFM to QQQ (glutamine) and single point mutation of F (phenylalanine, Phe) to Q have been shown to slow the inactivation of Nav1.2 (West *et al.*, 1992). So far, it is still not clear what the specific role that deletion of

F1486 plays in regulating biophysical properties of Nav1.5. In addition, it is unknown whether deletion of F1486 can modulate the channel's pharmacological response to antiarrhythmic drug such as lidocaine. Previous studies found that although the F to Q mutation impairs sodium channel inactivation, it does not alter lidocaine sensitivity (Balsler et al., 1996). The abnormal channel activity generated by the LQT3  $\Delta$ KPQ deletion mutation, also in the III-IV linker, is preferentially targeted by antiarrhythmics (Wang et al., 1997). However, an infant patient with severe cardiac arrhythmia (see ECG study result from (Yamamura et al., 2010) was identified to carry a *De Novo* F1486del within the IFM motif (Figure 6), and this patient showed reduced sensitivity to lidocaine (Yamamura et al., 2009). Based on this case report, we formed a hypothesis that "Deletion of F1486 on intracellular loop III of human Nav1.5 could alter the biophysical properties of the channel, and causes refractory pharmacological response to lidocaine". The aim of this study is to determine the electrophysiological consequence of deleting F1486 and investigate the role of Phe in determining the response to lidocaine. This is the first report to study the overexpression of LQT3 mutations in transfected native cardiomyocytes.

Although disease causing channelopathies are relatively rare, investigating the biophysical and functional consequence of these mutations will increase our knowledge on the roles that sodium channel plays in controlling the excitability of the cardiac cells. Understanding the biophysical response of the mutant sodium channels to particular pharmacological drug treatments will help

to improve the pharmacological approach to individual patient. Therefore, the specific aims of this thesis are:

- 1 To determine if deletion of F1486 on hNav1.5 affects the electrophysiological properties of the channel using both HEK293 cells and neonatal rat cardiomyocytes.
- 2 To determine the functional consequence of F1486del on cardiac action potential using neonatal rat cardiomyocytes.
- 3 To determine if the F1486del mutant channel has reduced response to the antiarrhythmic drug lidocaine.



hNav1.5	--KKGQDI	FMTEE	QKKYY	NAMK	KL	G--
hNav1.1	--KKGQDI	FMTEE	QKKYY	NAMK	KL	G--
hNav1.2	--KKGQDI	FMTEE	QKKYY	NAMK	KL	G--
hNav1.3	--KKGQDI	FMTEE	QKKYY	NAMK	KL	G--
hNav1.4	--KKGQDI	FMTEE	QKKYY	NAMK	KL	G--
hNav1.6	--KKGQDI	FMTEE	QKKYY	NAMK	KL	G--
hNav1.7	--KKGQDI	FMTEE	QKKYY	NAMK	KL	G--
hNav1.8	--KKGQDI	FMTEE	QKKYY	NAMK	KL	G--
hNav1.9	--KKGQDI	FMTEE	QKKYY	NAMK	KL	G--

**Figure 6. Schematic representation and sequence alignment of *Homo sapiens* VGSCs.** The top panel is the linear representation of *Homo sapiens* voltage-gated sodium channels (hNav) alpha subunit structure. Amino acids IFM which form the putative inactivation motif on the intracellular linker between DIII and DIV are shaded in grey. The voltage sensor on segment 4 of each domain is marked with “+” and highlighted in grey color. Below is the sequence alignment of all types of hNav. There is a 100% sequence identity for the IFM motif. The site of phenylalanine (F) deletion in our study is located in the center of IFM motif.

## **II. MATERIALS AND METHODS**

### **A. Ethical information and animal protocols**

Human embryonic kidney (HEK293) cells were ordered from ATCC (Manassas, VA, USA). Use of HEK293 cells was approved by the Institutional Biosafety Committee and conformed to the ethical guidelines for the National Institutes of Health for the use of human derived cell lines. The animal care and use protocol was approved by the Animal Resource Center of Indiana University and met National Institutes of Health and guidelines for the health and well being of the animals.

### **B. Animals**

Neonatal Sprague Dawley rats (pups of postnatal day 1: P1) were obtained from Harlan-Sprague Dawley, Inc. (Indianapolis, IN, USA). Animals were housed in the Laboratory of Animal Source Center (LARC) and used on the day of arrival. All procedures used in these studies were approved by the Animal Care and Use Committee at Indiana University School of Medicine, Indianapolis, IN.

### **C. Patch-clamp recording related instrument set up and general experimental procedures**

The patch-clamp set up rig contains an inverted microscope stage (Nikon Instruments Inc., Melville, NY, USA), which was equipped with a white (Nikon TE2-PS 100W) and fluorescent halogen light source (X-cite 120, Photonic Solutions Inc, Mississauga, ON, Canada), dual Nikon ocular lenses, and Nikon

contrast objectives (10 ×, and 40 ×). The rig also contains an isolated nitrogen infused air table (50-60 psi maintained air pressure) with a 2 inches stainless steel laminate (63-500 Series, Technical Manufacturing Company, Peabody, MA, USA). The function of the air table is to prevent vibration of the microscope and the recording chamber. The air table was grounded with metal wire to be connected to the ground input of the amplifier.

Detailed description of the patch-clamp technique can be found online from Axon or HEKA websites. In general, cells were selected based on their morphology and expression of EGFP. A polished glass electrode pipette was back filled with the appropriate intracellular solution. After filling with intracellular pipette solution, the ideal pipette resistances for recordings are around 0.9-1.3 MΩ in HEK293 cells, and 1.5-2.5 MΩ in neonatal cardiomyocytes. Liquid junction was adjusted to zero before forming the seal. Whole cell patch-clamp recordings were started after obtaining a Giga Ohm seal, which is formed between the glass pipette tip and the cell lipid membrane layer. The typical seal that can be achieved is around 1-20 GΩ.

#### **D. Preparation of the patch-clamp recording chamber**

The patch-clamp recording chamber was home-made and designed based on a 35 mm cell culture dish (Corning, Inc, Corning, NY, USA). The chamber was filled with silicone elastomer base (Sylgard, World Precision Instruments Inc.®, Sarasota, FL, USA), which was mixed with curing agent, and allowed to solidify. After the solidification, a 12 mm glass coverslip was placed in the center of the silicone coated dish and a razor blade scalpel was used in order

to cut the edge surrounding the glass coverslip. The loose inner portion was discarded after the edge surrounding the coverslip was completely removed from the chamber. The center portion of the chamber will be large enough to hold up to approximately 300  $\mu$ l recording solution.

### **E. Mutagenesis of VGSCs**

hNav1.5 cDNA (wild type or mutant hNav1.5 cDNA) was subcloned into pcDNA3.1 (+) vector (Invitrogen, Carlsbad, CA, USA) using HindIII (5' end) and XbaI (3' end) as restriction enzyme sites. Site-directed mutagenesis of voltage-gated sodium channels was performed to characterize voltage-dependent effects of single-point mutation on several constructs (Nav1.5 WT, F1486del, G1481E). An additional mutation is required to engineer a second chimeric point mutation in both wild type and disease causing SCN5A sequences to endow the channels with enhanced resistance to TTX (~100  $\mu$ M). Biophysical and biochemical properties of channels were examined using voltage-clamp, current-clamp and western blot experiments. Mutagenesis primers were designed to introduce the correct base pair change into wild type hNav1.5 channel cDNA using Vector NTI software (Invitrogen, Carlsbad, CA, USA). WT hNav1.5 with appropriate nucleotide changes resulting in hNav1.5 F1486del was produced using Quick Change XL site-directed mutagenesis kit (Agilent technologies, Santa Clara, CA, USA) according to the manufacturer's protocol. Full-length sequence was analyzed using ACGT (Wheeling, IL, USA) plasmid DNA sequencing services to verify the specific mutation at the targeted site. Primers that were used to generate human Nav1.5 cDNA mutation constructs are listed in Table 2.

The sequencing primer for hNav1.5 WT and F1486del construct is:

5'-AACCTCTACATGTACATCTAT-3'

The primer for sequencing the hNav1.5 G1481E mutation product is:

5'- AAC AAC AAG AGC CAG TGT GAG TCC -3'

Primers used in full-length sequencing analysis are listed in Table 3.

Table 2. Primers used for generating hNav1.5 mutant cDNA constructs

<b>Primer Name</b>	<b>Sequence (5' to 3')</b>
F1486del Forward	GGCCAGGACATCATGACAGAGGAGC
F1486del Reverse	GCTCCTCTGTCATGATGTCCTGGCC
G1481E Forward	CAGAAGAAAAAGTTAGAGGGCCAGGACATCTTC
G1481E Reverse	GAAGATGTCCTGGCCCTCTAACTTTTTCTTCTG
TTXR Forward	CTGATGACGCAGGACAGTTGGGAGCGCCTCTATC
TTXR Reverse	GATAGAGGCGCTCCCAACTGTCCTGCGTCATCAG

Table 3. Primers used in full-length sequence analysis of sodium channel

Nucleotide Position	Sequence (5' to 3')
364-386	ACC TGC AGG CCT CCA AAA AGC TG
816-839	GAA TTT GTG GAC CTG GGC AAT GTC
1566-1586	CGT AGC TCC TTG GAG ATG TCC
2726-2750	GGT GCT AGC CAT CAT CGT GTT CAT C
3432-3452	CCT GTG TCC GGT GGC CCA GAG
4084-4104	CCA TCA AGT CAC TGC GGA CGC
4807-4830	GCT TGA ATA TGG TGA CCA TGA TGG
5497-5519	GCT TGA ATA TGG TGA CCA TGA TGG
6139-6159	CCA CCA GCG ATA ACC TCC AGG
6792-6814	GCT GAA CCC CCA CTC ACA CAA GC
7467-7487	CCA TGG CAC CTT TGA GAG AGG
8116-7488	GCT TGG AGA GGT ATG TGC CC

All sequencing primers were designed to test the correct base-pair change in the hNav1.5 construct, and to confirm there is no nonspecific mutation.

## **F. Large-scale bacteria culture and DNA purification**

Bacterial colonies were grown up according to the Strategene's QuickChange<sup>®</sup> protocol. After antibiotic-resistant colonies had grown on LB/antibiotic agar plates, several single individual colonies were picked using 20-200  $\mu$ l pipette tips. Each individual colony was then transferred to a 14 ml sterile round bottom Falcon tube (Becton Dickinson Labware, Franklin Lakes, NJ, USA) containing 5 ml of LB broth and penicillin (100  $\mu$ g/ml) to initiate the mini culture. The mini bacteria cultures were then placed in a 37 °C Excella E25 incubator (NewBrunswick Scientific, Edison, NJ, USA) at a shaking speed of 250 rpm and incubated overnight. Bacteria mini culture plasmid purification was performed using Promega Pure Yield Plasmid Miniprep Kit (Promega, Madison, WI, USA). All procedures were performed according to the manufacture's protocol. Once the plasmid DNA was purified, the constructs were screened and confirmed by restriction enzymatic digestion, and DNA sequencing based on the appropriate DNA sequencing primers. Full-length DNA sequencing was performed using the DNA sequencing service from ACGT Company (ACGT, Wheeling, IL, USA). After the sequence of the construct was verified, large scale bacteria cultures (MaxiPrep) were performed in order to obtain sufficient amount plasmid DNA for the downstream studies. The purification of plasmid DNA from larger scale bacterial cultures were performed using Sigma GeneElute HP Plasmid Maxi Prep Kit (NA0300, Sigma, St. Louis, MO, USA). After the plasmid purification was completed, the yield plasmid cDNA constructs were checked for purity and concentration using Nanodrop ND-1000 spectrophotometer instrument (Thermo

Fisher Scientific Inc., Wilmington, DE, USA). The concentration was brought to 0.5 µg/µl using double distilled sterile water. Purified plasmid cDNA constructs were then used for transfection in the appropriate expression system.

## **G. Cell culture**

### **1. Culture of HEK293 cells**

HEK293 cells (from ATCC, American Type Culture Collection, Manassas, VA, USA) were grown on 35mm tissue culture dishes (Corning Inc, NY, USA) under standard tissue culture conditions (37 °C; 5% CO<sub>2</sub>) in Dulbecco's modified Eagle's medium containing high glucose (DMEM/H, Invitrogen, Grand Island, NY, USA) supplemented with 10% fetal bovine serum (FBS, Atlanta Biologicals, Lawrenceville, GA, USA), 1% penicillin/streptomycin (Invitrogen, Grand Island, NY, USA) and 1mM L-glutamine (Invitrogen, Grand Island, NY, USA). Cell culture media was changed every 2-3 days. Cells were replated into new sterile tissue culture dishes once the confluency reaches 80% to 90%.

### **2. Harvest, isolation and culture of neonatal rat cardiomyocytes**

Neonatal Wistar rats were used in each single preparation. Pups of post natal day 1 (P1 pups) were generally used. P1 rats were sacrificed and hearts were collected from all pups. Hearts were stored in calcium and magnesium-free PBS on ice. Hearts were gently squeezed with forceps to expel the blood from the lumen, and then transferred into fresh ice-cold PBS buffer. The atria tissues were cut out and the ventricles were saved for the subsequent dissociation procedure. The ventricle tissues were then transferred to a new 60 mm sterile Petri dish and minced into small pieces with a sterile scalpel blade. The minced

neonatal heart tissues were then transferred into a sterile T-25 cell culture flask under a laminar flow tissue culture hood. The bottom of the flask was filled with 5-7 ml of the pre-warmed digestion buffer containing 0.5 mg/ml collagenase and 0.4 mg/ml pancreatin. The flask containing the cardiac tissues was incubated in a 37 °C water bath for 30 minutes and the tissues were mixed by gentle shaking. The supernatant containing the suspended cells from the first round of the digestion were discarded. The remained tissue was saved and the bottom of the flask was filled with another 5 to 7 ml digestion buffer. Following these steps, the tissues were incubated in the 37 °C water bath for 20 minutes. This step was repeated for 5 to 6 times. After each 20-minute digestion, the suspension containing the isolated cells was collected and transferred into a 15 ml sterile conical tube. 1 ml of horse serum was added to the tube to terminate the enzymatic reaction. The tube was centrifuged at 700 rpm for 10 minutes. The supernatant containing the enzyme was discarded, and 2 ml of the neonatal calf serum was added to the tube. The cells were gently mixed into a suspension by tapping the bottom of the tube. 10 ml of complete cell culture medium was added to the tube to completely suspend the isolated cardiomyocytes, which were then plated into a 10 cm cell culture dish. Eventually, the total isolated cardiomyocytes were plated into four to five 10 cm cell culture dishes. The cardiomyocytes were incubated under tissue culture conditions (37 °C, 5% CO<sub>2</sub>) for 1 to 1.5 hours to let the fibroblast cells attach. The culture media containing the isolated cardiomyocytes was then collected after the centrifugation. Complete tissue culture media was added to the tube to resuspend the cells. Cell number was

counted using the hemocytometer (Hansser Scientific, Horsham, PA, USA). The cardiomyocytes were cultured using DMEM/F12 media containing 10% fetal bovine serum, 100 units/ml penicillin, 100 mg/ml streptomycin and 1mM L-glutamine. Following a 24 hour incubation period, the serum-containing medium was replaced with a low serum medium containing medium (0.5% horse serum, 0.5% fetal bovine serum) called “maintenance medium” to prevent hypertrophy. Cardiomyocytes were cultured for up to 48 hours in the maintenance medium. Electrophysiology studies were performed within 48 hours post transfection.

## **H. Gene transfection**

### **1. Plasmid map of cDNA construct for human Nav1.5**

DNA encoding human cardiac voltage-gated sodium channel Nav1.5 was subcloned into pCDNA3.1 vector. The restriction enzyme cutting site are BamH I (5' end) and Xba I (3' end). The detailed information is indicated in the vector map (Figure 7).

### **2. Plasmid map of cDNA construct for N<sub>2</sub>-EGFP**

cDNA encoding N<sub>2</sub>-EGFP was used in the transfection, and its product green fluorescence protein is used as an transfection control in order to visualize the transfected cells. The detailed information about the cDNA construct is described in Figure 8.

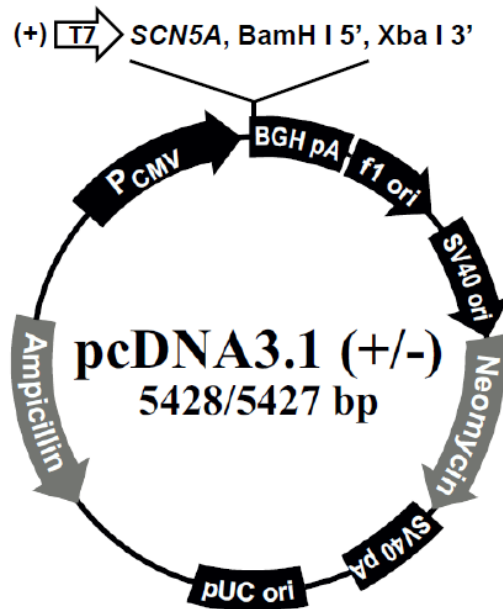


**Figure 7. Plasmid map of pcDNA3.1 (+) carrying the gene of *Homo Sapiens* full-length *SCN5A* encoding hNav1.5.** This map was modified based on the pcDNA3.1 (+) vector map. The gene was inserted into the vector between BamH I restriction enzyme site and Xba I site. The F1486del *SCN5A* gene carries an amino acid deletion at codon 1486. This amino acid is on the intracellular loop between transmembrane domain III (DIII) and domain IV (DIV). The total length of this plasmid DNA is around 12.8 kb.

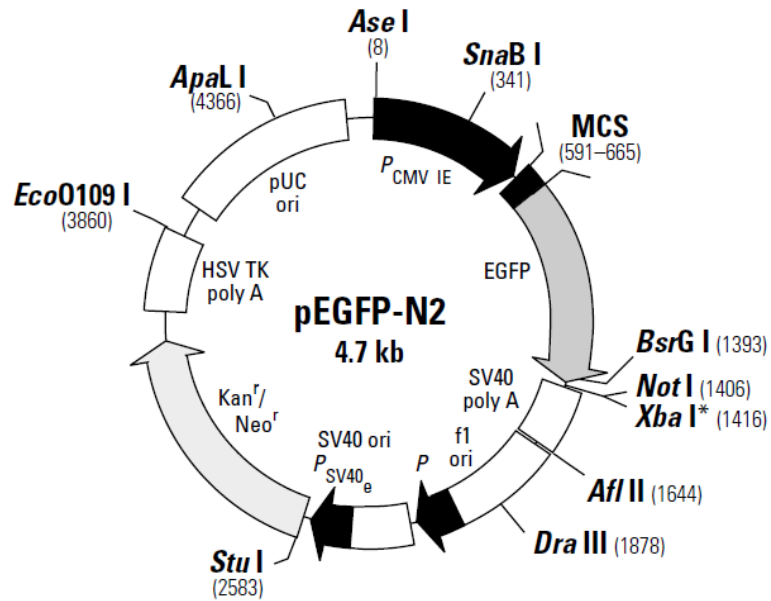


**Figure 8. Plasmid map of cDNA construct for N<sub>2</sub>-EGFP.** The copyright of this map belongs to the Clontech Inc. pEGFP-N<sub>2</sub> encodes a mutant fluorescent protein (GFP) with enhanced fluorescence as compared to the gene encoding WT green fluorescence protein. The total length of this vector is about 4.7 kb. EGFP was used as a transfection control in order to visualize the transfected cells in the electrophysiology studies.

### 3. Transient transfection of HEK293 cells

Unless otherwise stated, HEK293 cells were used to express various cardiac voltage-gated sodium channel Nav1.5 (WT, or different mutants). Equal amount of cDNA encoding sodium channel hNav1.5  $\alpha$  subunit and auxiliary  $\beta_1$  subunit were transiently cotransfected into HEK293 cells using calcium phosphate precipitation method. We chose to express the sodium channel  $\alpha$  subunit together with the  $\beta_1$  subunit since these two subunits have been shown to co-express in cardiomyocytes (Dhar Malhotra *et al.*, 2001). In addition, the  $\beta_1$  subunit was demonstrated to be able to modulate cardiac sodium channel function, while  $\beta_2$ -subunit function in heart maybe be limited to cell adhesion (Dhar Malhotra *et al.*, 2001). Plasmid DNA encoding N<sub>2</sub>-EGFP was also used as a transfection control in order to visualize the transfected cells which will be used in patch-clamp experiments.

30 minutes before the forming of the mixture of calcium phosphate, complete cell culture media was replaced by cell culture media containing 5% FBS. Next, the transfection reagents were brought to the room temperature or warmed in the 37 °C water bath. The transfection reagents contained: 2 x HEPES buffer (1.6 g NaCl, 0.021 g Na<sub>2</sub>HPO<sub>4</sub>, 1.3 g Na-HEPES per 100 ml, pH was adjusted to 7.0); sterile double distilled water; 2 M CaCl<sub>2</sub>. Various set of sterile 1.5 ml centrifuge tubes were labeled. For each transfection condition, 2 tubes will be used. The contents of the tubes were as follows, for example: Tube # 1, 50  $\mu$ l 2 x HEPES; tube # 2, 3  $\mu$ g  $\alpha$  subunit per transfection, 0.75  $\mu$ g  $\beta_1$  subunit per transfection, 0.75  $\mu$ g N<sub>2</sub>-EGFP per transfection, 5  $\mu$ l CaCl<sub>2</sub>, and use

sterile double distilled water to bring the total volume to 50  $\mu$ l. The 5  $\mu$ l  $\text{CaCl}_2$  was added to tube # 2 dropwise last, and mixed evenly. Each tube containing the content was allowed to sit in the cell culture hood for 2 minutes before combination. Then, the content in tube # 2 containing cDNA was added dropwise to tube # 1, which contained the 2  $\times$  HEPES buffer. The total content was mixed well by tapping the wall of the tube. Then bubbles were formed using the 100  $\mu$ l pipette tip, and this bubble-generating procedure was slowly repeated 5 to 10 times to allow the fine precipitate grains to be formed. The calcium-phosphate-DNA mixture was left in the sterile laminar tissue culture hood for 30 minutes to allow enough fine precipitate grains to be formed. 30 minutes later, the mixture of calcium phosphate and DNA was added to the cell culture medium with 5% reduced FBS and maintained in the media for 4-6 hours. After this, cells were washed with warmed fresh culture medium containing 10% FBS twice and replated onto 12 mm glass coverslips in 24 well plates (Costar, Corning Inc, Corning, NY, USA) with each well containing 500  $\mu$ l to 1ml 10% serum-complete medium. Typically, transfected cells were used for whole patch-clamp recording within 48-72 hours post transfection, given that this time-window is the best time for obtaining optimal expression level and single cell without contacting with adjacent cells. Cells were selected based on the expression of enhanced green fluorescence protein and used for data collection if current amplitude was greater than 500 pA under whole cell recording mode in order to minimize signal to noise ratio during data analysis.

#### **4. Transfection of neonatal rat cardiomyocytes**

$2 \times 10^6$  cells were used for each transfection reaction. Briefly,  $2 \times 10^6$  cells in suspension were transferred into a 1.5 ml sterile centrifuge tube and centrifuged at 600 rpm for 3 minutes. The supernatant was discarded. Then 100  $\mu$ l Amaxa Nucleofector transfection reagent was added to each tube. Then 100  $\mu$ l of cell suspension was combined with 3  $\mu$ g cDNA encoding  $\alpha$  subunit, 2  $\mu$ g pMaxGFP cDNA. Since the neonatal cardiomyocytes contains endogenous  $\beta_1$  subunit, the cDNA encoding  $\beta_1$  subunit was not included in each transfection. The mixture was evenly mixed with the plastic pasteur pipette with fine tips for 2 to 3 times. The mixture was then transferred into a cuvette for electroporation. The cuvette with cell/DNA suspension was transferred into the cuvette holder and the program G-009 for cardiomyocyte transfection was applied. The cell suspension was transferred into a 15 ml sterile conical tube and 12 ml of complete cell culture medium was added to the tube. The cells were mixed with the culture media gently and then plated into the 24-well plate containing the 12 mm coverslip in each well. Patch-clamp recordings were performed 24-48 hours post transfection.

## I. Chemicals

Detailed information about the chemicals used in the study is listed in Table 4.

Table 4. Chemical reagents and drugs used in the study

Chemical Name	Manufacture	Catalogue Number
lidocaine	Sigma	L5647
TTX	Alomone Lab	T-500
NaOH powder	Sigma	S8045
NaCl	Sigma	S7653
MgCl <sub>2</sub>	Sigma	M8266
KCl	Sigma	P9333
CaCl <sub>2</sub>	Sigma	C1016
HEPES	Sigma	H3375
CsF	Sigma	20989
EGTA	Sigma	E0396
sucrose	Sigma	S7903
glucose	Sigma	G7528
CoCl <sub>2</sub>	Sigma	60818
CsOH solution	Sigma	232068
NaH <sub>2</sub> PO <sub>4</sub>	Sigma	S8282
Na <sub>2</sub> -ATP	Sigma	A26209
KOH	Sigma	P5958
K-Aspartate	Sigma	A6558
NaOH solution	Sigma	S2770
CsOH solution	Sigma	232041

## **J. Solutions**

### **1. Preparation of lidocaine hydrochloride stock solution**

Lidocaine hydrochloride monohydrate (Sigma Aldrich) was dissolved in the standard external recording solution to make a stock solution of 100 mM. The stock solution was prepared shortly before the experiment and pH was adjusted to 7.3 using 1N NaOH. Subsequent dilutions to concentrations of 10 mM, 3 mM, 1 mM, 300  $\mu$ M, 100  $\mu$ M, 30  $\mu$ M, 10  $\mu$ M were performed using the standard external bathing solution.

### **2. Preparation of tetrodotoxin stock solution**

Citrate-free tetrodotoxin (TTX) powder (Alomone Lab, Israel; catalogue number: T-500) was dissolved in 50 mM acetic acid solution, and was further diluted to the desired concentration using the external bathing solution for  $I_{Na}$  recording in cardiomyocytes.

### **3. Standard extracellular bathing solution for voltage clamp recordings from HEK293 cells**

The standard extracellular bathing solutions were used to bathe HEK293 cells during all whole-cell voltage-clamp electrophysiology studies using transfected HEK293 cells. The osmolarity of the solution was adjusted to about 290 mOsm. The chemical components consisted of (in mM): 140 NaCl, 1 MgCl<sub>2</sub>, 3 KCl, 1 CaCl<sub>2</sub>, and 10 HEPES. pH was adjusted to 7.3 with NaOH.

#### **4. Standard intracellular pipette solution for voltage clamp recordings from HEK293 cells**

The standard pipette solution for  $I_{Na}$  recording from HEK293 cells contained (in mM): 140 CsF, 10 NaCl, 1.1 EGTA, and 10 HEPES, pH 7.3 (adjusted with CsOH). Osmolarity was adjusted to around 300 Osm. After obtaining the appropriate osmolarity and pH, the internal solution was filtered using fast flow and low binding syringe driven 0.22  $\mu$ M filter unit (Millipore, Carrigtwohill, Co, Cork, Ireland) to get rid of any potential substance that can block the pipette tip. The pipette solution was then aliquoted into 1.5 ml sterile centrifuge tubes and stored in a -20 °C freezer for future use.

#### **5. Standard extracellular bathing solution for $I_{Na}$ recordings from neonatal rat cardiomyocytes**

The bath solution for  $I_{Na}$  recordings was the same as described by Maier *et al.* in 2002. (Maier *et al.*, 2002). The chemical components of the extracellular bathing solution consisted of (in mM): 120 NaCl, 1.2  $MgCl_2$ , 1.5  $CaCl_2$ , 10 HEPES, 10 tetraethylammoniumchloride, 5.0 sucrose, 5.0 glucose, and 5.0  $CoCl_2$ , pH was adjusted to 7.4 with 1N NaOH.

#### **6. Standard intracellular pipette solution for $I_{Na}$ recordings from neonatal rat cardiomyocytes**

The pipette solution contained (in mM): 120 Cs-aspartate, 5.0 NaCl, 2.0  $MgCl_2$ , 10 HEPES, 10 EGTA. pH was adjusted to 7.3 with CsOH. After obtaining the appropriate osmolarity and pH, the internal solution was filtered using fast flow and low binding syringe driven 0.22  $\mu$ M filter unit (Millipore, Carrigtwohill, Co,

Cork, Ireland) in order to get rid of any potential substance that can block the pipette tip. The internal solution was then aliquot into a series of 1.5 ml sterile centrifuge tubes, and stored at -20 °C for future use.

### **7. Standard extracellular solution for action potential recordings from neonatal rat cardiomyocytes**

In order to record the action potential from primary rat neonatal cardiomyocytes, tyrode solution was used extracellularly. The tyrode solution used for action potential studies contained (in mM): NaCl 126, KCl 5.4, HEPES 10, NaH<sub>2</sub>PO<sub>4</sub> 0.33, MgCl<sub>2</sub> 1.0, CaCl<sub>2</sub> 1.8, glucose 10. pH was adjusted to 7.4 with NaOH. The osmolarity was adjusted to 300 Osm.

### **8. Standard intracellular pipette solution for action potential recordings from neonatal rat cardiomyocytes**

The current-clamp mode was used in order to study the action potential profile from native neonatal rat cardiomyocytes. The pipette solution used in current-clamp experiments contained (mM): KCl 20, potassium aspartate 110, MgCl<sub>2</sub> 1.0, HEPES 5.0, EGTA 10, Na<sub>2</sub>-ATP 5.0. pH was adjusted to 7.2 with KOH, and osmolarity was adjusted to around 290 using nanopure water. After obtaining the appropriate osmolarity and pH, the internal solution was filtered using fast flow and low binding syringe driven 0.22 µm filter unit (Millipore, Carrigtwohill, Co, Cork, Ireland) in order to get rid of any potential substance that can block the pipette tip. The internal solution was then aliquoted into a series of 1.5 ml sterile centrifuge tubes, and stored at -20 °C for future use.

### **K. Whole cell patch-clamp recordings on HEK293 cells**

Whole cell patch-clamp recordings were conducted at room temperature (~ 21 °C) using a HEKA EPC-10 amplifier. Data was collected using a computer with the Pulse program (v 8.65, HEKA Electronic, Germany). Fire-polished glass electrodes were fabricated from capillary glass (VWR International, Radnor, PA, USA), which were pulled using a Sutter P-97 puller (Novato, CA, USA) to have a resistance of 0.9-1.4 M $\Omega$ . Cells on glass coverslips were transferred to the recording chamber containing 300  $\mu$ l of external bathing solution. Series resistance was compensated to reduce the voltage error to less than 3 mV. Recordings were started 5 mins after forming whole cell configuration to allow for sufficient equilibration of the intracellular solution and pipette solution. Lidocaine solution was added to the recording chamber by first withdrawing 30  $\mu$ l of bath solution, and then adding 30  $\mu$ l of 10-fold concentrated lidocaine and mixing 10 to 15 times using a 100  $\mu$ l pipettor. Cells were kept in the external bathing solution for no more than one hour to allow the healthy condition during patch-clamp recordings.

### **L. Whole cell patch-clamp recordings from neonatal rat cardiomyocytes**

Whole-cell cardiac sodium current and action potentials were recorded at room temperature from rod-shaped cells within 24-48 h post transfection. The current-clamp technique was used to record the action potentials from neonatal cardiomyocytes. Action potentials were elicited by 2-ms stimulus pulses at frequency of 1 kHz. AP measurements were started 5 min after obtaining the

whole cell configuration, and the steady-state action potential duration was measured at 50% (APD<sub>50</sub>) and 90% (APD<sub>90</sub>) of full repolarization. Data sampling rate varied from 2 to 2.5 kHz. Cells generating spontaneous oscillatory potentials at depolarized potentials were defined to have early afterdepolarization (EAD). TTX was added to the external solution at a final concentration of 20  $\mu$ M to eliminate the contamination of endogenous sodium currents in neonatal cardiomyocytes in voltage-clamp studies (Figure 9). No TTX was applied to the extracellular recording solution for action potential studies under the current-clamp mode. Pipette resistance was 1.5-2.5 M $\Omega$  when filled with the internal solution.



### **M. Cysteine, lysine and arginine specific cell surface biotinylation assay**

Cell surface expression of WT and F1486del mutant proteins was analyzed by biotinylation using a cell impermeable reagent (Khanna *et al.*, 2001). Briefly, 6 µg of plasmid DNA was transfected into HEK293 cells cultured in a 6 cm cell culture dish. Four dishes were used for each group. 36-48 h post transfection, HEK293 cells were washed twice with cold PBS and then incubated at 4 °C for 30 min with EZ-link Sulfo-NHS-LC-Biotin (1 mg/ml; Thermochemical, Rockford, IL, USA) in PBS solution. The cells were then washed with glycine to quench the biotinylation reaction. Following this step, cells were washed with cold PBS two to three times to remove the excessive biotinylation reagent. The cells were lysed using 600 µl ice-cold RIPA cell lysis buffer containing protease inhibitors. The lysed cells were incubated on ice for 30 min, vortexed every 5 min, and then centrifuged at 4 °C to remove the insoluble component. 5% of the total volume of the solubilized protein was reserved for future use. 5 µl of the protein from each tube was used for protein concentration measurement using BCA assay. The rest of the solubilized material was incubated with 75 µl streptavidin-linked agarose beads (Thermochemical, Rockford, IL, USA) at 4 °C overnight. The beads were collected by brief centrifugation and washed 3 times with RIPA lysis buffer. Precipitated protein was then eluted by boiling in 50 µl gel loading buffer at 100 °C for 5 min followed by brief centrifugation. The streptavidin precipitated protein and the aliquoted total solubilized protein were subjected to electrophoresis using 4-12% acrylamide gels. The proteins were then transferred to a PVDF membrane, immunoblotted with a rabbit polyclonal anti-Nav1.5

antibody (ASC-005, Alomone Lab, Isarel) and mouse monoclonal anti- $\beta$  III tubulin antibody (G712A). The proteins were then visualized using an enhanced chemiluminescent western blotting substrate (Thermoscientific, Rockford, IL, USA, prod # 32106).

#### **N. Preparation of cell lysate**

HEK293 cells were transiently transfected with cDNA coding for WT Nav1.5 or F186del channels. Typically, 6 cm sterile cell culture dishes were used in these experiments. Before transfection, cells that grow in 6 cm cultures dishes reach 80%-90% confluency. 24 hours post transfection, cell culture media was aspirated from the culture dishes. Then, the cells were washed with 1 $\times$ PBS twice. 500  $\mu$ l cell lysis buffer was added to each dish. The cell lysis buffer contained: 20 mM Tris-HCl (pH 7.5), 150 mM NaCl, 1 mM Na<sub>2</sub>EDTA, 1 mM EGTA, 1% Triton, 2.5 mM sodium pyrophosphate, 1 mM beta-glycerophosphate, 1 mM Na<sub>3</sub>VO<sub>4</sub>, 1  $\mu$ g/ml leupeptin. Cells were then scraped off the plate and transferred to a 1.5 ml microcentrifuge tube. The sample was incubated on ice for 30 minutes, vortexed or mixed with the pipette every 5 minutes. The sample was sonicated for 30 seconds on ice in order to shear the genomic DNA and reduce the viscosity that could trap the protein. Thus, the purpose is to increase the protein content that is dissolved in the sample. The sample was then centrifuged at full speed for 20 minutes at 4 centigrade. The supernatant was then transferred to a 1.5 ml centrifuge tube and stored in a -80 °C freezer for future use.

## **O. Protein concentration measurement**

Protein concentration was measured using bicinchoninic acid (BCA) assay method. BCA assay is a detergent-compatible formulation for the colorimetric detection and quantification of protein concentration. In this assay, the  $\text{Cu}^{2+}$  was reduced to  $\text{Cu}^+$  under an alkaline medium. One cuprous ion  $\text{Cu}^+$  was chelated with two molecules of BCA, and the purple-colored product was formed. The colored product can be detected since it has a strong absorbance at 562 nm. BSA was used as a protein concentration standard. The standard BSA is diluted to a series of final concentrations ( $\mu\text{g/ml}$ ): 2000, 1500, 1000, 750, 500, 250, 125, and 25. The working BCR reagent (WR) was prepared by mixing 50 parts of BCA reagent with 1 part of BCA reagent B (50:1, reagent A:B). Samples were diluted with a ratio of 1:10 using  $1\times$  cell lysis buffer. 25  $\mu\text{l}$  of each standard or unknown sample replicate was added into a single microplate well. Then, 200  $\mu\text{l}$  of the working reagent was added to each well and mixed thoroughly. The plate was then covered with aluminum foil (Fisher Scientific, Cat No: 01-213-100) and incubated in the 37  $^{\circ}\text{C}$  incubator for 30 minutes. Protein concentrations were measured using a plate reader at 562 nm wavelength.

## **P. SDS-polyarylamide gel electrophoresis of protein and transfer**

50  $\mu\text{g}$  of protein was mixed with  $5\times$  sample loading buffer (250 mM Tris pH 6.8, 10% SDS, 50% glycerol, 0.02% bromophenol blue, add 10%  $\beta$ -mercaptoethanol as fresh before use) and then heated to 95-100 centigrade for 5 minutes to denature the protein. The total volume was balanced to the same volume for each sample. 50  $\mu\text{g}$  of each protein sample was loaded onto a 5%

SDS-PAGE gel. Electrophoresis was performed under a voltage of 80 V for the stacking gel and 120 V for the separating gel. After the appropriate separation of the protein molecular weight marker, proteins on the gel were transferred onto a 0.22  $\mu\text{m}$  PVDF membrane (Bio-Rad, Hercules, CA, USA) using a Bio-Rad electrotransfer apparatus. The transfer was performed at room temperature for 1 hour under a voltage of 15 V. The transfer buffer contained 25 mM Tris-HCl (pH 8.0), 190 mM glycine and 20% methanol.

#### **Q. Western immunoblotting analysis**

Immunoblotting analysis was used to analyze total Nav1.5 protein expression level in HEK293 cells transiently transfected with cDNA coding for WT Nav1.5 or F186del channels.

The membrane containing the transferred proteins was washed with 1 $\times$ TBST (10 mM Tris-HCl, 50 mM NaCl, and pH was adjusted to 7.6 with 6N HCl, and then add 0.1% Tween-20) for 5 minutes after the membrane was taken out from the transfer apparatus. The membrane was then incubated in blocking buffer containing 5% non-fat milk at room temperature with constant shaking for 1 hour. Membrane was then incubated with primary rabbit antibody for Nav1.5 (Alomone Lab, Israel) for 1.5 hours at room temperature. After the incubation with primary antibody, the membrane was then washed 3 times with 1 $\times$ TBST (10 minutes for each wash). The membrane was then incubated with secondary antibody against rabbit IgG under room temperature for 1 hour. After 3 washes, the membrane was exposed to ECL plus (PIERCE, Rockford, IL, USA) liquid

mixture for about 1 minute. Autographic film was used to detect the proteins following an optimal exposure time period.

## R. Data analysis

Voltage-clamp experiment data were analyzed offline using the Pulsefit (v 8.65, HEKA electronic), Microsoft Excel and Prism (GraphPad Software Inc, La Jolla, CA) software programs. Normalized conductance-voltage relationships ( $G-V$ ) were derived using the function:  $G_{Na} = I_{Max} / (V_m - E_{Na})$  (1).  $G_{Na}$  is conductance of sodium channel,  $I_{Max}$  is the peak current density in response to the test pulse,  $V_m$  stands for the test pulse potential, and  $E_{Na}$  is the measured sodium channel equilibrium potential. The conductance of activation, steady-state fast inactivation ( $h_{\infty}$ ) and slow inactivation curves were fitted using the general Boltzmann function:  $I = \text{offset} + \{ \text{amplitude} / [1 + \exp((V_{half} - V) / \text{Slope})] \}$ . Slope factors and  $V_{half}$  ( $V_{1/2}$ ) were also calculated based on Boltzmann function analysis.  $V_{1/2}$  is the voltage at which the current is half maximal. Data are presented as mean  $\pm$  SE.  $n$  is presented as the number of the separate experimental cells. The equations used for the dose-inhibition relationships for lidocaine and the Nav channels were as follows: Sigmoidal dose-response with variable slope:  $Y = \text{Bottom} + (\text{Top} - \text{Bottom}) / [1 + 10^{(\text{LogEC}_{50} - X) \cdot \text{Hillslope}}]$  (2). Bottom is the Y value at the bottom plateau. Top is the Y value at the top plateau.  $\text{LogEC}_{50}$  is the X value when the response is halfway between Bottom and Top. Hill Slope describes the steepness of the curve. Statistical difference was assessed using either student's unpaired t-test or one way ANOVA integrated in the Prism 4 software package. Specifically, for action potential duration (APD) comparison, membrane current density

comparison, and ramp current density comparison, data was analyzed using un-paired *t*-tests with a significance level of 0.05.

Protein bands were quantified by densitometry using Molecular Analyst software (version 1.4; Bio-Rad). The percentage of normalized biotinylated protein was compared using un-paired student's *t*-test.  $P < 0.05$  was considered statistically significant.  $P < 0.01$  was considered statistically very significant. Data was presented as mean  $\pm$  S.E.M (standard error of the mean).

### III. RESULTS

#### **A. Deletion of F1486 within the intracellular loop between DIII-DIV of hNav1.5 reduces peak current density in HEK293 cells and neonatal rat cardiomyocytes**

Wild-type (WT) hNav1.5 or the F1486del channel were transiently transfected with the auxiliary  $\beta_1$  subunit into HEK293 cells. Electrophysiological properties of the channels were investigated using standard whole-cell voltage-clamp techniques. Remarkably, the initial comparison of current traces from both channels revealed striking differences in current amplitude and channel kinetics. F1486del channels showed significantly decreased current density compared to WT channels (Figure. 10A). The averaged peak current density at -20 mV was significantly larger for WT channels ( $513.1 \pm 76.14$  pA/pF,  $n=14$ ) than for F1486del channels ( $100.2 \pm 24.13$  pA/pF,  $n=14$   $p < 0.001$ , Figure. 10C). Initially, this observation was surprising as the IFM motif was previously reported to be solely critical for channel inactivation and LQT3 mutations are typically associated with gain-of-function, not loss-of-function effects. To verify that the decrease in current density was not an artifact that was caused by the heterologous expression system, we sought to express the channel in neonatal cardiomyocytes.

In order to isolate sodium currents generated by recombinant channels in myocytes, the hNav1.5 constructs were mutated (C374S) to greatly increase their resistance to TTX. Endogenous sodium currents were largely blocked

(>95%) by application of 20  $\mu$ M TTX (Figure 11), allowing isolation and characterization of currents generated by the C374S channels.

We then compared the current density for each type of channel that was expressed in the primary cells, and found that in neonatal myocytes the F1486del channels still carried less current (Figure 12A and B), as in HEK293 cells. cardiomyocytes transfected with the WT channels had an averaged peak current density of  $385.6 \pm 87.7$  pA/pF (n=12), while the F1486del channels carried a current density of only  $117.3 \pm 18.9$  pA/PF (n=8) ( $p < 0.05$ , Figure 12C). The loss of function phenotype regarding the peak current density for F1486del channel suggests that possible defects in channel trafficking and/or cellular toxicity were induced by the mutation.

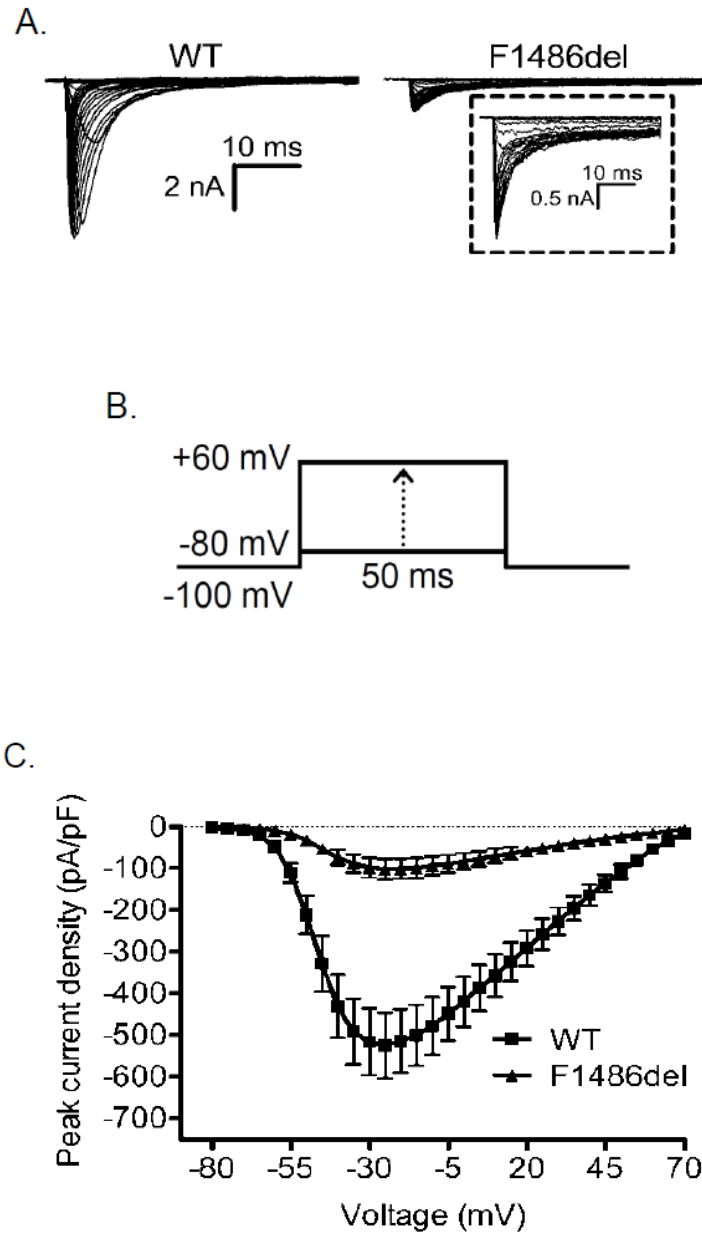


**Figure 10. F1486del within the intracellular loop between DIII-DIV of hNav1.5 reduced peak current density in HEK293 cells.** A. Representative sodium current traces recorded from HEK293 cells for WT versus F1486del channels elicited using an incremental depolarizing protocol. Both channels were co-expressed with human auxiliary  $\beta_1$  subunits. B. Test protocol used for the current density measurements is illustrated. The depolarization voltage step is

with 5 mV increments. C. Mean current-voltage relationships in response to 50 ms stimulation pulses from -80 mV to +60 mV (5 mV increments) for WT (n=25, closed squares) and F1486del (n=14, closed triangles) channels expressed in HEK293 cells.

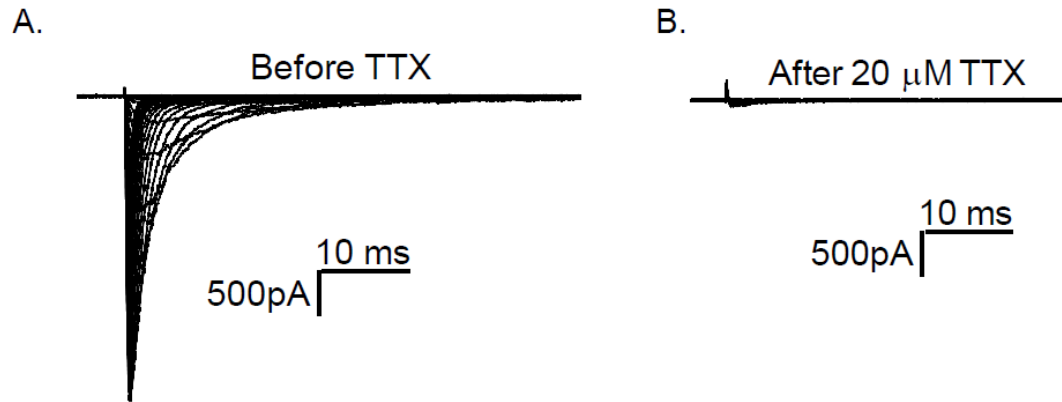


**Figure 11. Endogenous sodium currents in neonatal cardiomyocytes were blocked by TTX at a final concentration of 20  $\mu\text{M}$ .** A. Representative sodium current traces recorded from a neonatal cardiomyocyte without the transfection of recombinant voltage-gated sodium channels. B. Representative sodium current traces from the same cell as in A. After applying 20  $\mu\text{M}$  TTX, the currents carried by the endogenous sodium channels were largely blocked.

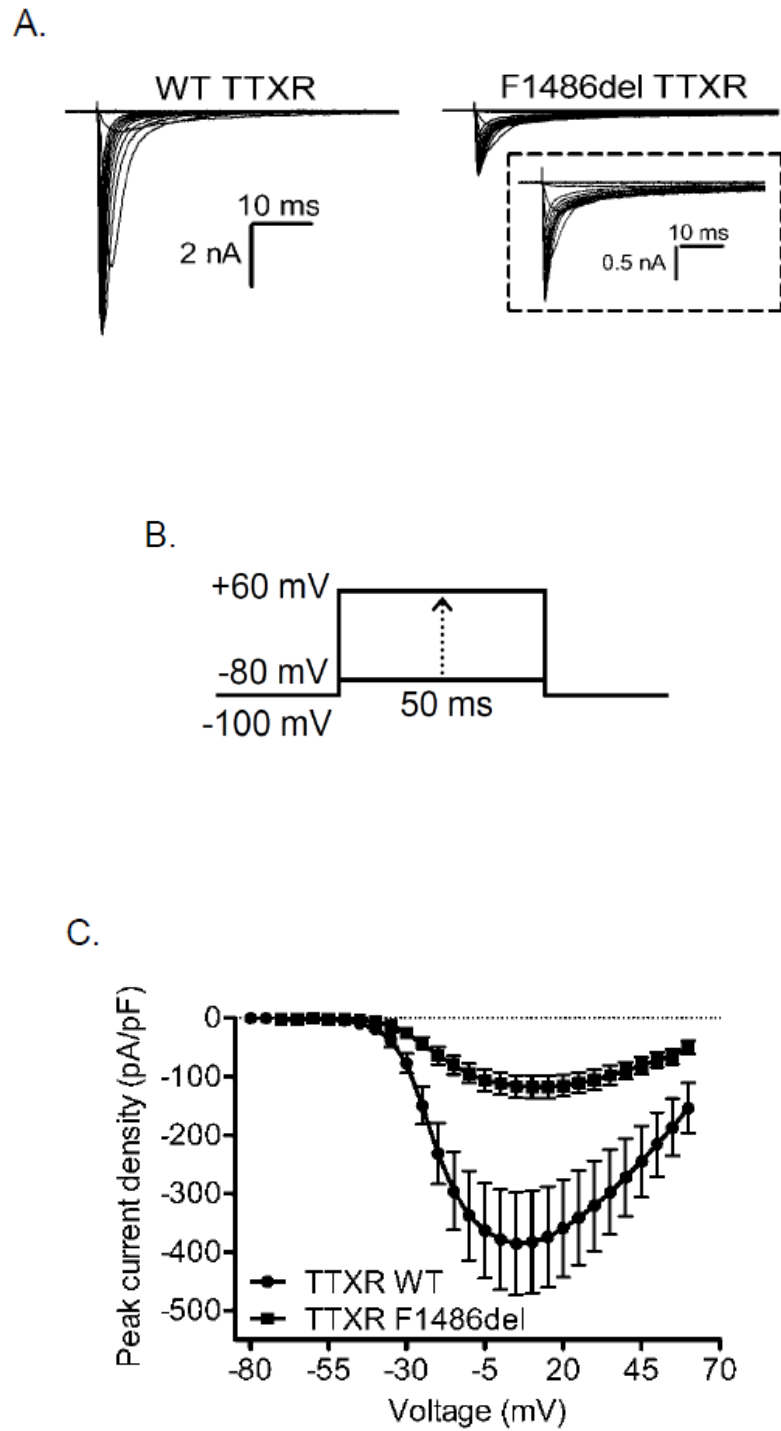


**Figure 12. F1486del results in decrease in membrane current density in neonatal rat cardiomyocytes.** A. Representative sodium current traces

recorded from neonatal cardiomyocytes expressing TTX resistant WT channel (n=12 for TTXR WT), or TTX resistant F1486del channel (n=8 for TTXR F1486del) in the presence of 20  $\mu$ M TTX. B. Test protocols used for the current density measurements; the depolarization voltage step is with a 5 mV increment. C. Mean current-voltage relationships for cardiomyocytes ectopically expressing each type of channel in response to the voltage stimulation.

## **B. Deletion of F1486 decreases sodium channel surface expression in HEK293 cells**

To quantitatively compare the levels of hNav1.5 protein at the cell surface, cell surface biotinylation experiments were performed. Since the cysteine and lysine residues were confirmed to exist in the extracellular loops, we used EZ-link Sulfo-NHS-LC-Biotin reagent to biotinylate the cell surface Nav1.5 protein. HEK293 cells expressing the WT or F1486del mutant proteins were incubated with the cysteine and lysine specific, cell impermeable EZ-link Sulfo-NHS-LC-Biotin reagent. Following cell lysate protein solubilization, the biotinylated protein was precipitated with streptavidin-agarose beads and subjected to electrophoresis and immunoblot reactions with the anti-Nav1.5 specific antibody. The non-fractionated aliquot (5%) of the solubilized protein was electrophoresed in parallel. The surface expression of  $\beta$ -tubulin was used as a control to indicate if there is a cytosolic protein contamination in the reaction. The total blotted  $\beta$ -tubulin protein was blotted in parallel to determine the fraction of sodium channel protein biotinylated by the procedure (Figure 13A). From the western blot analysis, surface expression and the total expression level of Nav1.5 were higher for WT protein (Figure 13A). The analyzed quantitative results indicate that the wild type sodium channel expression at the cell surface was significantly higher than the F1486del mutant protein (Figure 13B). We conclude that F1486del significantly decrease surface expression of the Nav1.5 protein in HEK293 cells, consistent with the data on current density collected using patch-clamp technique.

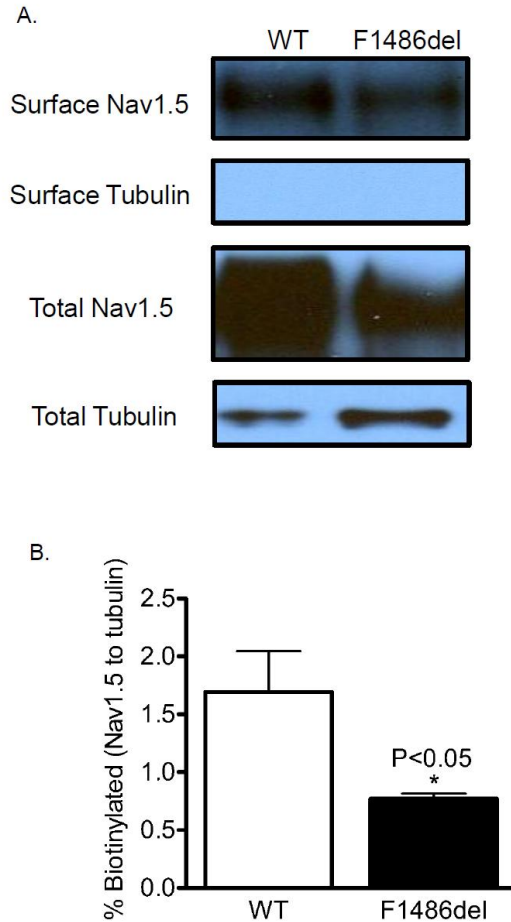


**Figure 13. Deletion of F1486 decreases sodium channel surface expression in HEK293 cells.** HEK293 cells expressing WT or F1486del mutant channel protein were labeled with sulfo-NHS-LC-biotin. 36-48 h post transfection, biotinylated proteins were precipitated with streptavidin-agarose beads. After electrophoresis, hNav1.5 proteins were identified by immunoblot analysis using a polyclonal rabbit Nav1.5 antibody (ASC-005). A. Surface fraction of Nav1.5 protein is higher in cells expressing the WT channel protein. Probe for surface  $\beta$ -tubulin indicates that there is no cytosolic protein contamination for the biotinylation experiment. B. The percentage of biotinylated hNav.15 protein was determined by normalizing the surface biotinylated protein to the total  $\beta$ -tubulin (n=4, performed in quadruplicate). “\*” indicates  $p < 0.05$  compared with WT. Statistic analysis was performed using un-paired student’s t- test.

### **C. Deletion of F1486 augments late sodium current (late $I_{Na}$ ) in HEK293 cells and neonatal rat cardiomyocytes**

In addition to the changes in sodium current density which were observed from the sodium current traces using the depolarizing protocol from -80 mV to +40 mV (for both WT and F1486del mutant channel), sodium current recorded in cells expressing WT channel activated and decayed rapidly (Figure 10A, and 12A). The inactivation was essentially complete during longer test pulses (Figure 10A and 12A). However, the mutant channel displays incomplete inactivation (Figure 10A and 12A). Therefore next we sought to quantify the late sodium current by normalizing the current remaining at the end of 200 ms depolarizing pulses to the peak amplitude derived from the same depolarizing stimulus. At the voltage of -10 mV, there was only 0.67% of the late sodium current remained in HEK293 cells expressing WT sodium channels, and only 0.18% late  $I_{Na}$  left in cardiomyocytes ectopically expressing the WT recombinant sodium channels. In comparison, cells expressing the F1486del mutant channels had incomplete decay of the sodium current. At the end of the 200 ms stimulation pulses, approximately 20.69% of the sodium current remaining in HEK293 cells and 19.8% late  $I_{Na}$  remained in cardiomyocytes. Representative traces of late sodium current recorded at -10 mV from each type of channel are shown in Figures 14A and 15A. At each of the test voltages we studied, the remaining late sodium current was significantly higher in cells expressing F1486del mutant channels than WT channels (Figure 14B and 15B). This relative amount of late current is

substantially higher than that reported with other LQT3 mutations (Wang *et al.*, 1996; Bankston *et al.*, 2007b), which is from ~0.4%.to less than 5%.

The marked increase in  $I_{Na}$  late sodium current by F1486del is consistent with the severe clinical phenotype found by Yamamura *et al.* (2009). We hypothesized that the increase in late sodium current should contribute to the delayed repolarization of cardiac cellular action potentials.

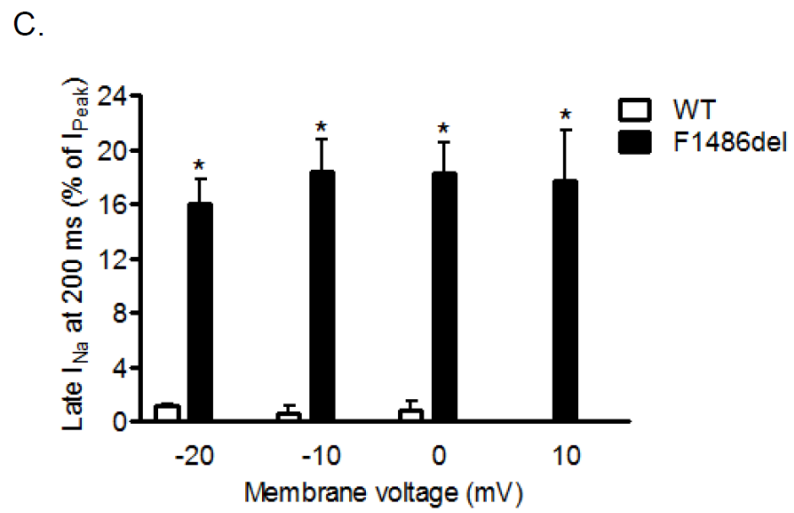
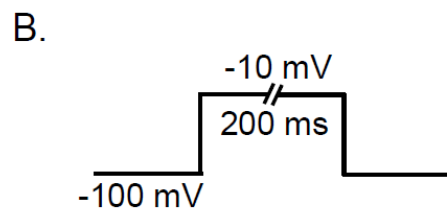
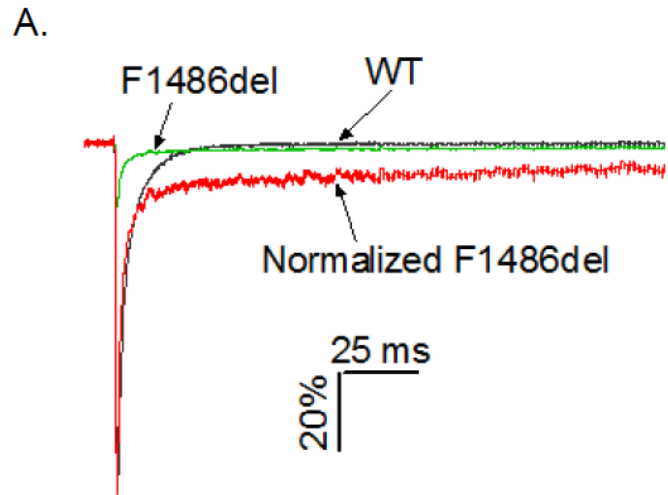


**Figure 14. F1486del augments late  $I_{Na}$  in HEK293 cells.** A. Representative traces of sodium current recorded at -10 mV from HEK293 cells transfected with each gene. The averaged raw data from F1486del mutant and WT channels are indicated in the graph. Augmented late  $I_{Na}$  was shown by normalizing the trace recorded from F1486del mutant channels to the trace recorded from WT channels, and is labeled “normalized”. B. Protocol used in measuring late  $I_{Na}$  shown in panel A. C. Bar graph indicates the summarized percentage of late  $I_{Na}$  (normalized to the peak current amplitude) in HEK293 cells recorded at each tested voltage. “\*” represent  $p < 0.01$ . F1486del mutant channel (n=12) vs.WT channel (n=6).

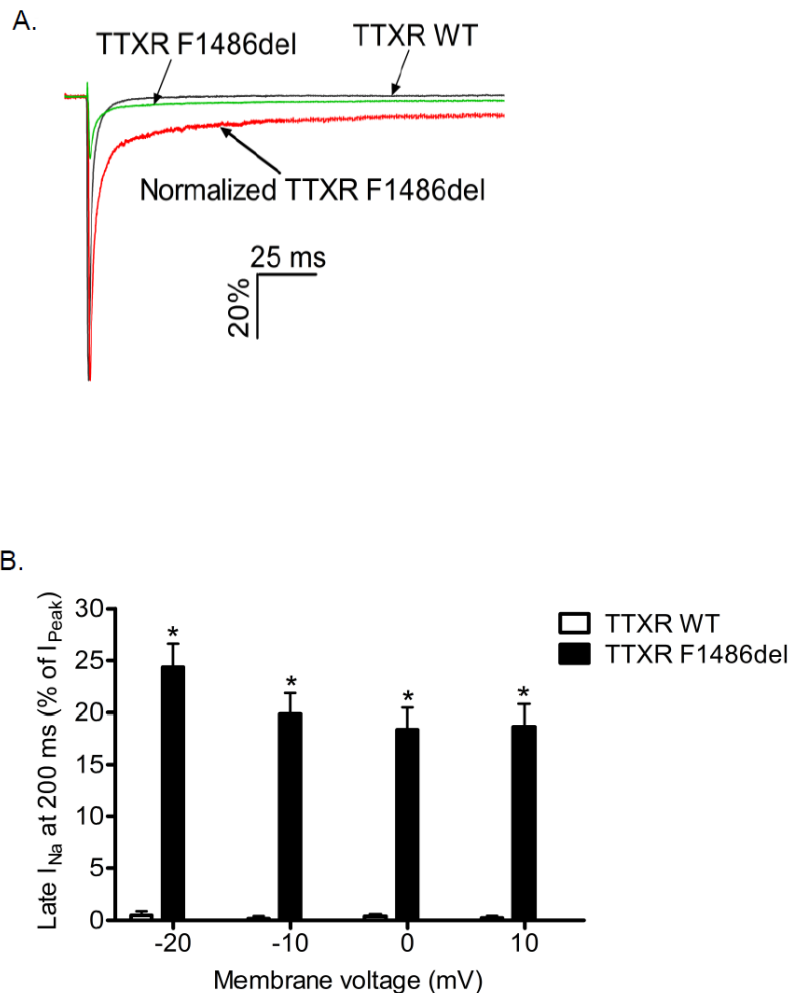


**Figure 15. F1486del augments late  $I_{Na}$  in neonatal rat cardiomyocytes.**

A. Representative traces of the mean sodium current recorded at -10 mV from cardiomyocytes expressing each channel in the presence of 20  $\mu$ M TTX. The trace for F1486del and WT channels are labeled respectively. The line indicating the normalized data from F1486del channels is labeled in the graph. B. Bar graph indicates the averaged late  $I_{Na}$  recorded from neonatal rat cardiomyocytes at each tested voltage in the presence of 20  $\mu$ M TTX. “\*” represent  $p < 0.01$ . F1486del (n=7) channel vs.WT channel (n=6).

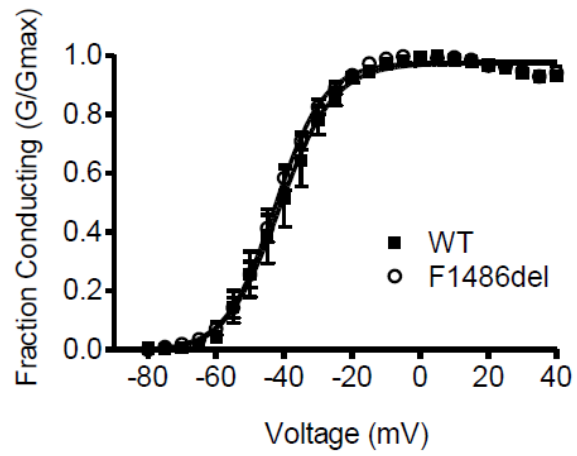
#### **D. F1486del does not alter voltage dependence of activation in both HEK293 cells and neonatal rat cardiomyocytes**

The location of the deletion site within the Nav1.5 inactivation gate (in the linker region between DIII and DIV), and the clinical cardiac phenotype of the patient triggered us to further characterize the mutant channel.

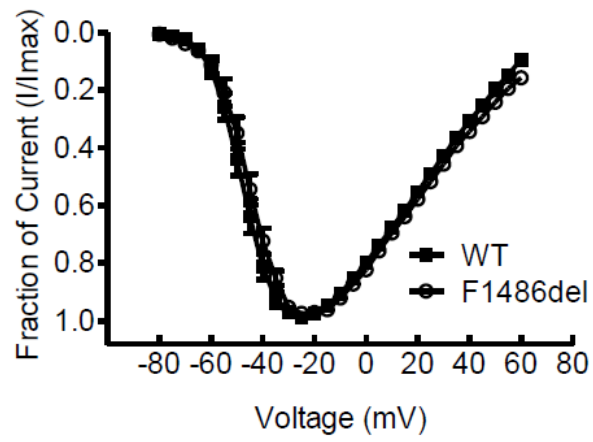
Cells expressing WT *SCN5A* exhibited rapid activation and inactivation in response to a series of depolarizing test pulse from -80 mV to +60 mV, which is typical for voltage-gated sodium channels. The F1486del mutant channel, however, shows a similar profile of fast activation, but with incomplete inactivation throughout the duration of stimulation pulse. The voltage dependence of activation for each type of channel was measured using a series of test pulses ranging from -80 mV to +60 mV with a 5-mV increment. Conductance-voltage (*G-V*) curve analysis revealed that there was no difference in the channel activation profile between these two types of channels (Figure 16A, B, and 17). The midpoint of channel activation and the conductance slope factor of the activation curve were calculated using Boltzmann function. The macroscopic voltage dependence of activation for the WT channel wasn't statistically different from that of the F1486del mutant channel expressed in HEK293 cells (Figure 16A, B and Table 5). Again, we observed a similar voltage dependence of channel activation profile in cardiomyocytes expressing these two types of channel respectively (Figure 17, Table 6). This result is consistent with previous results indicating that mutation of any of the amino acids within IFM motif does not alter the voltage dependence of channel activation in *Xenopus*

*oocytes* (West et al., 1992). The similarity in channel activation kinetics suggests that this mutation does not directly affect gating charge movement.

A.



B.



C.

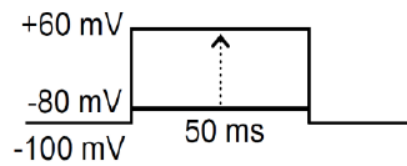


**Figure 16. F1486del does not affect the voltage dependence of Na<sup>+</sup> channel activation in HEK293 cells.** A. Mean steady-state activation curves generated under the 50 ms stimulation pulses from -80 mV to +60 mV with 5 mV increments for WT (n=14, closed squares) and mutant channels (n=13, open circles) that are expressed in HEK293 cells. Data indicate that F1486del does not affect the voltage dependence of activation. Both activation curves were fitted with Boltzmann function. There is no statistic difference in the parameters for steady-state activation. B. The I-V relationship analysis for both WT and F1486del mutant indicates there is no difference in sodium channel activation, since these two curves overlap with each other (n=14 for WT, closed squares; n=13 for F1486del, open circles). C. The protocol used to determine the voltage dependence of activation.

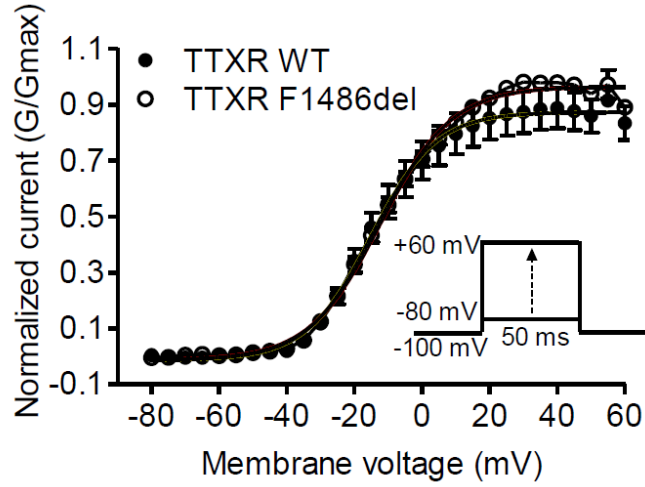


**Figure 17. F1486del does not affect the voltage dependence of Na<sup>+</sup> channel activation in neonatal rat cardiomyocytes.** Mean steady-state activation curve was generated using the same protocol as in the previous figure. n=12 for TTXR WT channel, and n=8 for TTXR F1486del mutant channel. These two activation curves overlap and there is no statistical difference for  $V_{1/2}$  between the two groups. Statistical significance was determined using a Student's unpaired t-test.

Table 5. Voltage-dependent gating parameters for WT and F1486del mutant Na<sup>+</sup> channels in HEK293 cells

	Activation			Inactivation		
	V <sub>1/2</sub> , mV	k, slope	n	V <sub>1/2</sub> , mV	k, slope	n
Wild type	-41.46±0.85	6.45±0.31	14	-82.94±2.99	9.99±1.56	11
F1486del	-42.66±0.46	6.92±0.32	13	-65.98±1.74*	8.69±0.81	16

v<sub>1/2</sub>, voltage at which the channel is half activated or half inactivated; k, slope factor; n, number of cells recorded. The values are presented as mean ± S.E.M. Student's unpaired t-test was used for statistic analysis. "\*" represents p < 0.05.

Table 6. Voltage-dependent gating parameters for WT and F1486del channels expressed in cardiomyocytes

	Activation			Inactivation		
	$V_{1/2}$ , mV	$k$ , slope	$n$	$V_{1/2}$ , mV	$k$ , slope	$n$
Wild type	-14.83±1.58	6.45±0.31	12	-71.66±0.03	7.13±1.16	12
F1486del	-12.02±1.47	6.92±0.32	7	-54.04±0.02*	6.63±0.81	8

$v_{1/2}$ , voltage at which the channel is half activated or half inactivated;  $k$ , slope factor;  $n$ , number of cells recorded. The values are presented as mean  $\pm$  S.E.M. Student's unpaired t-test was used for statistic analysis. "\*" represents  $p < 0.05$

## **E. F1486del does not alter the time constants for channel deactivation in HEK293 cells**

Action potential duration could also be regulated by the rate of transition from the open activated state to the close resting state, a gating process referred to as “deactivation”. Mediated by the integrated returning of the S4 “voltage sensor” to a primed position (Oxford, 1981; Kuo & Bean, 1994; Featherstone *et al.*, 1998), deactivation can affect cell excitability (Sheets *et al.*, 2007). Based on this idea, we attempted to evaluate the time constant of deactivation for both WT and the mutant channel. The analysis for the time constant for deactivation indicated that the F1486del mutant channel takes similar time to transition out of the open activated state as the WT channel. Therefore, there is no difference in the time constant and rate of deactivation between F1486del and WT channels (Figure 18).

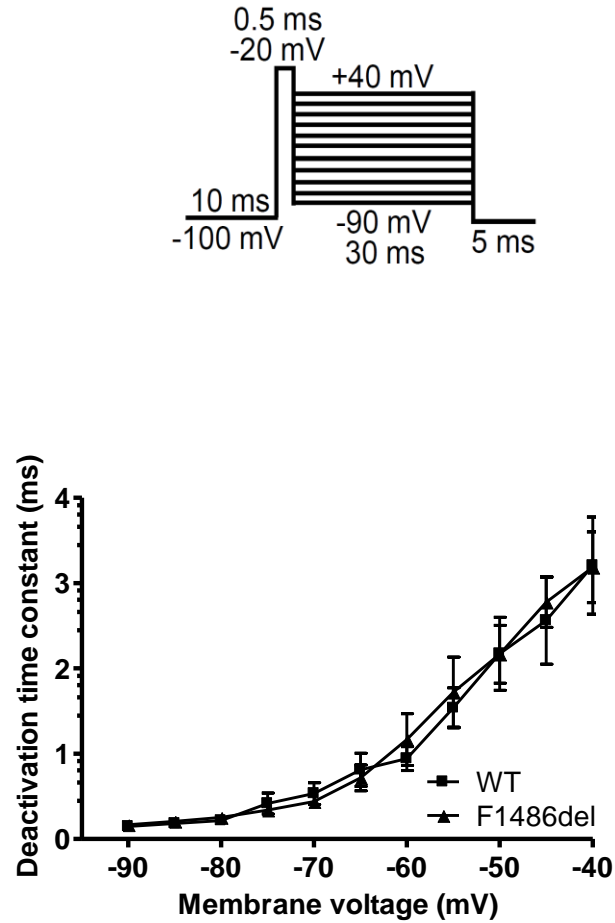


**Figure 18. F1486del does not alter the time constants of channel deactivation in HEK293 cells.** The upper panel illustrates the protocol used for testing channel deactivation time constants in HEK293 cells. Changes in channel deactivation for the F1486del channels determined under a range of membrane potentials by observing tail current properties. The lower panel indicates there is no difference in deactivation between F1486del and WT sodium channels at test voltages.

## **F. Multiple biophysical consequences of the F1486del may lead to delayed repolarization and APD prolongation**

The IFM motif in a neuronal form of sodium channel Nav1.2 has been demonstrated to be critical for channel inactivation. Triple mutation of these three amino acids to glutamine (Q) in Nav1.2 has been shown to slow the rate of channel inactivation in *Xenopus oocytes* (West *et al.*, 1992). In our study, deletion of F1486 increased the persistent late sodium current. Based on this observation, we next tested the hypothesis that deletion of amino acid of Phe on Nav1.5 could alter the voltage dependence of channel inactivation. In our experimental system using both HEK293 cells and cardiomyocytes, we observed a rightward shift of the steady-state fast inactivation curve for the mutant channel (Figure 19A), which suggests that inactivation was disrupted by deletion of F1486. When expressed in HEK293 cells, the F1486del mutation caused a +16.96 mV depolarizing shift in the  $V_{1/2}$  of channel availability (WT:  $V_{1/2} = -82.94 \pm 2.99$  mV,  $n=14$  and F1486del:  $V_{1/2} = -65.98 \pm 1.74$ ,  $n=13$ ;  $p < 0.01$ , Student's unpaired t-test) with little or almost no change in the slope factor of the fitted Boltzmann current-voltage relationships (WT:  $k$  slope =  $6.45 \pm 0.31$ ,  $n=14$  and F1486del  $k$  slope =  $6.92 \pm 0.32$ ,  $n=13$ ;  $p > 0.05$ , Student's unpaired t-test). In cardiomyocytes, the F1486del mutant channel caused a +17.13 mV depolarizing shift in the  $V_{1/2}$  of channel availability and a statistical difference in the slope factor (Figure 21A, Table 6). The  $V_{1/2}$  of inactivation is defined as the voltage at which 50% of the channel population has transitioned to a non-conducting inactivated state. The fraction of the available channels was almost zero when the prepulse potential

was close to and above -40 mV for WT channels (Figure 21A, and 23A). By contrast, nearly 20% of the mutant channels were still available when the cells were prepulsed to -40 mV (Figure 19A, and 21A).

Overall, the F1486del mutant channel has a clear defect in transition to the closed inactivated state. The marked increase in  $V_{1/2}$  toward positive potentials, the rightward shift of the inactivation curve, and the incomplete inactivation of the mutant channel are consistent with increased mutant channel activity, which may explain the prolongation of action potentials.

Destabilization of the inactivated state can affect the region in the voltage-conduction relationship curve where steady-state channel activation and inactivation overlap. This destabilization will result in an increased probability of channel re-opening at the membrane potential close to the resting potential. Therefore, the destabilization can develop persistent “window currents” (Hodgkin & Huxley, 1952b). The window current is thought to result from the opening of non-inactivated sodium current, so called “persistent  $I_{Na}$ ”. The depolarizing shift of the inactivation resulted in a bigger window current when the F186del mutant channel is expressed in both HEK293 cells and cardiomyocytes (Figure 20, and 22).

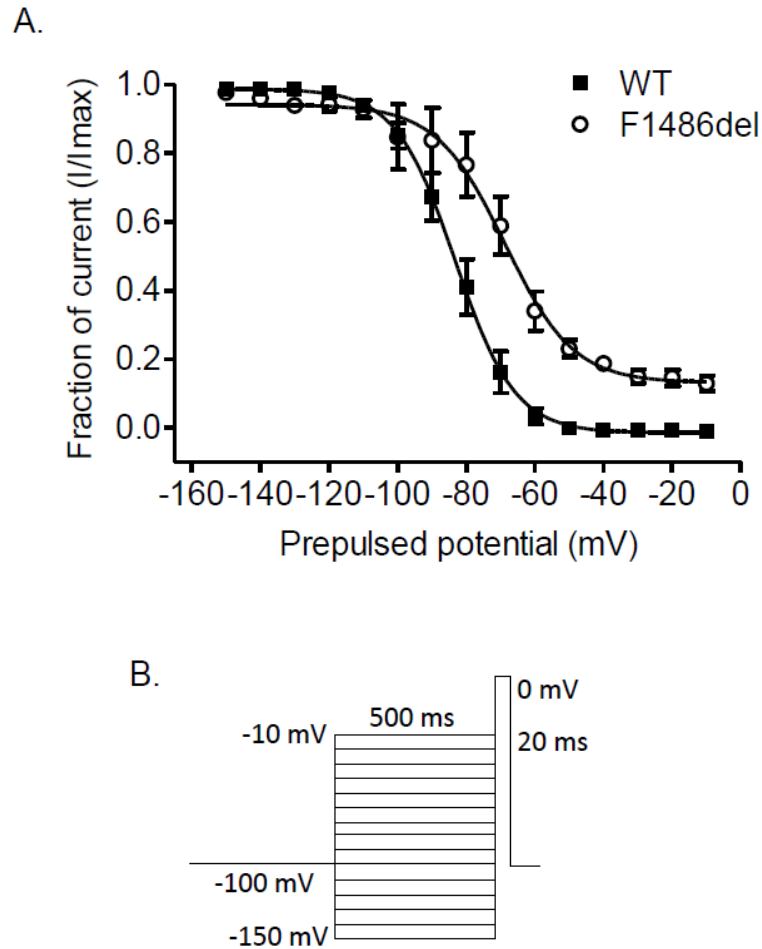


**Figure 19. F1486del causes a depolarizing shift in the voltage dependence of inactivation in HEK293 cells.** A. The steady-state fast inactivation curve for F1486del channels (open circles,  $n=16$ ) is shifted toward more positive potentials compared to the curve for wild type channel (filled squares,  $n=11$ ). The channels that remain available after each inactivating prepulse were evaluated by the peak current amplitude produced during a test pulse to  $-10$  mV for 20 ms. B. The protocol that was used to study steady-state inactivation of sodium channels is illustrated. Cells were held at  $-100$  mV and stepped to an inactivating repulse ( $-150$  mV to  $-10$  mV) for 500 ms.

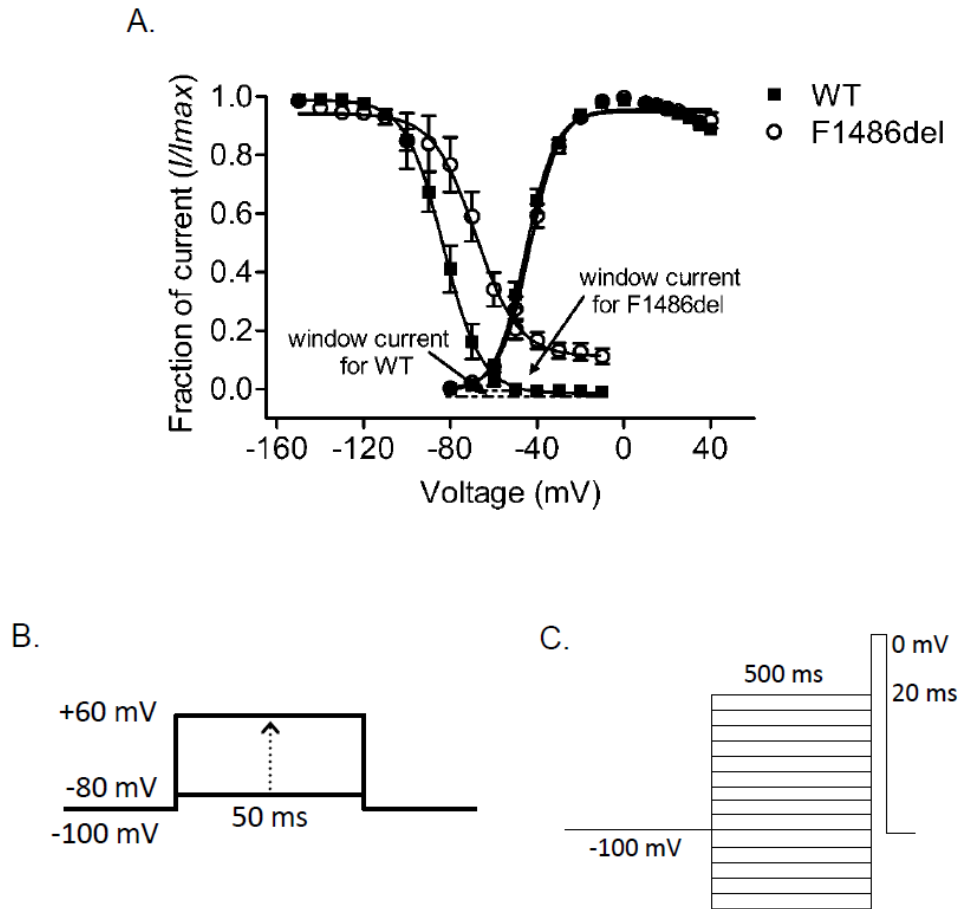


**Figure 20. F1486del increases window sodium current in HEK293 cells.** The window current is represented by the area which is created by the overlap of steady-state activation and steady-state fast inactivation curves. A. The shaded region represents the window current generated by WT hNav1.5 channels. Since the activation curves for both WT ( $n=14$ ) and F1486del ( $n=13$ ) channels overlap with each other, the shaded region plus the blank area (underneath both the activation curve and the inactivation curve for F1486del) represent the window current generated by F1486del sodium channels, which is indicated by the arrow line. Window current measurement indicates that F1486del channels expressed in HEK293 cells conduct more non-inactivating sodium current.  $N=11$  for WT steady-state inactivation curve, and  $n=16$  for F1486del steady-state inactivation curve. B, and C. Protocols used to analyze the steady-state window current are illustrated.

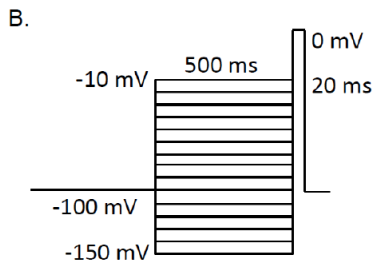
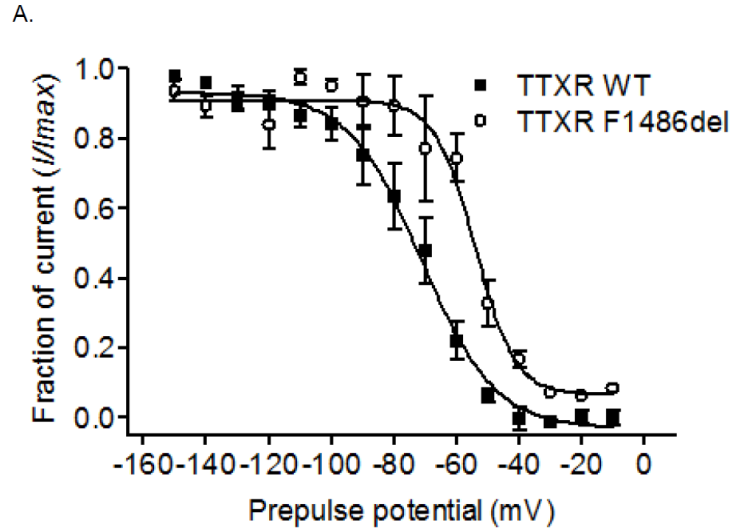


**Figure 21. F1486del causes a depolarizing shift in the voltage dependence of inactivation in neonatal rat cardiomyocytes.** A. The F1486del causes a +17.13 mV depolarizing shift in the steady-state availability curve. Data shown for TTXR WT (closed squares, n=15) and TTXR F1486del (open circles, n=18) channels. B. The protocol that was used for the study of steady-state inactivation of sodium channels is illustrated.

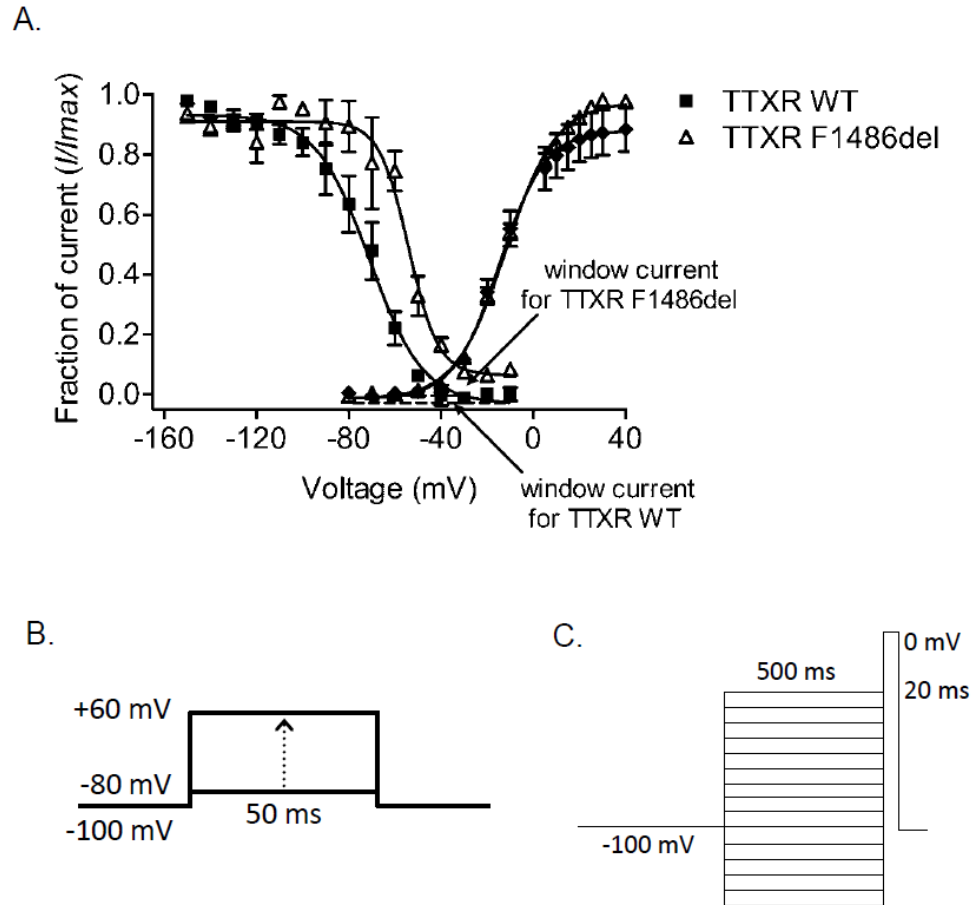


**Figure 22. F1486del causes an augmentation of window sodium current in neonatal rat cardiomyocytes.** A. The window current is indicated by the overlapping area covered by the steady-state activation and the steady-state inactivation curves. The shaded region represents the window current generated by TTXR WT hNav1.5 channels. Since the activation curves for both TTXR WT (closed squares,  $n=12$ ) and TTXR F1486del (open triangles,  $n=7$ ) channels overlap with each other, the shaded region plus the blank region (underneath both the activation curve and the inactivation curve for TTXR F1486del) represent the window current generated by TTXR F1486del hNav1.5 channels, which is indicated by the arrow line. Data indicates that TTXR F1486del channels

carry a significant larger non-inactivating window current. N=15 for TTXR WT steady-state inactivation curve, and n=18 for TTXR F1486del steady-state inactivation curve. B, and C. Protocols used to study the steady-state window current are illustrated.

## **G. F1486del leads to the increased time constants for recovery from inactivation**

Since inactivation is not the only factor that can alter the action potential duration, we further tested for the effects of the F1486del on the time constants of recovery from inactivation. The time constants of recovery from inactivation was investigated using a 100 ms conditioning pulse -10 mV to induce channel inactivation followed by a recovery pulse after returning to -120 mV for various durations and then a test pulse to -10 mV to assess the fraction of channels that had recovered from inactivation. Data from these experiments were fitted by the two-exponential function. The averaged time constant for channels to recover from inactivation was significantly different between these two groups. F1486del channels took a significantly longer time to recover from inactivation ( $\tau_{-120} = 70.20 \pm 14.55$ ,  $n=7$ ), while the WT channels recover much quicker from inactivation ( $\tau_{-120} = 14.58 \pm 1.38$ ,  $n=4$ ;  $p < 0.01$ , student's unpaired t-test). The F1486del slows the speed by which sodium channels recover from inactivation to the available (resting, closed) state. This result indicates that the F1486del mutant channel undergoes a slower transition process from the inactivated state to the resting state. The IFM motif forms a hydrophobic particle which binds to its receptor, the inactivation gate. We hypothesized that by deleting one hydrophobic amino acid, F1486, the hydrophobic strength is decreased thus the particle difficult to bind to or easy to come off from its receptor. Surprisingly, the channel paradoxically shows impaired inactivation as well as slower recovery from inactivation.

## **H. F1486del produces augmented ramp current in both HEK293 cells and neonatal rat cardiomyocytes**

The relatively slow transitions of sodium channels to closed-state inactivation are considered to produce ramp current in response to slow depolarizing voltage ramps at hyperpolarized potentials close to resting membrane potential (Cummins *et al.*, 1998; Rush *et al.*, 2006). Furthermore, the ramp current has been thought to contribute to action potential firing threshold and cellular excitability (Crill, 1996). Therefore, we sought to examine ramp currents in cells expressing either WT or F1486del channels. A broad duration of positive ramp voltages (0.28 mV/ms) was given to HEK293 cells expressing either WT or mutant channels. In response to the positive voltages, WT channels carry inward sodium current, but this conduction was only sustained over a narrow voltage range. By contrast, the F1486del mutant channels conduct over a broader range of voltages. A significant increase in the current amplitude of the ramp currents elicited especially at more depolarized potentials for the mutant F1486del channels was observed (Figure 23, 24). The ramp current generated in response to 500 ms slow depolarizing test pulse by the mutant channel was increased by 86.88% compared to the WT channel. There was a significant difference between these two types of channels regarding the averaged normalized ramp current (normalized to the peak current) (Figure 23A, 24A). In addition, the mutant channels showed delayed inactivation toward positive potential stimuli and never completely inactivated at the end of the voltage ramp when compared to WT channels (Figure 23A, 24A). The comparison of the

averaged normalized ramp current is shown in Figure 23B, and 24B. The characteristics for the ramp current generated by the F1486del mutant channel revealed an impaired transition to a non-conducting state. This increase in ramp current might reflect similar mechanisms that contribute to the increase of late current.

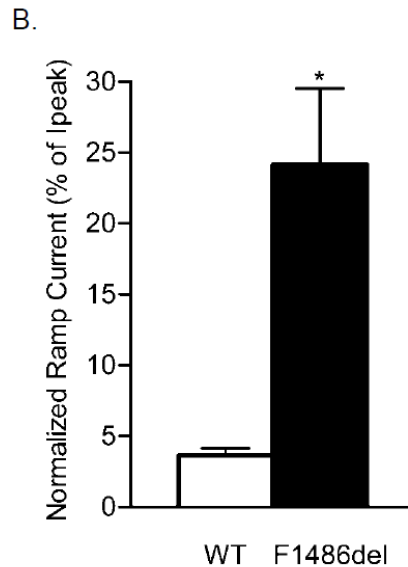
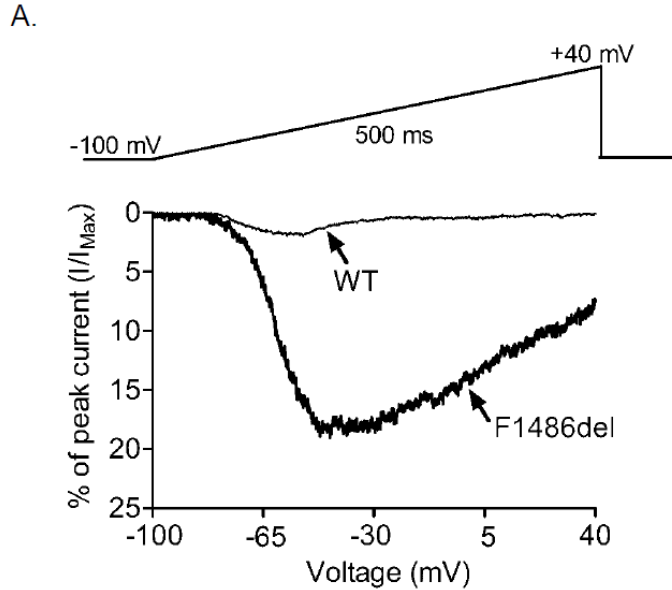
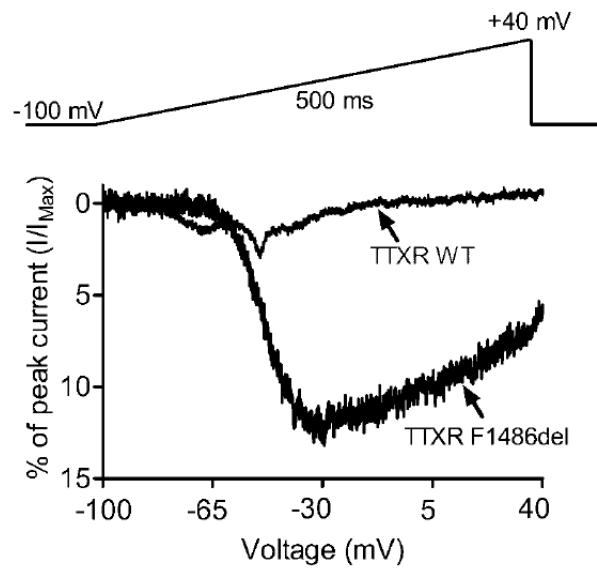


**Figure 23. F1486del increases ramp current in HEK293 cells.** A. Averaged normalized WT (n=10) and F1486del (n=10) ramp currents in response to a ramp protocol of 500 ms with a voltage from -100 mV to +40 mV. Data demonstrate that F1486del enhances inward sodium current within a broad range of membrane voltage. B. Bar graph interpretation of averaged ramp current as a percentage of peak transient current during the slow depolarizing ramp stimulus

for all channels examined in this study. (n=10 for WT, n=10 for F1486del). Ramp current amplitude is presented as a percentage of the peak transient current elicited with a standard *I-V* protocol. Unpaired student's t-test was used for data analysis. "\*" indicates  $p < 0.001$ .

A.



B.

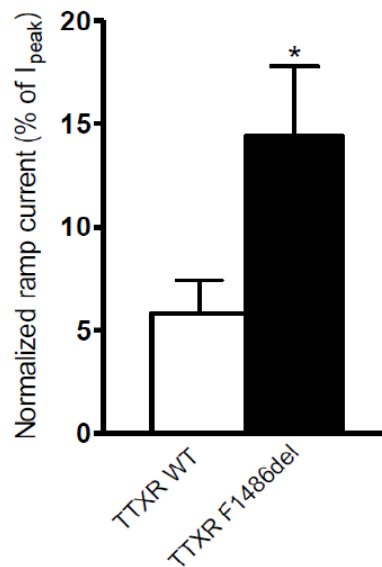


**Figure 24. F1486del causes an augmentation of ramp current in neonatal rat cardiomyocytes.** A. Averaged normalized ramp current elicited in response to a slow depolarizing stimulus for TTX-R WT (n=6) and F1486del (n=4) channels from -100 mV to +40 mV during 500 ms with a holding potential of -100mV. Data

demonstrate TTX-R F1486del enhances inward sodium ramp current. Ramp current was normalized to the peak current amplitude elicited with a standard *I-V* protocol. B. Bar graph interpretation of percentage peak current during the slow depolarizing ramp stimulus for all channels examined in this study. (n=6 for TTX-R WT, n=4 for TTX-R F1486del). Ramp current amplitude is presented as a percentage of the peak transient current elicited with a standard *I-V* protocol. Unpaired student's t-test was used in statistical analysis. "\*" indicates  $p < 0.001$ .

## **I. F1486del on hNav.15 prolongs APD and generates EADs in neonatal neonatal rat cardiomyocytes**

As the slow inactivating component of sodium current, late  $I_{Na}$  is a depolarizing current that increases the duration of the ventricular action potential (Kiyosue & Arita, 1989; Bennett *et al.*, 1995). In our studies, we observed the augmentation of sustained late  $I_{Na}$  by the F1486del mutation. The proband identified by Yamamura and his colleagues presented a severe cardiac arrhythmia with an extreme prolonged corrected QT interval (as long as 860 ms). Based on our experimental results, we hypothesized that the LQTs manifested in the patient was caused by the APD prolongation, which was subsequent to increased late  $I_{Na}$ . To further explore the functional consequence of deleting F1486, we chose to use primary neonatal rat cardiomyocytes as an expression system to study action potential profiles. Since the proband carried the heterologous deletion of hNav1.5 F1486 on one allele, we chose to study the function of the mutant channel in the presence of the endogenous sodium channel. Therefore, no TTX was added in this set of experiments. Representative action potential traces are shown in Figure 27A. Cardiomyocytes carrying the heterologously expressed WT sodium channel had an averaged APD of 88.9 ms, which is typical for neonatal cardiomyocytes (Figure 25A, and 25B). In contrast, cells expressing the F1486del mutant channel had a very significant prolongation of the action potential duration (Figure 25A and B, averaged APD 1001.0 ms,  $p < 0.0001$  compared to WT). In this study, the early phases of the action potential repolarization was indicated by  $APD_{30}$ , while the final steady-state repolarization

phase of the action potential repolarization was indicated by APD<sub>50</sub>, APD<sub>80</sub> and APD<sub>90</sub>. During each stage of the action potential repolarization phase, there were significant differences between these two groups (Figure 25C). We also observed the decrease in sodium current density and increase in late sodium current in cardiomyocytes expressing the mutant channel which were consistent with our findings using HEK293 cells. An increase in late I<sub>Na</sub> has been shown to be followed by sequential appearance of EADs (Song *et al.*, 2008), early afterdepolarizations that usually happen during the early phase of the action potential repolarization. In our experimental system with rat cardiomyocytes, we were interested in exploring whether increased late I<sub>Na</sub> induced by the channel mutation would facilitate occurrence of EADs, which are commonly associated with bradyarrhythmia-triggered arrhythmic activity (Clancy *et al.*, 2002). In cardiomyocytes expressing the mutant recombinant channel, we observed a series of spontaneous EADs in 33.3% of the cells we studied (4/12) (Figure 26). In contrast, cells expressing the WT recombinant channel mostly carry the normal profile of the action potential, with no observed EADs (0/22) (Figure 26). We predict that the APD prolongation, as a result of increased late I<sub>Na</sub>, causes the occurrence of EADs, and leads to the subsequent bradycardia-induced arrhythmia. We also predict that the APD prolongation is due to the deficit in inactivation.

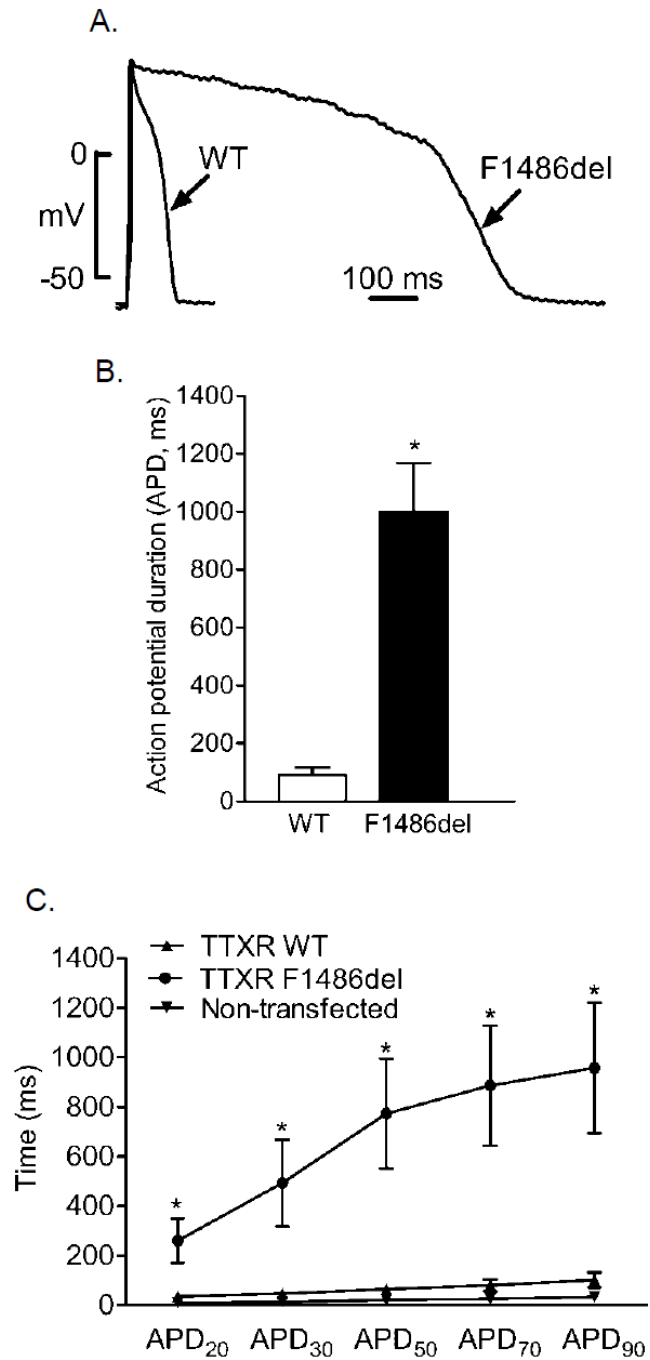


**Figure 25. hNav1.5 F1486del prolongs APD in neonatal rat cardiomyocytes.**

A. Representative traces for neonatal rat cardiomyocytes expressing either WT or F1486del channels. B. Averaged data analysis for the APD measurement.

Cardiomyocytes expressing the WT recombinant channel have an averaged APD of  $88.87 \pm 28.63$  ms ( $n=12$ ); whereas the averaged APD for cells expressing the F1486del channel is  $1001 \pm 167.1$  ( $n=11$ , \*  $p < 0.0001$ ). Data was analyzed using Student's unpaired t-test. C. Averaged APDs (APD at 20%, 30%, 50%, 70%, and 90% repolarization (APD<sub>20</sub>, APD<sub>30</sub>, APD<sub>50</sub>, APD<sub>70</sub>, and APD<sub>90</sub>, respectively) indicate that cells expressing the mutant channels take significantly longer time to repolarize to the resting membrane potential. Data was shown as mean  $\pm$  SE.  $n=15$  for WT,  $n=7$  for F1486del and  $n=5$  for non-transfected cells. "\*"  $p < 0.001$ , cells expressing F1486del channel vs. the other two types of channel. There is no statistical significance in APD analysis between cells expressing WT recombinant channels and non-transfected cells expressing endogenous sodium channels. Data was analyzed by one way ANOVA plus Bonferroni posthoc test.

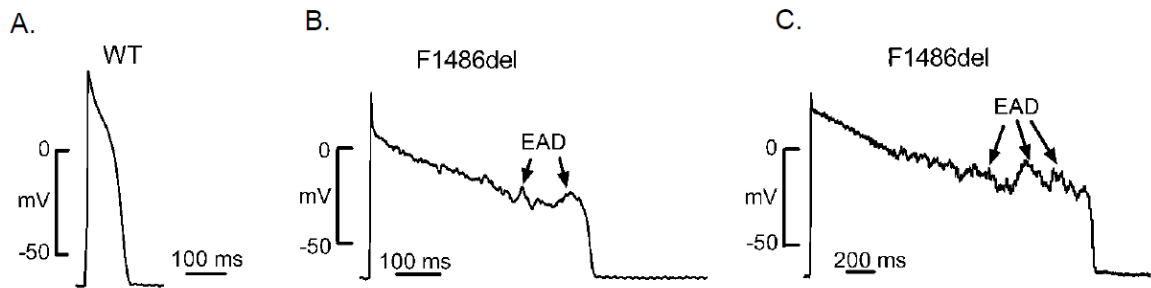


**Figure 26. Cardiomyocytes expressing F1486del mutant channels presented with spontaneous EADs.** A. A representative recording from a neonatal cardiomyocyte expressing the WT channels. One single current injection was given to the cell for 2.5 ms. The APD was within the normal range. There was no EAD observed. B, and C. Representative traces from two individual cells expressing the F1486del channels. Cells were also injected with one single current injection for 2.5 ms. Cells present not only prolonged APD, but prominent EADs, which may lead to LQTS and further trigger electrical activity.

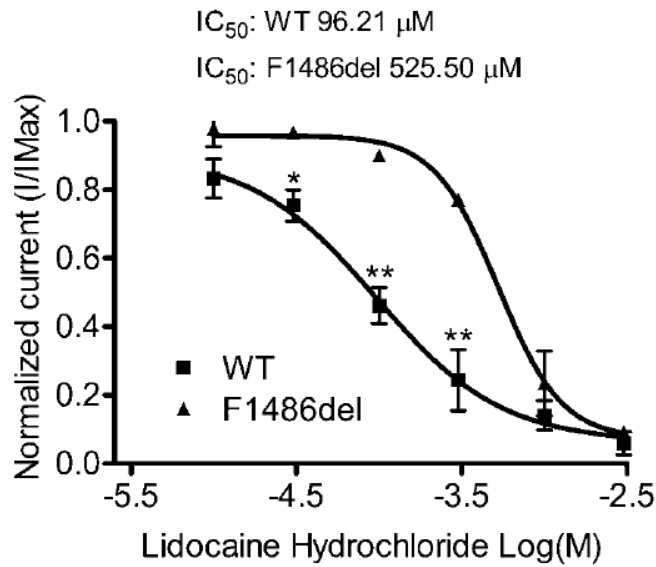
## **J. F1486del attenuates the response to antiarrhythmic drug lidocaine in HEK293 cells**

The poor response of the infant patient carrying mutant F1486del channels to therapeutic treatment with lidocaine (Yamamura *et al.*, 2009) and the location of the mutation site led us to determine: whether deletion of F1486 could modify the sensitivity of the sodium channel to the antiarrhythmic drug lidocaine?

As a local anesthetic and antiarrhythmic drug, lidocaine interferes with impulse conduction by binding to the inner pore of voltage-gated sodium channels to block the current (Hille, 2001). Experimental evidence suggests that local anesthetics can bind to the sodium channel in resting, open and inactivated states, but preferentially binds to the open and/or inactivated VGSCs (Hille, 1977; Hondeghem & Katzung, 1977; Yeh, 1978; Bean *et al.*, 1983). In order to examine the ability of lidocaine to inhibit channels in the resting state, cells expressing Nav1.5 channels were held at -120 mV for 10s (to allow all channels to move to the resting state) and then depolarized to 0 mV for 20 ms to elicit the current. Different concentrations of lidocaine were applied to the cells to test its inhibitory effect on sodium channel. Peak current amplitude was evaluated before and after application of lidocaine hydrochloride (10-3000  $\mu$ M; n = 3-5). Data points from each concentration that we studied were fitted to a dose-response curve (Figure 27A). The IC<sub>50</sub> (estimated by fitting the data points to a dose-response curve) of WT channel was 96.21  $\mu$ M, and was 525.50  $\mu$ M for mutant channel, suggesting that the F1486del decreases the sensitivity of the channel to lidocaine (Table 7). Representative traces recorded when cells expressing the WT and F1486del

mutant channels were treated with 100  $\mu$ M lidocaine are shown in Figure 28. Since the location of the F1486 site is essential for steady-state inactivation, we then compared the inhibitory effects of lidocaine on the inactivated channels for both WT and F1486del mutants. The ability of lidocaine to interact with inactivated channels was examined by holding cells expressing Nav1.5 channels at -50 mV for 10s (to allow channels to move to inactivated states) and then stepping the voltage to -120 mV for 100 ms (channels without drug bound would recover from fast inactivation). Finally, the cells were depolarized to 0 mV for 20 ms to elicit currents and measure channel availability. Peak current was also measured before and after application of lidocaine (10-1000  $\mu$ M; n = 3-6). Fits to the dose-response curve revealed that the IC<sub>50</sub> for lidocaine on inactivated WT Nav1.5 channels is 17.12  $\mu$ M (Figure 29, Table 7). Although WT channels did respond to lidocaine hydrochloride in a dose-response manner in the inactivated state, the F1486del mutant channel does not respond to lidocaine in the inactivated state, even at 1 mM drug concentration (Figure 29, 30). Therefore, it is possible that deletion of F1486del induces a channel conformational change that prevents lidocaine from binding. Putting these together, we hypothesize that the poor response of the patient to lidocaine is caused by the deletion of F1486 on Nav1.5.

A.



B.

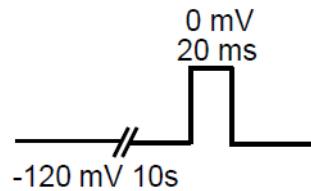


**Figure 27. Dose-response curve for the inhibitory effect of lidocaine on hNav1.5 WT and F1486del channels in the resting state.** A. hNav1.5 WT or F1486del mutant channels are expressed in HEK293 cells. F1486del causes a rightward shift of the concentration-response curve for the F1486del mutant channel, which indicates that deletion of F1486 attenuates the pharmacological effect of lidocaine on the sodium channel in the resting state. Data are presented as averaged normalized peak current  $\pm$  S.E.M (\*  $p < 0.05$ , \*\*  $p < 0.01$ ). The peak current amplitude after drug treatment was normalized to that before drug treatment. Data were fitted with Sigmoidal dose-response curve with variable slopes ( $R^2 = 0.97$  for F1486del,  $R^2=0.86$  for WT). 3-8 individual recordings were collected for each dose. B. Protocol used for testing the inhibitory effects of lidocaine on sodium channels in the resting state is illustrated.

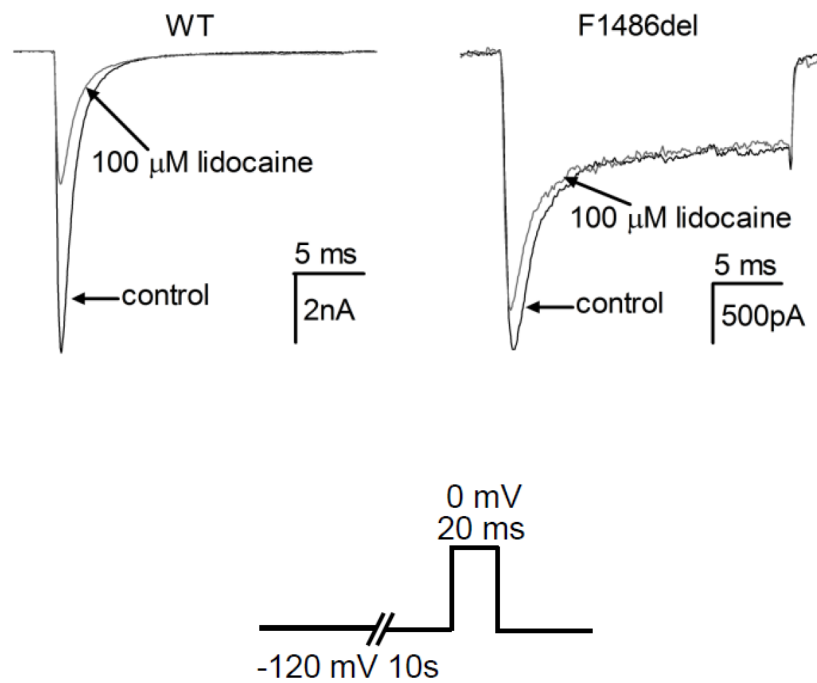


**Figure 28. Deletion of F1486 attenuates the effect of 100  $\mu$ M lidocaine on sodium channels in the resting state.** Representative traces recorded from HEK293 cells expressing the WT and F1486del mutant channels in the presence of 100  $\mu$ M lidocaine under the protocol for testing the inhibitory effect of lidocaine on resting-state channels. 100  $\mu$ M lidocaine has a differential effect on WT and F1486del mutant hNav.15 channels. The protocol used in this study is shown in the lower panel.

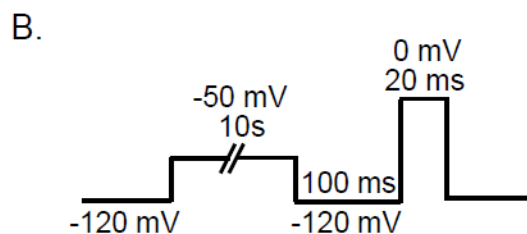
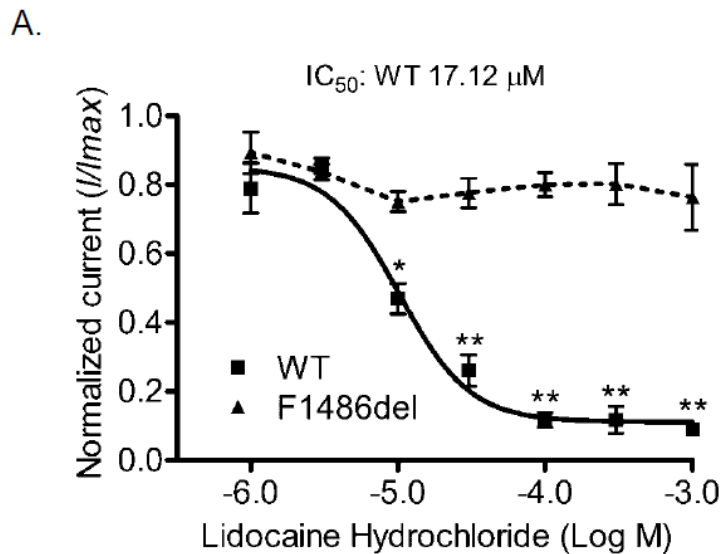


**Figure 29. Dose-response curve for the inhibitory effect of lidocaine on inactivated hNav1.5 channels.** A. The peak current amplitude after drug treatment was normalized to that before drug treatment. Only the data collected from WT channel can be fitted with Sigmoidal dose-response curve ( $R^2 = 0.92$ ,  $IC_{50} = 17.12 \mu\text{M}$ ). Data are presented as averaged normalized peak current  $\pm$  S.E.M (\*  $p < 0.01$ , \*\*  $p < 0.001$ ). The dotted line was drawn to manually connect the F1486del data point and serves as a guide to visualize the data. 3-8 individual recordings were collected for each dose. B. Protocol used for testing the inhibitory effects of lidocaine on sodium channels in the inactivated state is illustrated.

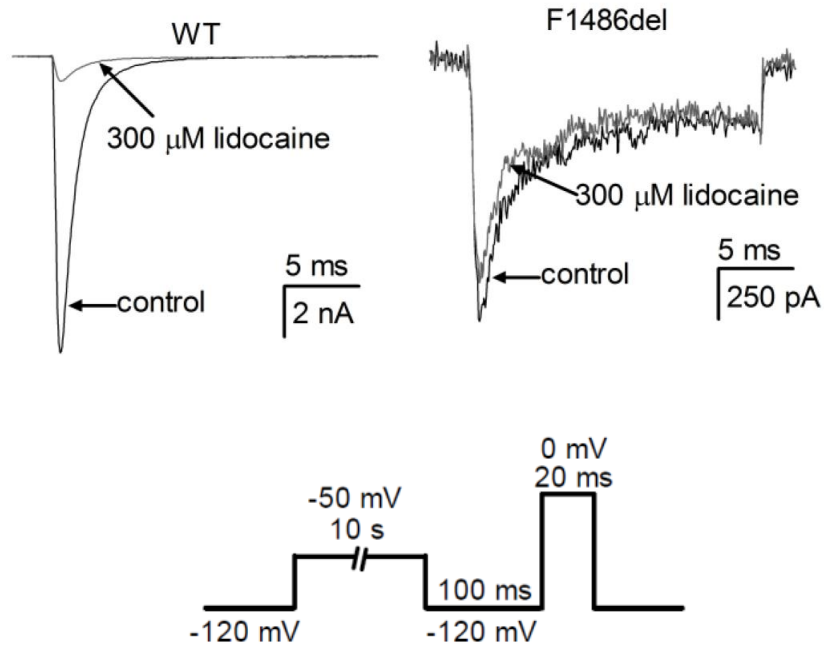


**Figure 30. F1486del reduces the effect of lidocaine on sodium channels in the inactivated state.** The upper panel shows representative traces recorded when cells expressing the WT and F1486del channels were treated with 300  $\mu\text{M}$  lidocaine, and tested for the inhibitory effect of lidocaine on inactivated channels. Voltage protocol for testing current amplitude generated after drug binding to the inactivated channel is diagramed in the lower panel.

Table 7. Summary of IC<sub>50</sub> values estimated for lidocaine inhibition of hNav1.5 channels in different states

<b>IC<sub>50</sub> (μM)</b>	<b>Resting State</b>	<b>Inactivated State</b>
<b>WT</b>	96.21	17.12
<b>F1486del</b>	525.50	N/A

## SUPPLEMENTAL RESULTS

### **K. Sodium channel mutation G1481E within the intracellular loop between DIII-DIV of hNav1.5 increases peak current density in HEK293 cells**

The location of G1481 is similar to the F1486 since both of these amino acids are located in the intracellular loop between DIII and DIV. Previously, it was shown that specific mutations within intracellular loop III are associated with LQT3 syndrome (Bankston *et al.*, 2007b; Ruan *et al.*, 2010). In a large group of cohort studies, a large cohort of consecutive, unrelated patients referred for long-QT syndrome were screened for mutations of LQTS related genes by Mayo Clinic from August 1997 to July 2004 (Tester *et al.*, 2005). A polymorphism was found at nucleotide 4442 where a G to A mutation was observed in a patient with LQT3. This change in nucleotide generates a G1481E mutation. Five amino acids upstream of F1486, the G1481E might be able to alter the electrophysiological function of hNav1.5, and lead to LQT3 syndromes. Thus, the hypothesis for studies on G1481E was formed: G1481E mutation on hNav1.5 could affect the electrophysiological function of cardiac sodium channel hNav1.5, and lead to LQT3 syndromes. Based on this hypothesis, several electrophysiological parameters of hNav1.5 G1481E were fully characterized. For this study, the expression system utilized is the HEK293 cell line. Transient transfection of sodium channel  $\alpha$  subunit,  $\beta_1$  subunit and EGFP were performed. First of all, the current density was investigated to explore if there is any change in the current density when G1481 is mutated to glutamine. Unlike the F1486del mutation

channel, G1481E mutation increases the peak current density (Figure 31). So far, the exact mechanism underlying this increase is unknown.

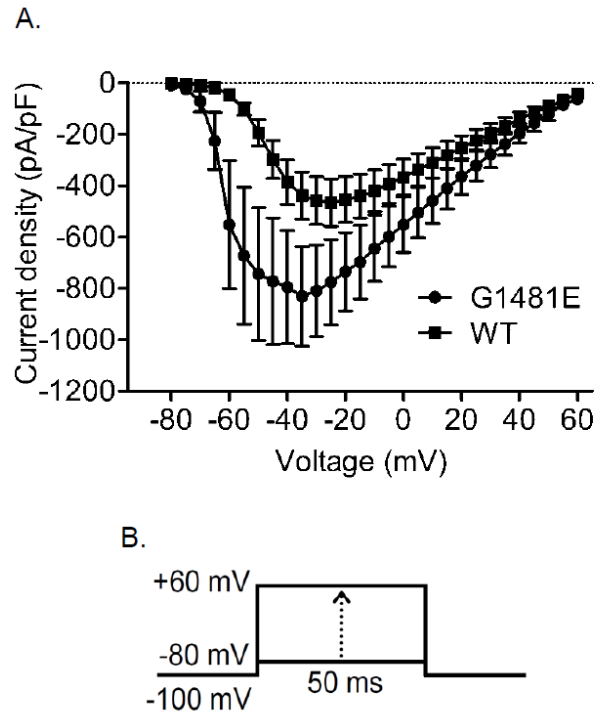


**Figure 31. Sodium channel mutation G1481E within the intracellular loop between DIII-DIV of hNav1.5 increases peak current density in HEK293 cells.**

A. Mean current-voltage relationships recorded in response to 50 ms stimulation pulse from -80 mV to +60 mV (5 mV increment) for WT (n=14, closed squares) and G1481E (n=7, closed circles) mutant channels expressed in HEK293 cells.

B. Test protocols used for the current density measurements. The depolarization voltage step is with 5 mV increment.

## **L. G1481E mutation causes a leftward shift of the steady-state activation curve in HEK293 cells**

Sodium channel activation profile was also investigated using a depolarization protocol from -80 mV to +40 mV with a 5 mV increment. Peak current amplitude under each voltage was measured, and normalized to the maximum peak current amplitude. The normalized fraction of current was then correlated with the membrane voltage to generate a current-voltage relationship curve, which was then fitted using the Boltzmann function. The activation curve of G1481E hNav1.5 mutation is shifted to the left as compared to that of WT hNav1.5, which suggests that the G1481E mutation causes the channel to activate at a more negative potential (Figure 32). The  $V_{1/2}$  (voltage at which channel is half activated) value of the mutant channel is more negative, although there is no statistical difference in  $k$  slope of channel inactivation. Overall, the G1481E mutation increases the percentage of sodium current that is activated at a broad range of membrane potentials, and induces the channel activation at a more negative membrane potential. The left-ward shift of the activation curve may explain why the patient carrying the G1481E mutation has LQT3 syndrome. A similar observation was made on steady-state activation in LQT3-causing mutant channel (Horne *et al.*, 2010).

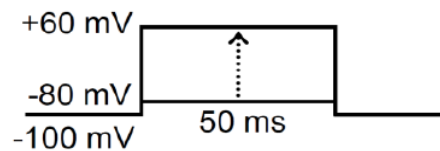
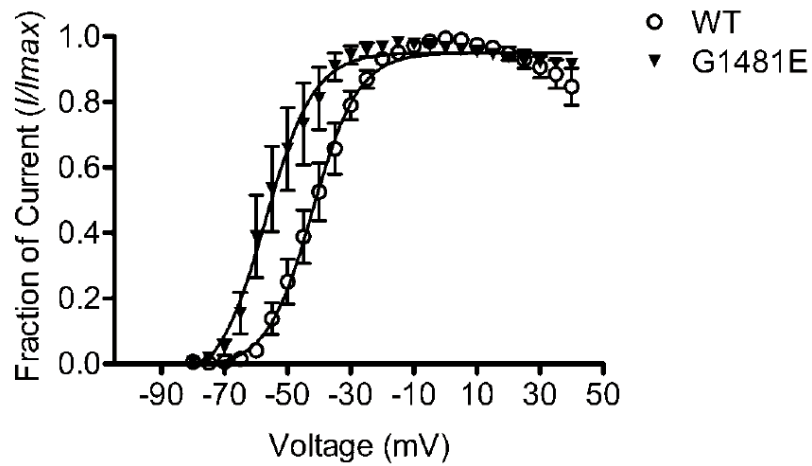


**Figure 32. G1481E mutation causes a leftward shift of the steady-state activation in HEK293 cells.** This figure shows the mean steady-state activation curves generated under the 50 ms stimulation pulses from -80 mV to +60 mV with 5 mV increments for WT ( $n=18$ , open circles) and G1481E mutant channels ( $n=14$ , closed triangles) that are expressed in HEK293 cells. Data indicate that G1481E mutation shifts the voltage dependence of activation to the left. Both activation curves were fitted using the Boltzmann function. The leftward shift of the activation curve means there are more channels available as compared to the WT. The panel below illustrates the protocol that was used to study the activation profile.

## **M. The G1481E mutation does not affect sodium channel steady-state fast inactivation**

The intracellular loop III within domain III and IV has been demonstrated to be critical for channel inactivation. In our study and West's study (West *et al.*, 1992), F1486 was found to be critical for channel inactivation and augmentation of late  $I_{Na}$ . G1481 is five amino acids upstream of F1486, and mutation of G1481 to E was found to be associated with long-QT syndrome. Based on these facts, we hypothesized that the G1481E mutation would lead to the disruption of sodium channel inactivation and lead to LQTS. In our experimental system using HEK293 cells, we didn't observe any change in inactivation parameters such as  $V_{1/2}$  and  $k$  slope when we compare the WT channel with the G1481E mutant channel (Figure 33), which suggests that the inactivation was not affected or disrupted by G1481E mutation. When expressed in HEK293 cells, the G1481E mutation channel has a  $V_{1/2}$  of -83.60 mV ( $n=18$ ),  $k$  slope of 7.0. The WT channel has a  $V_{1/2}$  of -83.15 mV, and  $k$  slope of 8.6 ( $n=15$ ). There are no statistical changes in these two parameters ( $p > 0.05$ ). The  $V_{1/2}$  of inactivation is defined as the voltage at which 50% of the channel population has transitioned to a non-conducting inactivated state. The above mentioned observation for both channel types suggests that mutation of G1481E does not affect sodium channel inactivation.

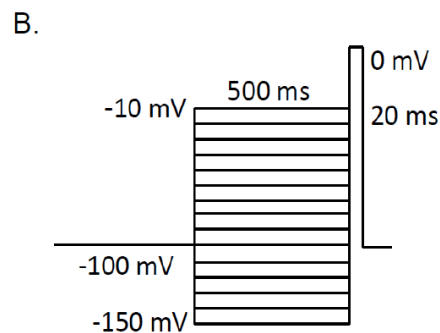
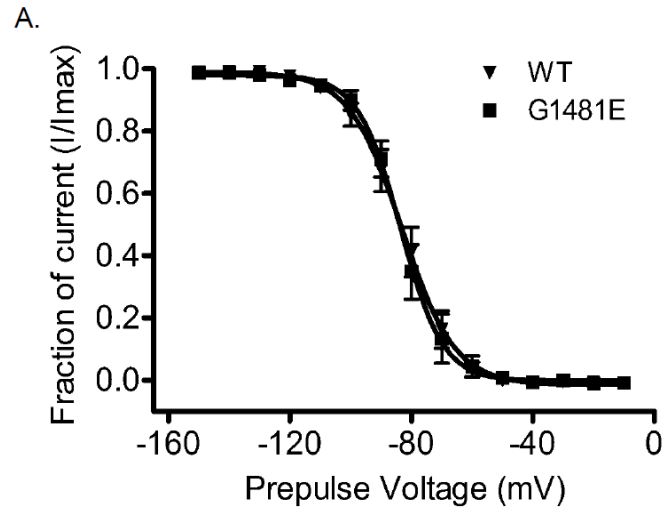


**Figure 33. G1481E mutation does not affect sodium channel steady-state fast inactivation in HEK293 cells.** A. The steady-state fast inactivation curve for G1481E mutant channels (closed squares,  $n=18$ ) is not significantly shifted but it is overlapped with the curve for WT channel (closed triangles,  $n=15$ ). The channels that remain available after each inactivating prepulse were evaluated by the peak current amplitude produced during a test pulse to  $-10$  mV for 20 ms. B. Illustrates the protocol that was used for to study steady state inactivation of sodium channels. Cells were held at  $-100$  mV and stepped to an inactivating prepulse (from  $-150$  mV to  $-10$  mV) for 500 ms.

## **N. Sodium channel G1481E mutation does not affect late $I_{Na}$**

LQT3 syndrome is associated with sodium channel gain-of-function mutations, which is typically presented as the increase in late sodium current. The fundamental basis for our studies on G1481E mutation is that this mutation was found to be correlated with the LQT3 syndrome in the retrospective clinical case study. It has been found in some other studies that sudden infant death and LQT3-causing mutations increases late  $I_{Na}$  (Bankston *et al.*, 2007a). Therefore, we hypothesized that G1481E mutation could cause increase in late sodium current, and lead to LQT3 syndrome. Based on this hypothesis, we measured remaining late  $I_{Na}$  at the end of a 200 ms depolarizing pulse under a series of voltages. The amplitude of late  $I_{Na}$  was normalized to each peak current amplitude. The summarized data is shown in Figure 34.

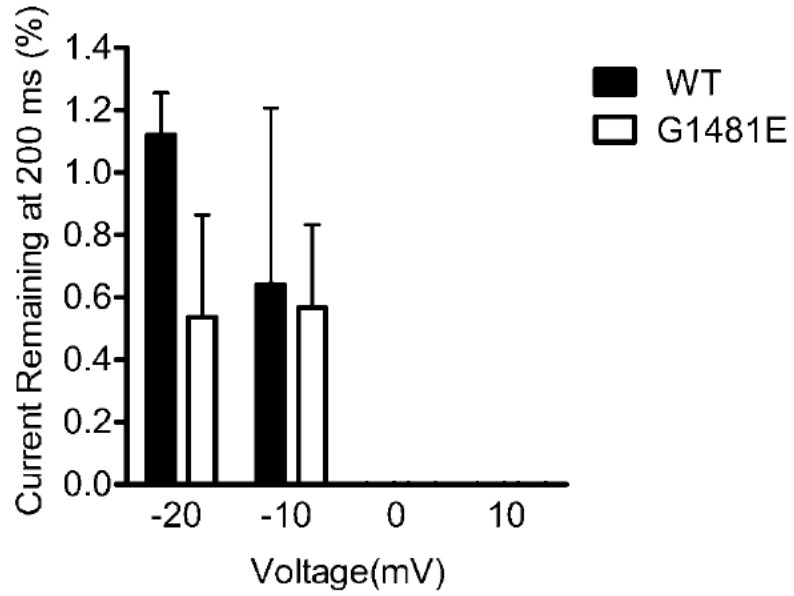


**Figure 34. G1481E mutation does not affect late  $I_{Na}$ .** Bar graph indicates the summarized percentage of late  $I_{Na}$  (normalized to the peak current amplitude) in HEK293 cells recorded at each tested voltage. There is no statistical difference between WT (n=18) and G1481E mutant channels (n=15).

## **O. The G1481E mutation enhances window current**

Based on the fact that patients carrying this mutation were proposed to be correlated with the LQT3, we decided to take further look at this mutation. The G1481E mutation causes the leftward depolarizing shift of the steady-state activation curve, but no change in the steady-state inactivation curve. Therefore, the averaged steady-state window currents were analyzed for both WT and G1481E channels. It was found that the G1481E mutation resulted in an increase in non-inactivating window current (Figure 35A), which could lead to APD prolongation and cause LQT3 in patients.

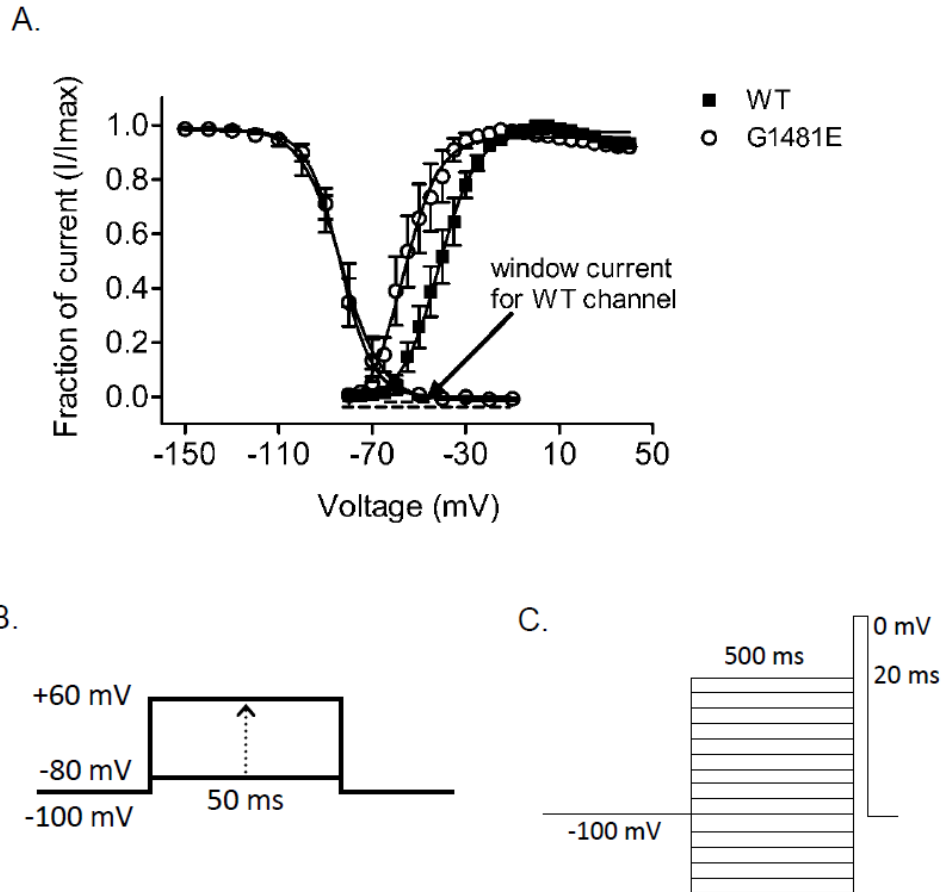
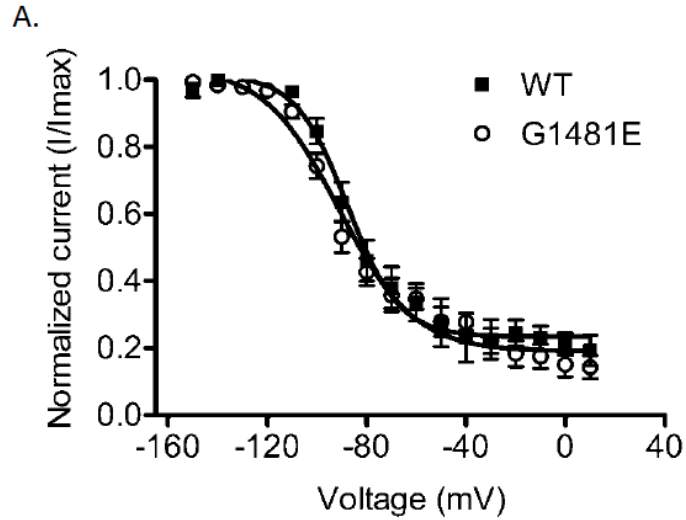


**Figure 35. The G1481E mutation increases sodium channel window current in HEK293 cells.** The window current is represented by the area which is created by the overlap of steady-state activation and steady-state fast inactivation curves. A. The shaded region represents the window current generated by WT hNav1.5 channels ( $n=9$  for activation curve,  $n=11$  for inactivation curve). The shaded region plus the blank area (underneath both the activation curve and the inactivation curve for G1481E) represent the window current generated by G1481E mutant channels ( $n=11$  for steady-state activation curve,  $n=10$  for steady-state inactivation curve). Window current measurement indicates that G1481E mutant channels conduct more non-inactivating sodium current. B, and C. Protocols used to analyze the window current are illustrated.

## **P. The G1481E mutation does not affect the slow inactivation**

In addition to fast inactivation, there is another type of channel inactivation which is termed “slow inactivation”. Development and recovery occur over the second to minute time scale for the “slow inactivation”. It was proposed that the ionic conductance decrease during a prolonged depolarization of several seconds is due to the slow inactivation process (Hille, 2001; Ulbricht, 2005). The kinetic analysis of steady-state activation and potential interactions between activation and slow inactivation suggested that slow inactivation might be coupled to the activation voltage sensors (Ruben *et al.*, 1992). It was demonstrated that mutation of phenylalanine (Phe, F) within the IFM motif in the sodium channel intracellular loop between DIII and DIV affects the steady-state fast inactivation but not slow inactivation regarding the study on Nav1.4 sodium channel (Cummins & Sigworth, 1996). As stated above, VGSCs can transit to an inactivation state called “slow inactivation”, which develops slowly and recover slowly (Vilin & Ruben, 2001). Certain mutations of skeletal muscle VGSCs that affect the channel availability due to defect in slow inactivation can lead to increased cellular excitability (Cummins & Sigworth, 1996). Since it was postulated that G1481E is associated with LQT3 syndrome, it is of importance to investigate if this mutation affects the voltage dependence of slow inactivation. An extended conditioning pulse was designed, after which a brief hyperpolarizing pulse (100 ms) was given to the cells to allow the channels to recover from fast inactivation. Then, a test depolarization pulse was given to the cell to test the fraction of the available channels (Figure 36). Both WT and G1481E mutant

channel availability curves were fit with a Boltzmann function. There was no notable alteration in the fraction of available channel for G1481E mutant, as compared to the WT hNav.1 channel. This result suggests that the LQTs which were identified in the patient is not related to slow inactivation.



B.

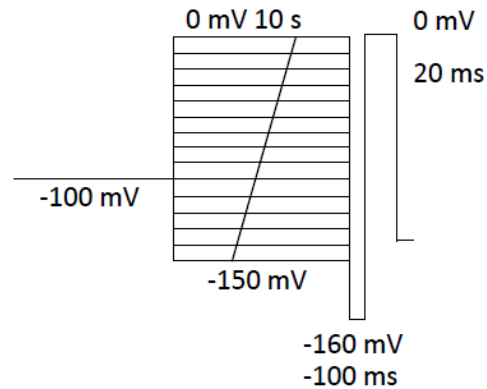


**Figure 36. G1481E mutation does not affect the slow inactivation.** WT and G1481E mutant sodium channels were tested in this study. To study slow inactivation, extended conditioning pulse ranging from -150 mV to +10 mV for 10 seconds were given to the cells. Cells were then applied with a brief hyperpolarized pulse to -100 mV to allow rapid recovery of fast inactivated channels before testing for the fraction of available channels for 20 ms at +10 mV. Both curves were fit with a Boltzmann function. The over-lapped curves indicate that there is no difference in slow inactivation.

## IV. DISCUSSION

### A. Overview of the dissertation research

As an inherited cardiac disorder, congenital LQTS is characterized by the prolongation of the QT interval. Patients with LQTS are susceptible to developing ventricular tachycardia (VT).

The cardiac voltage-gated sodium channel Nav1.5 is critical for the initiation and propagation of the action potential throughout the heart. Mutations of *SCN5A* are now considered to be associated with a number of cardiac diseases such as LQT3, Brugada syndrome, atrial fibrillation, and sudden infant death syndrome (Chen *et al.*, 1998; Wang *et al.*, 2007; Makiyama *et al.*, 2008). Since the first identification of the sodium channel mutation in a family with LQT history, about 80 *SCN5A* mutations have been reported to cause LQT3 (Inherited Arrhythmias Database). These studies have advanced our knowledge of the roles that sodium channel plays in cardiac function.

Yamamura and colleagues identified an infant patient with severe cardiac arrhythmia carrying a heterologous F1486 deletion (Yamamura *et al.*, 2009). Their ECG studies on this patient indicated prolonged QT interval, 2:1 atrioventricular block, and polymorphic VT. Surprisingly, the patient's VT was refractory to intravenous administration of lidocaine. We hypothesized that the F1486del of Nav1.5 would alter the sodium channel function, and therefore prolong the action potential duration, which would subsequently lead to cardiac

arrhythmia. We also speculated that the decreased sensitivity to antiarrhythmic drug lidocaine resulted from the deletion of F1486.

In the current study, we extensively characterized biophysical properties of the mutant sodium channel with F1486del within the intracellular loop between DIII and DIV. We found a loss-of-function alteration of current density and a series of gain-of-function changes. Ultimately, these alterations lead to the APD prolongation and lead to EADs in the infant patient.

### **B. Voltage-clamp studies on the F1486del channel**

This mutation site is within the IFM motif which was required for inactivation (Vassilev *et al.*, 1988; Stuhmer *et al.*, 1989; Patton *et al.*, 1992). In our study, using both the HEK293 cell line and neonatal rat cardiomyocytes as expression systems, we consistently found that cells expressing F1486del mutant channels had reduced current density compared to cells expressing WT channels. This is a sodium channel loss-of-function phenotype. Although the mechanism is not clear, one possibility is that the decreased current density reflects from a deficiency in channel trafficking. The *SCN5A* F1473S mutation, within the same intracellular loop as F1486del, has been identified to cause a channel trafficking defect (Ruan *et al.*, 2010).

Sodium current has a slow inactivating persistent component, which is called late sodium current (late  $I_{Na}$ ). In rat cardiomyocytes, persistent late  $I_{Na}$  usually has a magnitude of less than 1% of the size of peak transient sodium current (Saint *et al.*, 1992). As an inward depolarizing current, late  $I_{Na}$  can increase the duration of the ventricular action potential in cardiomyocytes.

Increases in late  $I_{Na}$  can also facilitate the onset of EADs and cause sustained triggered activity (Song *et al.*, 2008). Certain mutations of Nav1.5 associated with LQTS and sudden infant death have been shown to increase late sodium current when these mutants were expressed in HEK293 cells (Bankston *et al.*, 2007b; Ruan *et al.*, 2010). To determine to what extent the F1486del could affect the late sodium current, we chose to use a step depolarizing pulse lasting for 200 ms. The percentage of late sodium current remaining at 200 ms for WT channel was less than 1% percent, consistent with previous findings (Saint *et al.*, 1992). Our study clearly demonstrates a significant increase of late  $I_{Na}$  in cells expressing the F1486del mutant channels, which may explain why the infant patient carrying this deletion had LQTS and subsequent incessant tachycardia and reduced cardiac function. The remarkable effect of the F1486del is an increase in late sodium current to ~20% of the peak transient current. It is important to note that this increase of late  $I_{Na}$  is substantially greater than that typically observed with other LQT3 mutations. For example, the  $\Delta$ KPQ mutation only increases the late current to ~4% of the peak transient current (An *et al.*, 1996).

Inactivation is mediated by the inactivation gate (loop region between DIII and DIV) and the intracellular C-terminal domain (Vassilev *et al.*, 1988; Kass, 2006). Mutations associated with LQT3 and sudden infant death generally disrupt the voltage-dependent transition to the inactivated state. In our study, the F1486del caused a rightward depolarizing shift of the steady-state inactivation, suggesting that deletion of F1486 can possibly destabilize the inactivated

channel configuration and increase the percentage of channels that retain the capability to be activated and stay in the open state (Wang *et al.*, 1996).

The analysis for I-V relationship and activation curve demonstrates that the deletion of F1486 does not affect steady-state fast activation and these data are in accordance with previous findings demonstrating that the activation kinetics are not affected by other mutations within this region (Vassilev *et al.*, 1988; Bankston *et al.*, 2007b).

The process of a voltage-gated channel to transit from open activated state back to closed state before the channel goes into inactivation state is defined as deactivation. The time constant for deactivation is one of the factors that determine cell excitability (Featherstone *et al.*, 1998). Our data show that the time constants for the F1486del channel is similar to that for the WT channel.

The data from time constant analysis for mutant channel recovery from inactivation seems contradictory with the fact that the patient has action potential prolongation, since a number of *SCN5A* mutation associated with LQT3 have been presented with decreased Tau value for recovery from inactivation (Wang *et al.*, 2007). The observation on the time constants for the recovery from inactivation suggests that once the channel overcomes the energy barrier and goes to the inactivated state, it is difficult for the channel to transition out of the open inactivated state.

### **C. Therapeutic outcomes of lidocaine on F186del channels**

Lidocaine, with a tertiary amine structure, is widely used as an antiarrhythmic drug. We found that lidocaine has a significantly lower IC<sub>50</sub> for

resting WT Nav1.5 channels than the mutant channels. Lidocaine hydrochloride is more potent on inhibiting inactivated WT sodium channels, which is in accordance with the previous findings that lidocaine preferentially binds to the sodium channel in the inactivated state, and then inhibits the channel (Butterworth & Strichartz, 1990; Ragsdale *et al.*, 1996). Interestingly, the  $\Delta$ KPQ mutant channel was not less sensitive to lidocaine than WT channels (An *et al.*, 1996). The absolute insensitivity for the F1486del channel in the inactivated state to lidocaine indicates that the deficit in inactivation leads to the loss of response to lidocaine. Based on our findings, we predict that F1486 is crucial to the stabilization of the high-affinity lidocaine binding site in Nav1.5. This is surprising to us as the mutation of F1486 to Q did not alter the peak current dose-response curve of Nav1.5 for lidocaine (Balsler *et al.*, 1996). Therefore, for the first time, our mutagenesis study on sodium channel Nav1.5 reveals a critical role for F1486 on the potency and efficacy of lidocaine on cardiac sodium channels.

#### **D. Current-clamp studies on neonatal cardiomyocytes ectopically expressing recombinant F1486del channels**

We used neonatal rat ventricular cardiomyocytes as an expression system and studied the functional consequence of the mutant channel on cardiac action potential profile from a single cell aspect. Substantial prolongation of the action potential duration and the subsequent triggered EADs in these neonatal cardiomyocytes were observed. We also observed the late  $I_{Na}$  augmentation in cardiomyocytes. We hypothesized that in the patients the long-QTs is caused by the increase in late  $I_{Na}$ , which was induced by deletion of F1486. The increased in

late  $I_{Na}$  then led to the initiation of EADs, which are followed by the cardiac tachycardia.

Taken together, the F1486del produces a loss-of-function alteration of sodium current density and gain-of-function alterations such as impairment of inactivation, augmentation of late sodium current, increase of ramp current, increase of window current. Although the peak current density is reduced by the deletion of F1486, our data indicate that the substantial gain-of-function changes induced by the F1486del appear to be sufficient to overcome this deficit and prolong the APD. The data we collected from our studies on lidocaine efficacy and potency test proved our idea that additional therapeutic interventions are required to overcome the relative insensitivity to lidocaine displayed by the F1486del mutant channel. Uncovering the effect of lidocaine on both WT and the F1486del mutant channels should provide a better understanding of role that a specific residue plays in mediating the sensitivity to a therapeutic reagent. Our study will further validate the concept that gene specific therapeutic drugs need to be developed and characterized to reverse the cardiac arrhythmia which is caused by different mutations in *SCN5A*.

#### **E. Trafficking and cellular localization of voltage-gated F1486del sodium channels**

In reality, the electrical excitability of excitable cells such as neurons and cardiomyocytes depends not only on the expression level of the voltage-gated sodium channels, but also upon their appropriate targeting to the plasma membrane. So far, several sodium channel mutations have been found to

underlie sodium channel trafficking defects, and these mutations were also shown to cause life-threatening cardiac arrhythmia. For example, in some Brugada syndrome cases, mutations have been described to reduce the surface expression since the channel cannot fold correctly and is retained with the cytoplasmic compartment ER (Valdivia *et al.*, 2004). The sodium channel blocker lidocaine has been shown to be able to rescue the tsA 201 cells from attenuated Nav1.8 sodium current (Zhao *et al.*, 2007). In addition, the application of pharmacological reagents aiming at blocking sodium channels can rescue the channel from trafficking defects. One example of this is the research performed by Priori's group (Ruan *et al.*, 2010). In their study, the application of the sodium channel blocker Mexiletine can facilitate the mutation protein targeting to the plasma membrane surface without changing the channel's gating properties. Their study provided evidence that sodium channel trafficking can be modified by certain pharmacological Nav blockers. In my study, the cell surface sodium current density was decreased for F1486del mutant channel compared to WT hNav1.5 channel. Although the reasons for the low current density for the F1486del mutant channel are not known, one hypothesis is that this resulted from a channel trafficking defect that reduces the cell surface expression of functional channels. The low current densities for voltage-gated channels such as Nav1.5, Nav1.8, and HERG have been believed to be caused by trafficking defects (Okuse *et al.*, 2002; Anderson *et al.*, 2006; Ruan *et al.*, 2010). There also exists the possibility that excessive activation of the sodium channel causes a toxic effect to the cells expressing the mutant F1486del protein. Thus, only those

cells expressing low level of the mutant protein can survive and were able to be investigated. To test these two hypotheses, there are a series of experiments that have been designed to find out the determinants of Nav1.5 F1486del channel expression in HEK293 cells. These future experiments will combine biochemistry, immunochemistry, and electrophysiology techniques.

To test the hypothesis that F1486del can decrease the trafficking of sodium channels to the cell surface membrane, cell surface biotinylation experiment has been performed. The surface portion of the sodium channel protein was labeled with biotin and immunoprecipitated using streptavidin beads. Surface biotinylated protein was normalized to the  $\beta$ -tubulin protein. In my study, F1486del protein has a lower level of surface expression, which is consistent with the result from the patch-clamp study. However, this experimental strategy is not sufficient to rule out the possibility that the surviving cells express lower levels of F1486del mutant channels. Since the F1486del channel has a defect in the channel inactivation, which may cause secondary toxic effects to cells that express these channels. Additional experiments need to be performed further to test the hypothesis that cellular toxicity that is caused by the F1486del sodium channel.

In order to test the hypothesis that cellular toxicity causes the decreased channel distribution at plasma membrane, I have designed a hNav1.5 cDNA construct bearing a cysteine to tyrosine mutation at amino acid 374 (C374Y). Previous studies indicated that this particular site is critical in determining the sensitivity to TTX (Leffler *et al.*, 2005). TTX sensitive VGSCs such as Nav1.3,

Nav1.4, Nav1.6, and Nav1.7 carry a tyrosine residue at the corresponding site, which endows the channel with the property of being extremely sensitive to TTX (at nM level). 4-6 hours after transfection, cells will be replated onto 12 mm coverslips in a 24-well plate. At this step, 100 nM TTX will be added to the cell culture media and maintained in the culture media until starting the patch-clamp study. Since both WT and F1486del mutant channel carry this C374Y mutation, VGSCs will be inhibited in the presence of TTX. After washing out the residual TTX in the recording chamber, current densities will be compared to test the hypothesis that it is the cellular toxicity that causes the attenuated plasma membrane distribution of the sodium channel. The goal of this experiment is to test whether TTX can enhance the cell surface expression of the hNav1.5 F1486del channel. If the surface fraction is augmented after incubating with TTX, then we can conclude that it is the over activation of the sodium channel that causes the cellular toxicity, which then leads to the overall decrease in the surface sodium channel protein.

## **F. Summary and conclusions**

The overall results of my thesis are summarized as follows:

1. Deletion of amino acid Phenylalanine (F) 1486 on Nav1.5 cause decrease in membrane current density. This is a sodium channel loss-of-function phenotype. The decrease in sodium current density happens not only in heterologous expression system of human embryonic kidney (HEK293) cells, but in native primary neonatal rat cardiomyocytes. This means the decrease in current density

is not the artifact caused by the difference in the expression system, but it indicates a phenotype caused by deletion of F1486 on Nav1.5.

2. In both HEK293 cells and neonatal rat cardiomyocytes, deletion of F1486 does not cause any change in cardiac sodium channel Nav1.5 activation profile. Both the voltage at which channel half-activated ( $V_{1/2}$ ) and the slope factor of activation were not affected by F1486del.

3. In comparison to the activation profile, the inactivation of the sodium channel was disrupted by deletion of F1486 on Nav1.5. The disruption was presented as the positively shift of the  $V_{1/2}$  (voltage at which channel is half inactivated) in both HEK293 cells and neonatal cardiomyocytes. However, the slope factor was not significantly altered.

4. hNav1.5 F1486del causes augmentation of late component of sodium current (late  $I_{Na}$ ) in both HEK293 cells and cardiomyocytes.

5. hNav1.5 F1486del enhanced window current.

6. F1486del does not alter the time constants for channel deactivation. Again, the observations were seen in both HEK293 cells and cardiomyocytes.

7. hNav1.5 F1486del channels cause significant prolongation of cardiac action potential duration (APD) in neonatal rat cardiomyocytes, and initiates spontaneous early afterdepolarizations (EADs). The presence of EADs is a potential cause of QT interval prolongation, which underlines the occurrence of long-QT syndrome (LQTS). The EADs also can trigger the increase in cardiac automaticity.

8. Lidocaine lost its pharmacological effect on hNav1.5 F1486del mutant channels. The reduced response was reflected by the increase of  $IC_{50}$  for lidocaine on the F1486del sodium channel in the resting state. In the inactivated state, F1486del sodium channel doesn't respond to lidocaine in a dose-dependent manner, which suggests amino acid F1486 can stabilize the sodium channel at a certain conformation that can facilitate lidocaine binding to the sodium channel. The poor pharmacological response of the F1486del mutant channel to antiarrhythmic drug lidocaine explains why the pediatric patient is refractory to lidocaine treatment.

The results presented here reveal a relationship of hNav1.5 F1486del and the LQT syndrome found in the pediatric patient who had severe cardiac arrhythmia. The pharmacological studies on the mutant cardiac sodium channels reveals the causal relationship between the patient's refractory response to lidocaine treatment and the linear structural changes induced by F1486del. Finally, the current thesis work demonstrates the cardiac functional changes in the single working cardiomyocyte level, meaning the changes in action potential duration and the occurrence of EADs. The work demonstrated here can explain why the patient has severe QT interval prolongation, and subsequent ventricular tachycardia. It will be important to elucidate the structural change that is induced by F1486del, and further identify potential pharmacological reagents that can inhibit the F1486del channels more efficaciously. Overall, the current study supports the idea of gene specific therapy, since alteration of one single amino

acid on hNav1.5 greatly alters the pharmacological response to certain antiarrhythmic drugs.

**G. Discussion on supplemental results: G1481E mutation increases window current and may lead to LQT3 in patients**

The initiation of the patch-clamp study on the G1481E sodium channel site mutation is based on the retrospective clinical case study by Tester *et al.* (Tester *et al.*, 2005). Patients who carry this mutation were thought to be associated with LQT3 syndrome. In addition, as the F1486del site, the G1481E is also located in the intracellular loop III between transmembrane DIII and DIV. We did detailed biophysical studies on this mutant channel, and realized that unlike the F1486del channel, the G1481E mutant channel does not result in the shift of steady-state inactivation curve, which happens for most of the site mutations within the intracellular loop III (Bankston *et al.*, 2007a; Bankston *et al.*, 2007b; Ruan *et al.*, 2010). The G1481E mutation does not cause the statistical change in late sodium current either. However, the G1481E mutation does result in the depolarizing leftward shift in the steady-state activation, which will enhance the non-inactivating window current. Therefore, the overall increase in window sodium current could explain why the patients carrying this mutation present with LQT3. Detailed action potential studies on cardiomyocytes expressing the G1481E mutant channels will be necessary in the near future.

## REFERENCE LIST

Inherited Arrhythmias Database. <http://www.fs.mit/cardmoc/> **Online June, 2010.**

Agnew WS, Levinson SR, Brabson JS & Raftery MA. (1978). Purification of the tetrodotoxin-binding component associated with the voltage-sensitive sodium channel from *Electrophorus electricus* electroplax membranes. *Proc Natl Acad Sci U S A* **75**, 2606-2610.

Akopian AN, Sivillotti L & Wood JN. (1996). A tetrodotoxin-resistant voltage-gated sodium channel expressed by sensory neurons. *Nature* **379**, 257-262.

An RH, Bangalore R, Rosero SZ & Kass RS. (1996). Lidocaine block of LQT-3 mutant human Na<sup>+</sup> channels. *Circ Res* **79**, 103-108.

An RH, Wang XL, Kerem B, Benhorin J, Medina A, Goldmit M & Kass RS. (1998). Novel LQT-3 mutation affects Na<sup>+</sup> channel activity through interactions between alpha- and beta1-subunits. *Circ Res* **83**, 141-146.

Anderson CL, Delisle BP, Anson BD, Kilby JA, Will ML, Tester DJ, Gong Q, Zhou Z, Ackerman MJ & January CT. (2006). Most LQT2 mutations reduce Kv11.1 (hERG) current by a class 2 (trafficking-deficient) mechanism. *Circulation* **113**, 365-373.

Armstrong CM. (1981). Sodium channels and gating currents. *Physiol Rev* **61**, 644-683.

Arnestad M, Crotti L, Rognum TO, Insolia R, Pedrazzini M, Ferrandi C, Vege A, Wang DW, Rhodes TE, George AL, Jr. & Schwartz PJ. (2007). Prevalence of long-QT syndrome gene variants in sudden infant death syndrome. *Circulation* **115**, 361-367.

Attwell D, Cohen I, Eisner D, Ohba M & Ojeda C. (1979). The steady-state TTX-sensitive ("window") sodium current in cardiac Purkinje fibres. *Pflugers Arch* **379**, 137-142.

Backx PH, Yue DT, Lawrence JH, Marban E & Tomaselli GF. (1992). Molecular localization of an ion-binding site within the pore of mammalian sodium channels. *Science* **257**, 248-251.

Balser JR, Nuss HB, Orias DW, Johns DC, Marban E, Tomaselli GF & Lawrence JH. (1996). Local anesthetics as effectors of allosteric gating. Lidocaine effects on inactivation-deficient rat skeletal muscle Na channels. *J Clin Invest* **98**, 2874-2886.

Bankston JR & Kass RS. (2010). Molecular determinants of local anesthetic action of beta-blocking drugs: Implications for therapeutic management of long QT syndrome variant 3. *J Mol Cell Cardiol* **48**, 246-253.

Bankston JR, Sampson KJ, Kateriya S, Glaaser IW, Malito DL, Chung WK & Kass RS. (2007a). A novel LQT-3 mutation disrupts an inactivation gate complex with distinct rate-dependent phenotypic consequences. *Channels (Austin)* **1**, 273-280.

Bankston JR, Yue M, Chung W, Spyres M, Pass RH, Silver E, Sampson KJ & Kass RS. (2007b). A novel and lethal de novo LQT-3 mutation in a newborn with distinct molecular pharmacology and therapeutic response. *PLoS One* **2**, e1258.

Baroudi G, Carbonneau E, Pouliot V & Chahine M. (2000). SCN5A mutation (T1620M) causing Brugada syndrome exhibits different phenotypes when expressed in *Xenopus* oocytes and mammalian cells. *FEBS Lett* **467**, 12-16.

Bean BP, Cohen CJ & Tsien RW. (1983). Lidocaine block of cardiac sodium channels. *J Gen Physiol* **81**, 613-642.

Benhorin J, Taub R, Goldmit M, Kerem B, Kass RS, Windman I & Medina A. (2000). Effects of flecainide in patients with new SCN5A mutation: mutation-specific therapy for long-QT syndrome? *Circulation* **101**, 1698-1706.

Bennett PB, Yazawa K, Makita N & George AL, Jr. (1995). Molecular mechanism for an inherited cardiac arrhythmia. *Nature* **376**, 683-685.

Black JA & Waxman SG. (1996). Sodium channel expression: a dynamic process in neurons and non-neuronal cells. *Dev Neurosci* **18**, 139-152.

Bloise R, Napolitano C & Priori SG. (2002). Romano-Ward and other congenital long QT syndromes. *Cardiovasc Drugs Ther* **16**, 19-23.

Brugada P & Brugada J. (1992). Right bundle branch block, persistent ST segment elevation and sudden cardiac death: a distinct clinical and electrocardiographic syndrome. A multicenter report. *J Am Coll Cardiol* **20**, 1391-1396.

Butterworth JFt & Strichartz GR. (1990). Molecular mechanisms of local anesthesia: a review. *Anesthesiology* **72**, 711-734.

Chen Q, Kirsch GE, Zhang D, Brugada R, Brugada J, Brugada P, Potenza D, Moya A, Borggrefe M, Breithardt G, Ortiz-Lopez R, Wang Z, Antzelevitch C, O'Brien RE, Schulze-Bahr E, Keating MT, Towbin JA & Wang Q. (1998). Genetic basis and molecular mechanism for idiopathic ventricular fibrillation. *Nature* **392**, 293-296.

Chiamvimonvat N, Perez-Garcia MT, Ranjan R, Marban E & Tomaselli GF. (1996). Depth asymmetries of the pore-lining segments of the Na<sup>+</sup> channel revealed by cysteine mutagenesis. *Neuron* **16**, 1037-1047.

Chopra SS, Stroud DM, Watanabe H, Bennett JS, Burns CG, Wells KS, Yang T, Zhong TP & Roden DM. (2010). Voltage-gated sodium channels are required for heart development in zebrafish. *Circ Res* **106**, 1342-1350.

Clancy CE, Tateyama M & Kass RS. (2002). Insights into the molecular mechanisms of bradycardia-triggered arrhythmias in long QT-3 syndrome. *J Clin Invest* **110**, 1251-1262.

Cohen SA. (1996). Immunocytochemical localization of rH1 sodium channel in adult rat heart atria and ventricle. Presence in terminal intercalated disks. *Circulation* **94**, 3083-3086.

Crill WE. (1996). Persistent sodium current in mammalian central neurons. *Annu Rev Physiol* **58**, 349-362.

Crotti L, Celano G, Dagradi F & Schwartz PJ. (2008). Congenital long QT syndrome. *Orphanet J Rare Dis* **3**, 18.

Cummins TR, Howe JR & Waxman SG. (1998). Slow closed-state inactivation: a novel mechanism underlying ramp currents in cells expressing the hNE/PN1 sodium channel. *J Neurosci* **18**, 9607-9619.

Cummins TR & Sigworth FJ. (1996). Impaired slow inactivation in mutant sodium channels. *Biophys J* **71**, 227-236.

Cusdin FS, Clare JJ & Jackson AP. (2008). Trafficking and cellular distribution of voltage-gated sodium channels. *Traffic* **9**, 17-26.

Deal KK, England SK & Tamkun MM. (1996). Molecular physiology of cardiac potassium channels. *Physiol Rev* **76**, 49-67.

Dhar Malhotra J, Chen C, Rivolta I, Abriel H, Malhotra R, Mattei LN, Brosius FC, Kass RS & Isom LL. (2001). Characterization of sodium channel alpha- and beta-subunits in rat and mouse cardiac myocytes. *Circulation* **103**, 1303-1310.

Dominguez JN, de la Rosa A, Navarro F, Franco D & Aranega AE. (2008). Tissue distribution and subcellular localization of the cardiac sodium channel during mouse heart development. *Cardiovasc Res* **78**, 45-52.

Fabritz L, Kirchhof P, Franz MR, Nuyens D, Rossenbacker T, Ottenhof A, Haverkamp W, Breithardt G, Carmeliet E & Carmeliet P. (2003). Effect of pacing and mexiletine on dispersion of repolarisation and arrhythmias in DeltaKPQ SCN5A (long QT3) mice. *Cardiovasc Res* **57**, 1085-1093.

Fahmi AI, Patel M, Stevens EB, Fowden AL, John JE, 3rd, Lee K, Pinnock R, Morgan K, Jackson AP & Vandenberg JI. (2001). The sodium channel beta-subunit SCN3b modulates the kinetics of SCN5a and is expressed heterogeneously in sheep heart. *J Physiol* **537**, 693-700.

Featherstone DE, Fujimoto E & Ruben PC. (1998). A defect in skeletal muscle sodium channel deactivation exacerbates hyperexcitability in human paramyotonia congenita. *J Physiol* **506 ( Pt 3)**, 627-638.

Funck-Brentano C & Jaillon P. (1993). Rate-corrected QT interval: techniques and limitations. *Am J Cardiol* **72**, 17B-22B.

Glaaser IW, Bankston JR, Liu H, Tateyama M & Kass RS. (2006). A carboxyl-terminal hydrophobic interface is critical to sodium channel function. Relevance to inherited disorders. *J Biol Chem* **281**, 24015-24023.

Goldin AL. (2001). Resurgence of sodium channel research. *Annu Rev Physiol* **63**, 871-894.

Goodman LS, Hardman JG, Limbird LE & Gilman AG. (2001). *Goodman and Gilman's the pharmacological basis of therapeutics*. McGraw-Hill, New York.

Hedley PL, Jorgensen P, Schlamowitz S, Wangari R, Moolman-Smook J, Brink PA, Kanters JK, Corfield VA & Christiansen M. (2009). The genetic basis of long QT and short QT syndromes: a mutation update. *Hum Mutat* **30**, 1486-1511.

Heinemann SH, Terlau H, Stuhmer W, Imoto K & Numa S. (1992). Calcium channel characteristics conferred on the sodium channel by single mutations. *Nature* **356**, 441-443.

Henderson R & Wang JH. (1972). Solubilization of a specific tetrodotoxin-binding component from garfish olfactory nerve membrane. *Biochemistry* **11**, 4565-4569.

Hille B. (1977). Local anesthetics: hydrophilic and hydrophobic pathways for the drug-receptor reaction. *J Gen Physiol* **69**, 497-515.

Hille B. (2001). *Ion channels of excitable membranes*. Sinauer, Sunderland, Mass.

Hodgkin AL. (1958). Ionic movements and electrical activity in giant nerve fibres. *Proc R Soc Lond B Biol Sci* **148**, 1-37.

Hodgkin AL & Huxley AF. (1952a). Currents carried by sodium and potassium ions through the membrane of the giant axon of *Loligo*. *J Physiol* **116**, 449-472.

Hodgkin AL & Huxley AF. (1952b). A quantitative description of membrane current and its application to conduction and excitation in nerve. *J Physiol* **117**, 500-544.

Hondeghem LM & Katzung BG. (1977). Time- and voltage-dependent interactions of antiarrhythmic drugs with cardiac sodium channels. *Biochim Biophys Acta* **472**, 373-398.

Horne AJ, Eldstrom J, Sanatani S & Fedida D. (2010). A novel mechanism for LQT3 with 2:1 block: A pore-lining mutation in Nav1.5 significantly affects voltage dependence of activation. *Heart Rhythm*.

Isom LL, De Jongh KS, Patton DE, Reber BF, Offord J, Charbonneau H, Walsh K, Goldin AL & Catterall WA. (1992). Primary structure and functional expression of the beta 1 subunit of the rat brain sodium channel. *Science* **256**, 839-842.

Jackman WM, Friday KJ, Anderson JL, Aliot EM, Clark M & Lazzara R. (1988). The long QT syndromes: a critical review, new clinical observations and a unifying hypothesis. *Prog Cardiovasc Dis* **31**, 115-172.

Jervell A & Lange-Nielsen F. (1957). Congenital deaf-mutism, functional heart disease with prolongation of the Q-T interval and sudden death. *Am Heart J* **54**, 59-68.

Jiang C, Atkinson D, Towbin JA, Splawski I, Lehmann MH, Li H, Timothy K, Taggart RT, Schwartz PJ, Vincent GM & et al. (1994). Two long QT syndrome loci map to chromosomes 3 and 7 with evidence for further heterogeneity. *Nat Genet* **8**, 141-147.

Kallen RG, Sheng ZH, Yang J, Chen LQ, Rogart RB & Barchi RL. (1990). Primary structure and expression of a sodium channel characteristic of denervated and immature rat skeletal muscle. *Neuron* **4**, 233-242.

Kass RS. (2006). Sodium channel inactivation in heart: a novel role of the carboxy-terminal domain. *J Cardiovasc Electrophysiol* **17 Suppl 1**, S21-S25.

Keating M, Atkinson D, Dunn C, Timothy K, Vincent GM & Leppert M. (1991a). Linkage of a cardiac arrhythmia, the long QT syndrome, and the Harvey ras-1 gene. *Science* **252**, 704-706.

Keating M, Dunn C, Atkinson D, Timothy K, Vincent GM & Leppert M. (1991b). Consistent linkage of the long-QT syndrome to the Harvey ras-1 locus on chromosome 11. *Am J Hum Genet* **49**, 1335-1339.

Kellenberger S & Schild L. (2002). Epithelial sodium channel/degenerin family of ion channels: a variety of functions for a shared structure. *Physiol Rev* **82**, 735-767.

Kenyon JL & Gibbons WR. (1979). 4-Aminopyridine and the early outward current of sheep cardiac Purkinje fibers. *J Gen Physiol* **73**, 139-157.

Kenyon JL & Sutko JL. (1987). Calcium- and voltage-activated plateau currents of cardiac Purkinje fibers. *J Gen Physiol* **89**, 921-958.

Khanna R, Myers MP, Laine M & Papazian DM. (2001). Glycosylation increases potassium channel stability and surface expression in mammalian cells. *J Biol Chem* **276**, 34028-34034.

Kiyosue T & Arita M. (1989). Late sodium current and its contribution to action potential configuration in guinea pig ventricular myocytes. *Circ Res* **64**, 389-397.

Kuo CC & Bean BP. (1994). Na<sup>+</sup> channels must deactivate to recover from inactivation. *Neuron* **12**, 819-829.

Leffler A, Herzog RI, Dib-Hajj SD, Waxman SG & Cummins TR. (2005). Pharmacological properties of neuronal TTX-resistant sodium channels and the role of a critical serine pore residue. *Pflugers Arch* **451**, 454-463.

Lenegre J. (1964). Etiology and Pathology of Bilateral Bundle Branch Block in Relation to Complete Heart Block. *Prog Cardiovasc Dis* **6**, 409-444.

Lev M, Kinare SG & Pick A. (1970). The pathogenesis of atrioventricular block in coronary disease. *Circulation* **42**, 409-425.

Levinson SR & Ellory JC. (1973). Molecular size of the tetrodotoxin binding site estimated by irradiation inactivation. *Nat New Biol* **245**, 122-123.

Levinson SR, Thornhill WB, Duch DS, Recio-Pinto E & Urban BW. (1990). The role of nonprotein domains in the function and synthesis of voltage-gated sodium channels. *Ion Channels* **2**, 33-64.

Maier SK, Westenbroek RE, McCormick KA, Curtis R, Scheuer T & Catterall WA. (2004). Distinct subcellular localization of different sodium channel alpha and beta subunits in single ventricular myocytes from mouse heart. *Circulation* **109**, 1421-1427.

Maier SK, Westenbroek RE, Schenkman KA, Feigl EO, Scheuer T & Catterall WA. (2002). An unexpected role for brain-type sodium channels in coupling of cell surface depolarization to contraction in the heart. *Proc Natl Acad Sci U S A* **99**, 4073-4078.

Makita N, Bennett PB & George AL, Jr. (1996). Molecular determinants of beta 1 subunit-induced gating modulation in voltage-dependent Na<sup>+</sup> channels. *J Neurosci* **16**, 7117-7127.

Makita N, Bennett PB, Jr. & George AL, Jr. (1994). Voltage-gated Na<sup>+</sup> channel beta 1 subunit mRNA expressed in adult human skeletal muscle, heart, and brain is encoded by a single gene. *J Biol Chem* **269**, 7571-7578.

Makiyama T, Akao M, Shizuta S, Doi T, Nishiyama K, Oka Y, Ohno S, Nishio Y, Tsuji K, Itoh H, Kimura T, Kita T & Horie M. (2008). A novel SCN5A gain-of-function mutation M1875T associated with familial atrial fibrillation. *J Am Coll Cardiol* **52**, 1326-1334.

Mandel G. (1992). Tissue-specific expression of the voltage-sensitive sodium channel. *J Membr Biol* **125**, 193-205.

Mantegazza M, Yu FH, Catterall WA & Scheuer T. (2001). Role of the C-terminal domain in inactivation of brain and cardiac sodium channels. *Proc Natl Acad Sci U S A* **98**, 15348-15353.

Maron BJ, Clark CE, Goldstein RE & Epstein SE. (1976). Potential role of QT interval prolongation in sudden infant death syndrome. *Circulation* **54**, 423-430.

Michowitz MK, Michowitz Y, Zaidenstien R & Golik A. (2000). Drug-induced QT prolongation. *Isr Med Assoc J* **2**, 924-928.

Miller AW & Robyt JF. (1983). Sodium cyanoborohydride in the immobilization of proteins to glutaraldehyde-activated aminoalkyl silica. *Biotechnol Bioeng* **25**, 2795-2800.

Morgan K, Stevens EB, Shah B, Cox PJ, Dixon AK, Lee K, Pinnock RD, Hughes J, Richardson PJ, Mizuguchi K & Jackson AP. (2000). beta 3: an additional auxiliary subunit of the voltage-sensitive sodium channel that modulates channel gating with distinct kinetics. *Proc Natl Acad Sci U S A* **97**, 2308-2313.

Moss AJ, Schwartz PJ, Crampton RS, Tzivoni D, Locati EH, MacCluer J, Hall WJ, Weitkamp L, Vincent GM, Garson A, Jr. & et al. (1991). The long QT syndrome. Prospective longitudinal study of 328 families. *Circulation* **84**, 1136-1144.

Neher E & Sakmann B. (1976). Single-channel currents recorded from membrane of denervated frog muscle fibres. *Nature* **260**, 799-802.

Nemec J, Hejlik JB, Shen WK & Ackerman MJ. (2003). Catecholamine-induced T-wave lability in congenital long QT syndrome: A novel phenomenon associated with syncope and cardiac arrest. *Mayo Clinic Proceedings* **78**, 40-50.

Nuss HB, Chiamvimonvat N, Perez-Garcia MT, Tomaselli GF & Marban E. (1995). Functional association of the beta 1 subunit with human cardiac (hH1) and rat skeletal muscle (mu 1) sodium channel alpha subunits expressed in *Xenopus* oocytes. *J Gen Physiol* **106**, 1171-1191.

Okuse K, Malik-Hall M, Baker MD, Poon WY, Kong H, Chao MV & Wood JN. (2002). Annexin II light chain regulates sensory neuron-specific sodium channel expression. *Nature* **417**, 653-656.

Oxford GS. (1981). Some kinetic and steady-state properties of sodium channels after removal of inactivation. *J Gen Physiol* **77**, 1-22.

Palmer LG & Frindt G. (1986). Amiloride-sensitive Na channels from the apical membrane of the rat cortical collecting tubule. *Proc Natl Acad Sci U S A* **83**, 2767-2770.

Patton DE & Goldin AL. (1991). A voltage-dependent gating transition induces use-dependent block by tetrodotoxin of rat IIA sodium channels expressed in *Xenopus* oocytes. *Neuron* **7**, 637-647.

Patton DE, West JW, Catterall WA & Goldin AL. (1992). Amino acid residues required for fast Na(+)-channel inactivation: charge neutralizations and deletions in the III-IV linker. *Proc Natl Acad Sci U S A* **89**, 10905-10909.

Perez-Garcia MT, Chiamvimonvat N, Ranjan R, Balsler JR, Tomaselli GF & Marban E. (1997). Mechanisms of sodium/calcium selectivity in sodium channels probed by cysteine mutagenesis and sulfhydryl modification. *Biophys J* **72**, 989-996.

Ragsdale DS, McPhee JC, Scheuer T & Catterall WA. (1994). Molecular determinants of state-dependent block of Na<sup>+</sup> channels by local anesthetics. *Science* **265**, 1724-1728.

Ragsdale DS, McPhee JC, Scheuer T & Catterall WA. (1996). Common molecular determinants of local anesthetic, antiarrhythmic, and anticonvulsant block of voltage-gated Na<sup>+</sup> channels. *Proc Natl Acad Sci U S A* **93**, 9270-9275.

Roden DM. (2006). Long QT syndrome: reduced repolarization reserve and the genetic link. *J Intern Med* **259**, 59-69.

Rogart RB, Cribbs LL, Muglia LK, Kephart DD & Kaiser MW. (1989). Molecular cloning of a putative tetrodotoxin-resistant rat heart Na<sup>+</sup> channel isoform. *Proc Natl Acad Sci U S A* **86**, 8170-8174.

Romano C, Gemme G & Pongiglione R. (1963). [Rare Cardiac Arrhythmias of the Pediatric Age. II. Syncopal Attacks Due to Paroxysmal Ventricular Fibrillation. (Presentation of 1st Case in Italian Pediatric Literature)]. *Clin Pediatr (Bologna)* **45**, 656-683.

Roudier-Pujol C, Rochat A, Escoubet B, Eugene E, Barrandon Y, Bonvalet JP & Farman N. (1996). Differential expression of epithelial sodium channel subunit mRNAs in rat skin. *J Cell Sci* **109 ( Pt 2)**, 379-385.

Ruan Y, Denegri M, Liu N, Bachetti T, Seregni M, Morotti S, Severi S, Napolitano C & Priori SG. (2010). Trafficking defects and gating abnormalities of a novel SCN5A mutation question gene-specific therapy in long QT syndrome type 3. *Circ Res* **106**, 1374-1383.

Ruben PC, Starkus JG & Rayner MD. (1992). Steady-state availability of sodium channels. Interactions between activation and slow inactivation. *Biophys J* **61**, 941-955.

Rush AM, Dib-Hajj SD, Liu S, Cummins TR, Black JA & Waxman SG. (2006). A single sodium channel mutation produces hyper- or hypoexcitability in different types of neurons. *Proc Natl Acad Sci U S A* **103**, 8245-8250.

Saenen JB & Vrints CJ. (2008). Molecular aspects of the congenital and acquired Long QT Syndrome: clinical implications. *J Mol Cell Cardiol* **44**, 633-646.

Saint DA, Ju YK & Gage PW. (1992). A persistent sodium current in rat ventricular myocytes. *J Physiol* **453**, 219-231.

Sangameswaran L, Delgado SG, Fish LM, Koch BD, Jakeman LB, Stewart GR, Sze P, Hunter JC, Eglén RM & Herman RC. (1996). Structure and function of a novel voltage-gated, tetrodotoxin-resistant sodium channel specific to sensory neurons. *J Biol Chem* **271**, 5953-5956.

Satin J, Kyle JW, Chen M, Bell P, Cribbs LL, Fozzard HA & Rogart RB. (1992a). A mutant of TTX-resistant cardiac sodium channels with TTX-sensitive properties. *Science* **256**, 1202-1205.

Satin J, Kyle JW, Chen M, Rogart RB & Fozzard HA. (1992b). The cloned cardiac Na channel alpha-subunit expressed in *Xenopus* oocytes show gating and blocking properties of native channels. *J Membr Biol* **130**, 11-22.

Sato C, Sato M, Iwasaki A, Doi T & Engel A. (1998). The sodium channel has four domains surrounding a central pore. *J Struct Biol* **121**, 314-325.

Sato C, Ueno Y, Asai K, Takahashi K, Sato M, Engel A & Fujiyoshi Y. (2001). The voltage-sensitive sodium channel is a bell-shaped molecule with several cavities. *Nature* **409**, 1047-1051.

Schmidt JW & Catterall WA. (1986). Biosynthesis and processing of the alpha subunit of the voltage-sensitive sodium channel in rat brain neurons. *Cell* **46**, 437-444.

Schmidt JW & Catterall WA. (1987). Palmitoylation, sulfation, and glycosylation of the alpha subunit of the sodium channel. Role of post-translational modifications in channel assembly. *J Biol Chem* **262**, 13713-13723.

Schwartz PJ. (1985). Idiopathic long QT syndrome: progress and questions. *Am Heart J* **109**, 399-411.

Schwartz PJ, Periti M & Malliani A. (1975). The long Q-T syndrome. *Am Heart J* **89**, 378-390.

Schwartz PJ, Stramba-Badiale M, Crotti L, Pedrazzini M, Besana A, Bosi G, Gabbarini F, Goulene K, Insolia R, Mannarino S, Mosca F, Nespoli L, Rimini A, Rosati E, Salice P & Spazzolini C. (2009). Prevalence of the congenital long-QT syndrome. *Circulation* **120**, 1761-1767.

Sheets PL, Jackson JO, 2nd, Waxman SG, Dib-Hajj SD & Cummins TR. (2007). A Nav1.7 channel mutation associated with hereditary erythromelalgia contributes to neuronal hyperexcitability and displays reduced lidocaine sensitivity. *J Physiol* **581**, 1019-1031.

Song Y, Shryock JC & Belardinelli L. (2008). An increase of late sodium current induces delayed afterdepolarizations and sustained triggered activity in atrial myocytes. *Am J Physiol Heart Circ Physiol* **294**, H2031-2039.

Stuhmer W, Conti F, Suzuki H, Wang XD, Noda M, Yahagi N, Kubo H & Numa S. (1989). Structural parts involved in activation and inactivation of the sodium channel. *Nature* **339**, 597-603.

Sunami A, Dudley SC, Jr. & Fozzard HA. (1997). Sodium channel selectivity filter regulates antiarrhythmic drug binding. *Proc Natl Acad Sci U S A* **94**, 14126-14131.

Tester DJ, Will ML, Haglund CM & Ackerman MJ. (2005). Compendium of cardiac channel mutations in 541 consecutive unrelated patients referred for long QT syndrome genetic testing. *Heart Rhythm* **2**, 507-517.

Tian XL, Yong SL, Wan X, Wu L, Chung MK, Tchou PJ, Rosenbaum DS, Van Wagoner DR, Kirsch GE & Wang Q. (2004). Mechanisms by which SCN5A mutation N1325S causes cardiac arrhythmias and sudden death in vivo. *Cardiovasc Res* **61**, 256-267.

Towbin JA & Friedman RA. (1998). Prolongation of the QT interval and the sudden infant death syndrome. *N Engl J Med* **338**, 1760-1761.

Towbin JA & Vatta M. (2001). Molecular biology and the prolonged QT syndromes. *Am J Med* **110**, 385-398.

Ulbricht W. (2005). Sodium channel inactivation: molecular determinants and modulation. *Physiol Rev* **85**, 1271-1301.

Valdivia CR, Tester DJ, Rok BA, Porter CB, Munger TM, Jahangir A, Makielski JC & Ackerman MJ. (2004). A trafficking defective, Brugada syndrome-causing SCN5A mutation rescued by drugs. *Cardiovasc Res* **62**, 53-62.

Vassilev P, Scheuer T & Catterall WA. (1989). Inhibition of inactivation of single sodium channels by a site-directed antibody. *Proc Natl Acad Sci U S A* **86**, 8147-8151.

Vassilev PM, Scheuer T & Catterall WA. (1988). Identification of an intracellular peptide segment involved in sodium channel inactivation. *Science* **241**, 1658-1661.

Vilin YY & Ruben PC. (2001). Slow inactivation in voltage-gated sodium channels: molecular substrates and contributions to channelopathies. *Cell Biochem Biophys* **35**, 171-190.

Wang DW, Desai RR, Crotti L, Arnestad M, Insolia R, Pedrazzini M, Ferrandi C, Vege A, Rognum T, Schwartz PJ & George AL, Jr. (2007). Cardiac sodium channel dysfunction in sudden infant death syndrome. *Circulation* **115**, 368-376.

Wang DW, Yazawa K, George AL, Jr. & Bennett PB. (1996). Characterization of human cardiac Na<sup>+</sup> channel mutations in the congenital long QT syndrome. *Proc Natl Acad Sci U S A* **93**, 13200-13205.

Wang DW, Yazawa K, Makita N, George AL, Jr. & Bennett PB. (1997). Pharmacological targeting of long QT mutant sodium channels. *J Clin Invest* **99**, 1714-1720.

Wang Q, Shen J, Splawski I, Atkinson D, Li Z, Robinson JL, Moss AJ, Towbin JA & Keating MT. (1995). SCN5A mutations associated with an inherited cardiac arrhythmia, long QT syndrome. *Cell* **80**, 805-811.

Ward OC. (1964). A New Familial Cardiac Syndrome in Children. *J Ir Med Assoc* **54**, 103-106.

West JW, Numann R, Murphy BJ, Scheuer T & Catterall WA. (1991). A phosphorylation site in the Na<sup>+</sup> channel required for modulation by protein kinase C. *Science* **254**, 866-868.

West JW, Patton DE, Scheuer T, Wang Y, Goldin AL & Catterall WA. (1992). A cluster of hydrophobic amino acid residues required for fast Na<sup>(+)</sup>-channel inactivation. *Proc Natl Acad Sci U S A* **89**, 10910-10914.

White MM, Chen LQ, Kleinfeld R, Kallen RG & Barchi RL. (1991). SkM2, a Na<sup>+</sup> channel cDNA clone from denervated skeletal muscle, encodes a tetrodotoxin-insensitive Na<sup>+</sup> channel. *Mol Pharmacol* **39**, 604-608.

Yamamura K, Muneuchi J, Uike K, Ikeda K, Inoue H, Takahata Y, Shiokawa Y, Yoshikane Y, Makiyama T, Horie M & Hara T. (2009). A novel SCN5A mutation associated with the linker between III and IV domains of Na(v)1.5 in a neonate with fatal long QT syndrome. *Int J Cardiol*.

Yamamura K, Muneuchi J, Uike K, Ikeda K, Inoue H, Takahata Y, Shiokawa Y, Yoshikane Y, Makiyama T, Horie M & Hara T. (2010). A novel SCN5A mutation associated with the linker between III and IV domains of Na(v)1.5 in a neonate with fatal long QT syndrome. *Int J Cardiol* **145**, 61-64.

Yang P, Kanki H, Drolet B, Yang T, Wei J, Viswanathan PC, Hohnloser SH, Shimizu W, Schwartz PJ, Stanton M, Murray KT, Norris K, George AL, Jr. & Roden DM. (2002). Allelic variants in long-QT disease genes in patients with drug-associated torsades de pointes. *Circulation* **105**, 1943-1948.

Yeh JZ. (1978). Sodium inactivation mechanism modulates QX-314 block of sodium channels in squid axons. *Biophys J* **24**, 569-574.

Yu FH & Catterall WA. (2003). Overview of the voltage-gated sodium channel family. *Genome Biol* **4**, 207.

Zhao J, Ziane R, Chatelier A, O'Leary M E & Chahine M. (2007). Lidocaine promotes the trafficking and functional expression of Na(v)1.8 sodium channels in mammalian cells. *J Neurophysiol* **98**, 467-477.

## CURRICULUM VITAE

### Weihoa Song

#### **EDUCATION AND TRAINING**

Ph.D. Pharmacology	Indiana University, USA	08/2004-05/2011
Research Fellow	Montreal Heart Institute, Canada	07/2003-07/2004
M.S. Pharmacology	Harbin Medical University, China	09/1999-07/2002
M.D. Clinical Medicine	Harbin Medical University, China	09/1992-07/1997

#### **WORKING EXPERIENCE**

##### **Professional Teaching Experience**

07/1997-08/2004	Lecturer, Department of Pharmacology, Harbin Medical University (HMU), P.R. CHINA.
05/2001-07/2001	Supervised three medical students on the project "Effects of several anticancer drugs on HeLa and HLE cancer cells."
05/1999-07/1999	Supervised one graduate student of master program in HMU for her thesis project on "Cardiac anti-arrhythmia effects of berbamine in rats."
03/1998-09/1998	"Medical Pharmacology" Course manager, at Department of Pharmacology, Harbin Medical University.

##### **Professional Research Experience**

06/2005-04/2011	Graduate student and research assistant, Pharmacology Department, Indiana University, School of Medicine. Thesis work "Human Nav1.5 F1486 deletion associated with long-QT syndrome leads to deficiency in inactivation and reduces lidocaine sensitivity" Investigated "Involvement of TRPV1 phosphorylation sites in the acute sensitization by nerve growth factor and bradykinin"
07/2003-07/2004	Research Fellow, Montreal Heart Institute, Canada. Investigated effects of Human ether a-go-go related channel on cardiac arrhythmia
09/1999-02/2002	Conducted extensive research on anticancer pharmacology. My research was focused on "Selecting traditional Chinese herbs that have anticancer effects "
02/1999-06/1999	Group leader of developing the model of hepatitis in rats; conducted experiments on an anti-hepatitis herbal drug.
04/1998-06/1999	Co-investigator of the project, "The relationship between the cardiac anti-arrhythmic effect of several Chinese

traditional herbs and the potassium channel” supported by the National Science Foundation (NNSF). I was in charge of the pharmacodynamics part of that project.

10/1998-12/1998 Design and set up the cell culture core facility in our department.

## **PUBLICATIONS & PRESENTATIONS**

1. Hao XM, Yuan SH, Song WH, He SZ, Yang BF. Effects of thymosin on lymphocyte transformation rate in rats. *Journal of Harbin Medical University* 1999; 33 (2): 100-101.
2. Liu FY, He SZ, Yang BF, Song WH. Effects of HPD on protection of experimental acute hepatic injury. *Journal of Harbin Medical University* 1999; 33 (5): 360-362.
3. Handbook for Pharmacology Experiments. Published by Harbin Medical University in Jan, 2001.
4. Song WH, Sun JP, Yang BF. Anticancer effect of mineral extract MICOM *in vitro*. *Journal of Harbin Medical University* 2001; 35 (6): 402-403.
5. Song WH, Sun JP, Yang BF. The effect of MICOM on the colorectal cancer cell line Ls-174-T. *Journal of Harbin Medical University* 2002; 36 (5): 23-25.
6. Dong HY, Song WH, Sun JP, Wang L, Yang BF. Effects of artemisinin on the growth of HeLa cells. *Journal of Harbin Medical University* 2002; 36(6): 423-424.
7. Wang L, Song WH, Wu ZJ, Yang BF. The therapeutic effect of “Weiyanyao” on chronic atrophic gastritis in rat. *Chinese Journal of Medical Hygiene* 2002; 1(7): 44-46.
8. Dong HY, Song WH, Wang L, Yang BF. Apoptosis was induced by artemisinin in K562 cells. *Chinese Journal of Tumor* 2003; 12(8): 473-475.
9. Wang L, Sun HL, Song WH, Yang BF. GABA has protective effect on Ca<sup>2+</sup> overload induced by glutamate in cultured human oligodendrogloma cell. *The Korean Journal of Physiology & Pharmacology*. 2003; 7(Supplement 1): 179.
10. Liu Y, Sun HL, Song WH, Yang BF. Effects of emodin on the intracellular calcium concentration in the single cell of ventricular myocytes of guinea pig. *Journal of Harbin Medical University* 2003; 37(2):122-124.
11. Dong DL, Liu Y, Zhou YH, Song WH, Wang H, Yang BF. Decreases of voltage-dependent K<sup>+</sup> currents densities in ventricular myocytes of guinea pigs by chronic oxidant stress *in vitro*. *Acta Pharmacologica Sinica* 2004; 25 (6):751-755.
12. Dong DL, Li Z, Wang HZ, Du ZM, Song WH, Yang BF. Acidification alters antiarrhythmic drug blockade of the human HERG channels. *Basic & Clinical Pharmacology & Toxicology* 2004; 94(5):209-212.
13. Dong DL, Song WH, Ma PL, Yang BF. Arsenic trioxide-induced HeLa cell death is partially prevented by K<sup>+</sup> channel blockers. *Yao Xue Xue Bao* 2005; 40 (7): 644-648.

14. Song WH, Zhu WG, Oxford GS. Involvement of protein kinase C phosphorylation sites of TRPV1 in acute sensitization by nerve growth factor. Society for Neuroscience, Neuroscience Conference, 2008, Washington DC.
15. Song WH, Xiao YC, Chen HY, Piekarz AD, Yong WD, Hudmon A, Cummins TR\*, Shou W\* (\*co-correspondence author) Human Nav1.5 F1486 deletion associated with long-QT syndrome leads to deficiency in inactivation and reduces lidocaine sensitivity (paper in preparation).
16. Song WH, Xiao YC, Chen HY, Piekarz AD, Yong WD, Hudmon A, Cummins TR\*, Shou W\* (\*co-correspondence author) Abstract and poster presentation for Midwest Cardiologist Symposium, 2010, Indianapolis.
17. Song WH, Xiao YC, Chen HY, Piekarz AD, Yong WD, Hudmon A, Cummins TR\*, Shou W\*, (\*co-correspondence author) Poster presentation for Riley Heart Symposium, 2010, Indianapolis.

## **EXPERIMENTAL SKILLS**

Cell biology: Primary neonatal cardiomyocyte culture, Primary dorsal root ganglion neuron culture, mammalian cell line culture, mammalian cell and primary cell transfection, generating stable cell line.

Molecular biological techniques: regular PCR, RT-PCR, molecular cloning, ShRNA construction, siRNA knock down experiments, lentivirus and retrovirus production, DNA agarose gel electrophoresis, DNA & RNA purification, DNA transformation.

Biochemistry techniques: protein extraction, western blot, protein immunoprecipitation (IP), protein electrophoresis, cellular cAMP assay, MTT assay.

*In vivo* animal experiments: eg. mouse tail vein drug injection, ip injection.

Patch-clamp techniques, whole cell electrophysiological recording under both voltage-clamp and current-clamp conditions using both HEKA and Axon software.

## **HONORS**

1. Recipient of 2008 Indiana University Graduate School Education Enhancement Grant.
2. First place in the oral talk competition of "2003 Chinese National Conference for Pharmacology". As a winner, I was supported by the Chinese Pharmacological Society to attend the "Asian and West Pacific Pharmacological Meeting in Korea", 2003.
3. Scholarship from China Scholarship Council for Visiting Research Scholar in Canada, 2003.
4. National "Suzuki Graduate Student Fellowship", P.R. CHINA, 2002.
5. "Outstanding Junior faculty", Harbin Medical University, 1999.

6. Excellent Undergraduate Student Fellowship, Harbin Medical University, 1993-1997.

**AFFILIATION**

Member	American Heart Association	2010
Member	Society for Neuroscience	2007-2008
Member	Chinese Pharmacological Society	1998-present
Chair	Student Organization, HMU	1995-1997
Chair	English Corner of No.1 Middle School, Hulan	1990-1992